2020

Investigating diel, seasonal, and interannual variability of dissolved and particulate stable carbon isotope values in a eutrophic boreal lake

Rachel Henderson
hend3120@mylaurier.ca

Investigating diel, seasonal, and interannual variability of dissolved and particulate stable carbon isotope values in a eutrophic boreal lake

by
Rachel Henderson
Bachelor of Science, University of Waterloo, 2016

THESIS
Submitted to the Department of Geography and Environmental Studies
in partial fulfilment of the requirements for
Master of Science in Geography (Environmental Science)
Wilfrid Laurier University

Abstract

Lakes are globally significant sources, sinks, and conduits of carbon. Cultural eutrophication of freshwater promotes the growth of phytoplankton blooms, which can transform, respire, and sequester large amounts of carbon. Analysis of stable carbon isotopes is a common tool to study the movement of carbon through the aquatic carbon cycle. The causes of temporal variability in $\delta^{13}C$ values at different timescales are not well understood, and differ between lakes. In this study, I investigated diel, seasonal, and interannual variability in $\delta^{13}C$ values of dissolved inorganic carbon (DIC) and particulate organic carbon (POC) in Lake 227, an artificially eutrophic lake at the IISD Experimental Lakes Area in northwestern Ontario, Canada. Weekly phosphorus additions to Lake 227 promote the growth of annual phytoplankton blooms. I interpreted hourly overnight change in $\delta^{13}C$-DIC values to determine the relative contributions of atmospheric gas exchange and ecosystem respiration (ER) to the DIC pool on a diel timescale. I also interpreted the drivers of temporal variability in $\delta^{13}C$-DIC and $\delta^{13}C$-POC values on weekly to seasonal timescales from regular sampling events during the ice-free season since 2010.

Collecting $\delta^{13}C$-DIC samples overnight is labour-intensive and this study is one of few that reports overnight $\delta^{13}C$-DIC values for a lake. I collected hourly samples between sunset and sunrise on three occasions: during an epilimnion phytoplankton bloom dominated by cyanobacteria, a bloom composed of cyanobacteria and chlorophytes, and a period of biomass decline between the two blooms. 1 m samples represented conditions in the well-mixed epilimnion, and 3 m samples represented a depth of highly-concentrated biomass in the metalimnion. Overnight change in $\delta^{13}C$-DIC values varied between a 3 ‰ increase and 18 ‰ decrease. The values of $\delta^{13}C$-DIC at 1 m were closer to the value of $\delta^{13}C$-DIC produced by ER during the blooms, but closer to the $\delta^{13}C$-DIC value in equilibrium with the atmosphere during the lower-biomass period. Gas exchange and lake metabolism calculations confirmed that ER was the dominant source of DIC to the epilimnion during the blooms. The rate of ER controls the overnight increase in [DIC] and decline in pH. Daytime pH tended to reach 9.5-9.7 during the blooms, which

allowed for a low rate of chemically enhanced diffusion (CED). Accounting for CED, the rate of gas exchange was lower or equal to the rate of ER during the ice-free season. The 3 m sampling depth acted as a closed system as lake metabolism drove changes in DIC concentration. Understanding diel variability in DIC concentration and δ^{13}C-DIC is important for modeling values of photosynthetic fractionation, and interpreting seasonal δ^{13}C-DIC and δ^{13}C-POC values.

Changes in weekly mid-morning δ^{13}C-DIC and δ^{13}C-POC values were driven by changes in the concentration of phytoplankton biomass. Phytoplankton blooms in Lake 227 lower the DIC concentration below equilibrium with the atmosphere. Lower DIC concentrations occurred in conjunction with high δ^{13}C-POC values and low δ^{13}C-DIC values. Since sampling began in 2010, when the epilimnion concentration of chlorophyll a was greater than 30 µg L^{-1} and the DIC concentration was less than 50 µg L^{-1}, the range in δ^{13}C-POC values was narrow: between -26 ‰ and -23 ‰. Outside of these thresholds, observed values of δ^{13}C-POC were as low as -36 ‰. Similar relationships did not exist at 3 m, as the phytoplankton peak shifted vertically in the water column over each ice-free season. The lowest daytime δ^{13}C-DIC values at 1 m corresponded with the lowest DIC concentrations, and the overnight δ^{13}C-DIC values were also lowest when the DIC concentration was low during the phytoplankton blooms. DIC fixation caused pH to increase during the phytoplankton blooms, reducing the proportion of DIC that was dissolved CO_2, and decreasing the amount of photosynthetic fractionation. These trends repeated across years, and should lead to a high, consistent δ^{13}C value of the lake sediments.

Lake 227 is an ideal setting to investigate the drivers of temporal variability in δ^{13}C-DIC and δ^{13}C-POC in a eutrophic lake. The concentration of biomass and phytoplankton species composition tends to repeat each year, and there is a long history of comprehensive physical, geochemical, and biological monitoring. The data I present in this thesis provide new insight into how changes in phytoplankton concentration and carbonate geochemistry drive temporal variability in δ^{13}C values on diel, seasonal, and interannual timescales.

Acknowledgements

I have had such a fun and rewarding time in grad school. The friendships I've made, the skills I've learned, and the confidence I've gained are thanks to many kind, smart, and hardworking people. I would not have enjoyed my research nearly as much, nor would my thesis be as thoughtful, pretty, comprehensive, or absent of the passive voice as it is, without their help.

First of many is my supervisor, Dr. Jason Venkiteswaran. Thank you for challenging and trusting me to figure things out on my own, but for having an open office door and only ever being a Slack message away. Thank you for your fair and helpful comments that have made my work clearer, more correct, and more relevant. And thank you for your patience, encouragement, and understanding as I've sought out opportunities to learn and travel; I've gotten more out of my degree because of it. I might be biased, but you've built a lab that puts people first, and that attracts the friendliest students and researchers who really care about their science. You're the coolest, and I'm so lucky to have joined your team.

This thesis and my own professional development have benefitted greatly from input and advice from my committee members: Dr. Sherry Schiff, Dr. Kateri Salk, and Dr. Nora Casson. Thank you Sherry for many years of thoughtful questions and comments on my work, for giving me opportunities to practice my research skills, and for setting high expectations that pushed me to excel. Thank you Kateri for leading by example; your drive for excellence in teaching, field work, and science is contagious. Thank you Nora for your thoughtful feedback, for making time to meet with me whenever I was in Winnipeg, and for always making me feel like I was on the right track.

I ended up working for the Environmental Geochemistry Lab serendipitously, but I stayed for so long because of the fantastic people there. Thank you Richard Elgood for years of training, encouragement, office chats, and logistical support. You've opened some doors for me and given me a push through others, and I am so grateful for all of those opportunities. Thank you to Rich, and to Rhys Gwynne and Bill Mark of the Environmental Isotope Lab, for sharing your technical expertise and for analysing so many of my δ^{13}C-DIC and δ^{13}C-POC samples. And thank you to the students, post docs, and lab techs past and present who have made the fifth floor of EIT such a fun, friendly place to work.

I had the incredible opportunity to spend two summers at the IISD Experimental Lakes Area (IISD-ELA). Before I had ever even heard of IISD-ELA, the federal government cut its funding. Thank you to everyone who worked tirelessly to keep the doors and lakes of this research station open, and to those who continue to work to ensure IISD-ELA will always support world-class freshwater research.

During my time at IISD-ELA I had the support of knowledgeable and passionate researchers. Thank you Dr. Sonya Havens for welcoming me to your lab and accommodating my sample analysis – I am so appreciative of your time, your help, and the very fun atmosphere of the chem lab. Thank you Ken Sandilands and Paul Fafard for your outstanding generosity: sharing your expertise, your field equipment, your data, your boats, and even your truck. Most of what I know about doing good limnology field work is thanks to your help and patience. Thank you Dr. Scott Higgins for graciously hosting me in your lab, helping me land on my feet when I arrived in camp, and for your thoughtful advice on my research. And thank you Sonya, Ken, Paul, Scott, and to Cyndy Desjardins for your remote support: collecting, filtering, and shipping samples; deploying, retrieving, and off-loading data loggers; compiling data requests; and responding to my emailed questions. I have learned so much from you all.

An extra big thank you to the following grad students and research assistants, who made my time at IISD-ELA the absolute best: Jared Wolfe, for being such a competent and friendly field partner from the chaotic get-go; Bryanna Sherbo, for your immediate friendship and your fun, fearless attitude as we figured out our field work together; Joey Tonin, for showing me the ropes and always being someone I could go to for help; Justin Budyk, for literally teaching me how to drive a boat; and Sonya Michaleski, for being so generous with your friendship and never even giving me a chance to be shy. I miss you all!

Nights in the boreal forest are chilly and full of mosquitos. Thank you Kateri, Bethany Gruber, and Jennifer Mead for your willingness and excitement to sleep on a boat and wake up hourly to sample with me. You made a daunting task into an adventure, and three nights I'll never forget. And thank you Laura Alsip, Desiree Langenfeld, Stefano Strapazzon, and Blake Cooney for analysing so many DIC and pH samples afterward!

Next to field work, learning to program in R has been one of my favourite parts of grad school. Thank you Dr. Megan Larsen, Kateri, and Jason for teaching me the basics early, and for your enthusiastic help in troubleshooting my more elaborate ideas. Thank you also to Scott Tolksdorf for the brilliant advice to use AutoHotkey for entering the many δ's and ‰'s in this thesis.

The grad school gods were smiling on the day they put me in the same cohort as Jordyn Atkins, Emily Barber, and Puru Shah. You are all stellar officemates, field partners, grad students, and friends. It may have taken us a while to graduate, but that just meant I got to hang out with you all for longer!

My past and current roommates are my best friends and biggest cheerleaders. Thank you Wynona Klemt, Stephanie Slowinski, and Katie Brown for your encouragement, advice, and for all the fun times we've had together – not just as grad students, but since we met during frosh week *nine years ago*.

Finally, thank you to my parents, Ken and Kathy Henderson, who have supported me in everything I've ever set out to do. Thank you for the rides to the airport, moving me and my furniture too many times, and for always encouraging my love of learning.

Contents

List of Tables

List of Figures

Chapter 1: Introduction

Lakes are an active component of the global carbon (C) cycle, serving as sources of carbon to the atmosphere, sinks of carbon to lake sediments, and conduits of carbon to downstream water bodies (Cole et al., 2007; Tranvik et al., 2009). Globally lakes emit approximately 0.32-0.53 Pg C yr^{-1} to the atmosphere and bury 0.05-0.12 Pg C yr^{-1} in sediments (Anderson et al., 2020; Raymond et al., 2013; Tranvik et al., 2009). Lakes account for 2.2% of global land area, but these fluxes are 2-4 times less than the annual amounts of carbon accumulated in the ocean and buried in marine sediments: 2.2 Pg C yr^{-1} and 0.2 Pg C y^{-1}, respectively (Battin et al., 2009; Raymond et al., 2013). Phytoplankton are key to many of the biological and chemical processes of the aquatic carbon cycle, as they fix dissolved inorganic carbon (DIC) through photosynthesis, produce DIC through respiration, and ultimately bury organic carbon as cells die and settle at the bottom of lakes. In this work, I investigate the relationship between phytoplankton and DIC in the aquatic carbon cycle using stable isotope analysis.

1.1 Algal Blooms

The terms 'algal bloom' and 'phytoplankton bloom' are used by scientists and the general public to describe the visible accumulation of phytoplankton in a body of water (Watson et al., 2016). Algal blooms affect the drinking water quality, aquatic health, recreation potential, and the overall aesthetic of a variety of water bodies (Schindler & Vallentyne, 2008). They can be composed of a diverse algal community or dominated by one or more taxa; create an unpleasant surface scrum or congregate at depth; and be harmful to human, animal, and aquatic life or be a benign nuisance. Overall, algal blooms are a wide-reaching and diverse problem, becoming increasingly common globally due to nutrient pollution and climate change (Carpenter et al., 1998; Heisler et al., 2008).

Harmful algal blooms

A harmful algal bloom (HAB) has the potential to be toxic to human, animal, and fish health, and is typically associated with the release of toxins by cyanobacteria as they die (Watson et al., 2015). Cyanobacteria, commonly referred to as 'blue-green algae', are a phylum of photosynthetic bacteria that macroscopically resemble eukaryotic algae. Colonizing (e.g. *Microcystis* spp.) and filamentous (e.g. *Anabaena* spp*., Aphanizomenon* spp.) taxa are common in freshwater blooms, although specific species and strains within these taxa may or may not produce toxins (Carpenter, 2008; Schindler & Vallentyne, 2008). In addition to the potential for toxin release, cyanobacteria-dominated blooms can have negative effects on water taste and odour, and lead to shading, fouling, hypoxia, and reduced biodiversity in water bodies (Watson et al., 2015). The economic costs associated with HABs include increased healthcare, loss of tourism revenue from beach and lake closures, reduced aquaculture, loss of access to drinking water sources, and the associated costs of mitigation, monitoring, and water treatment (Hoagland & Scatasta, 2006). Researchers have estimated that the effects of HABs in Lake Erie alone cost $272 million annually in Canada (2015 Canadian dollars; Smith et al., 2019).

The costs and harmful effects associated with algal blooms have spurred significant scientific research across disciplines and environments, leading to a more nuanced approach to preventing and managing blooms (Heisler et al., 2008). Major successes have occurred as a result of past research, including the reversal of hypoxia in Lake Erie during the 1970s through reduced loading of phosphorus (P; Charlton et al., 1993; Dove & Chapra, 2015). While phytoplankton biomass can be controlled by managing P, reduction is often difficult and algal blooms persist. Researchers have been studying the role of other macro- and micronutrients in bloom development and species composition to offer additional management strategies (Molot et al., 2014; Sunda, 2006; Van Dam et al., 2018).

Nutrient stoichiometry

Phytoplankton require carbon, nitrogen (N) and P to grow. Marine phytoplankton cells are typically composed of C, N, and P in a molar ratio of 106:16:1, respectively, which indicates sufficient nutrient availability (Goldman et al., 1979; Redfield, 1958). The molar ratios C:N, C:P, and N:P of phytoplankton in freshwater systems are more variable than in the ocean, and tend to be greater than the Redfield ratio (Hecky et al., 1993). These ratios are indicators of nutrient deficiency, with ratios above a certain threshold indicating N or P limitation (Wetzel, 2001).

Atmospheric exchange of CO_2 provides a sufficient supply of DIC to promote the growth of phytoplankton in lakes (Schindler et al., 1972). The atmosphere also supplies lakes with dissolved N_2, which diazotrophic phytoplankton taxa can fix in sufficient quantities to overcome N-limitation (Higgins et al., 2018). There is no gaseous form of P that enters lakes; natural weathering of phosphate-rich rocks supply lakes with varying amounts of P, and anthropogenic sources such as fertilizer and wastewater can contribute high amounts of N and P (Carpenter, 2008).

Lakes with high nutrient supply and high rates of primary productivity are classified as eutrophic. Eutrophic lakes tend to be turbid, with an abundance of phytoplankton and aquatic plants in the epilimnion and a low-oxygen hypolimnion. Conversely, oligotrophic lakes are clear, have low nutrient concentrations and low rates of primary productivity, and high hypolimnetic oxygen concentrations. While naturally eutrophic lakes do exist, it is more common that human activities cause oligotrophic lakes to become eutrophic by releasing high amounts of N and P into waterways (Schindler & Vallentyne, 2008). This process, referred to as cultural eutrophication, results mainly from nutrient-rich agricultural run-off and wastewater effluent (Carpenter et al., 1998).

The concentrations of dissolved C, N, and P in lakes are variable over time, and freshwater phytoplankton have adapted to access these elements when they are scare (Heisler et al., 2008).

Cyanobacteria may dominate blooms in lakes that have a low concentration of N or C. Some species of cyanobacteria have heterocyte cells, enabling them to fix atmospheric N_2 and thrive in aquatic environments with low concentrations of NO_3^- and NH_4^+ (Flett et al., 1980; Paerl, 1990). All cyanobacteria rely on carbon concentrating mechanisms (CCMs) to support photosynthesis at low concentrations of dissolved CO_2 (Badger & Price, 2003; Giordano et al., 2005).

Carbon concentrating mechanisms

Phytoplankton fix CO_2 during photosynthesis. Uptake of dissolved CO_2 into the phytoplankton cell can occur passively by diffusion, but phytoplankton also use CCMs to more effectively increase their internal CO_2 concentration (Giordano et al., 2005). In lakes with low DIC concentrations, or alkaline lakes where the majority of DIC is HCO_3^-, CCMs are necessary to saturate RuBisCO with CO_2 for fixation.

CCMs differ between cyanobacteria and eukaryotic algae, and also between taxa. Cyanobacteria concentrate HCO_3^- in their cytosol and then convert HCO_3^- to CO_2 in their carboxysome (Badger & Price, 2003). Most freshwater cyanobacteria can actively take up HCO_3^- at low and high concentrations or convert CO_2 to HCO_3^- as it passes through the plasmalemma (Kaplan & Reinhold, 1999; Giordano et al., 2005). Freshwater β-cyanobacteria are better able to transport CO_2 and HCO_3^- under changing conditions than marine α- and β-cyanobacteria, as freshwater cyanobacteria have adapted to the frequent changes in dissolved CO_2 concentrations in lakes (Badger, 2003). Eukaryotic algae CCMs are diverse, and include membrane transporters, pyrenoids, photosynthetic pathways similar to C4 photosynthesis, and secreting carbonic anhydrase between the plasma membrane and cell wall (Giordano et al., 2005). Low concentrations of dissolved CO_2 in lakes may promote the growth of phytoplankton species with CCMs (Van Dam et al., 2018).

1.2 The Aquatic Carbon Cycle

Primary production by phytoplankton is a key component of the aquatic carbon cycle, as phytoplankton fix, respire, and sequester carbon (Cole et al., 2007). Figure 1.1 summarizes some of the major reactions involving DIC, dissolved organic carbon (DOC), and organic matter (OM) in the aquatic carbon cycle. Allochthonous carbon originates from the atmosphere, surrounding catchment, and from groundwater and surface water inputs (Dillon & Molot, 1997). In-lake processes including photosynthesis, ecosystem respiration (ER), photolysis, and redox reactions involving methane produce autochthonous carbon by transforming allochthonous and autochthonous DIC, DOC, and OM (Bastviken et al., 2008; Molot & Dillon, 1997; Schindler & Fee, 1973). Aquatic carbon may be emitted back into the atmosphere as CO_2, buried in lake sediments, or transported downstream (Cole et al., 2007).

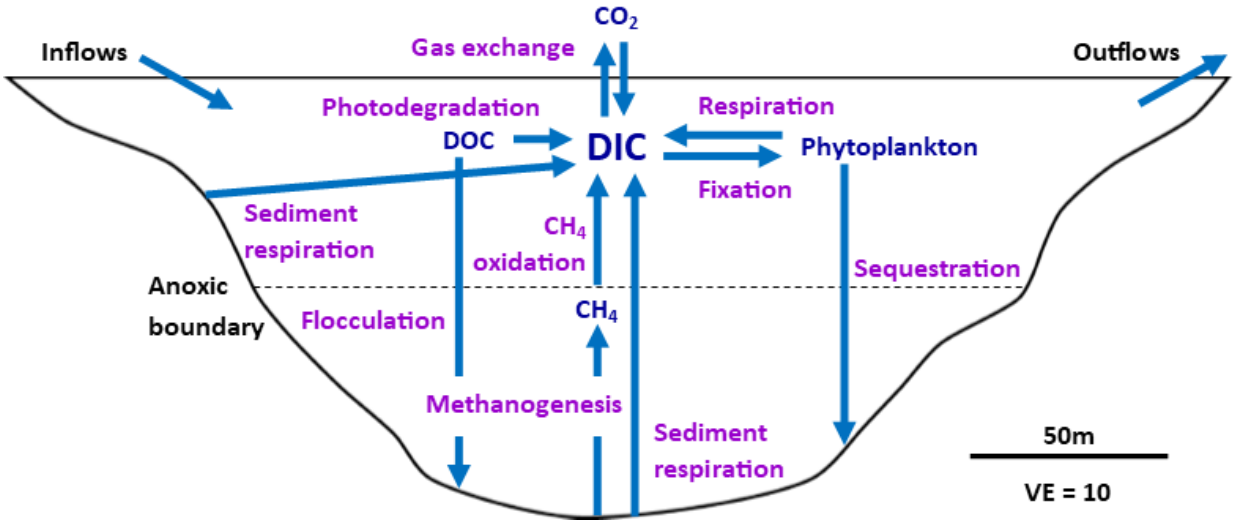

Figure 1.1: Summary of aquatic carbon sources, fates, and in-lake transformations in Lake 227. Lake 227 is a freshwater, thermally stratified lake with no groundwater inputs at the IISD Experimental Lakes Area in northwestern Ontario, Canada.

Primary productivity in lakes

Individual lakes can serve as net sources or sinks of carbon relative to the atmosphere (Cole et al., 1994). Whether a lake is a source or sink is related to its rate of net ecosystem production (NEP; Equation 1.1), the difference between gross primary productivity (GPP) and ER (Odum, 1956). Net autotrophic lakes

(GPP > R) are net sinks of carbon and tend to be eutrophic: larger standing crops of phytoplankton fix CO_2 and sequester that carbon in lake sediments. Net heterotrophic lakes (GPP < R) are net sources of carbon emissions and tend to be oligotrophic, as ER is greater than the amount of CO_2 sequestered by a smaller standing crop of phytoplankton (del Giorgio and Peters, 1993).

$$NEP = GPP - R \tag{1.1}$$

The concentration of dissolved CO_2 in a lake is linked to primary productivity in a way that is "bidirectional and intrinsically complex" (Vogt et al., 2017). Supersaturation of CO_2 in oligotrophic lakes can lead to increased rates of GPP as phytoplankton fix more CO_2 (Jansson et al., 2012). If GPP is already high, as in eutrophic lakes with anthropogenic inputs of N and P, large crops of phytoplankton fix enough dissolved CO_2 during the day to cause undersaturation (Balmer & Downing, 2011; Schindler et al., 1972). Although phytoplankton can acquire sufficient DIC from the atmosphere to support phytoplankton blooms, access to DIC can become limiting on diel timescales as phytoplankton drawn down the concentration (Verspagen et al., 2014). In both oligotrophic and eutrophic lakes with sufficient allochthonous carbon inputs, dissolved CO_2 can be supersaturated with respect to the atmosphere and promote higher rates of GPP (Bogard & del Giorgio, 2016; Dubois et al., 2009).

The carbonate system

The concentration of dissolved CO_2 in any body of water is related to many of its chemical properties through the carbonate system, the species produced through a series of equilibrium reactions when CO_2 dissolves in water (Equation 1.2; Falkowski & Raven, 2007). Biological production and consumption of CO_2, inputs from the atmosphere, and the interaction of water with the geology of the surrounding area control the concentration of CO_2 and its ions (Wetzel, 2001).

$$CO_{2(aq)} + H_2O \leftrightarrow H_2CO_3 \leftrightarrow {HCO_3}^- + H^+ \leftrightarrow {CO_3}^{2-} + 2H^+ \tag{1.2}$$

Carbonic acid, H_2CO_3, exists in very low concentrations compared to $CO_{2(aq)}$. It is standard practice to combine $[H_2CO_3]$ and $[CO_2]$ as one term, because $[H_2CO_3] + [CO_{2(aq)}] \approx [CO_{2(aq)}]$ (Stumm & Morgan, 1996). Total DIC is therefore the sum of dissolved CO_2, HCO_3^- and CO_3^{2-}. The relative amounts of these three species vary with pH at a given temperature and pressure (Figure 1.2). Most freshwater lakes have a pH between 6 and 9, a range over which the fraction of DIC that is CO_2 changes from nearly half to < 1% (Wetzel, 2001). As CO_2 is added to water, the equilibria in Equation 1.2 shifts to the right, decreasing pH by causing an increase in $[H^+]$. If CO_2 is removed, pH increases.

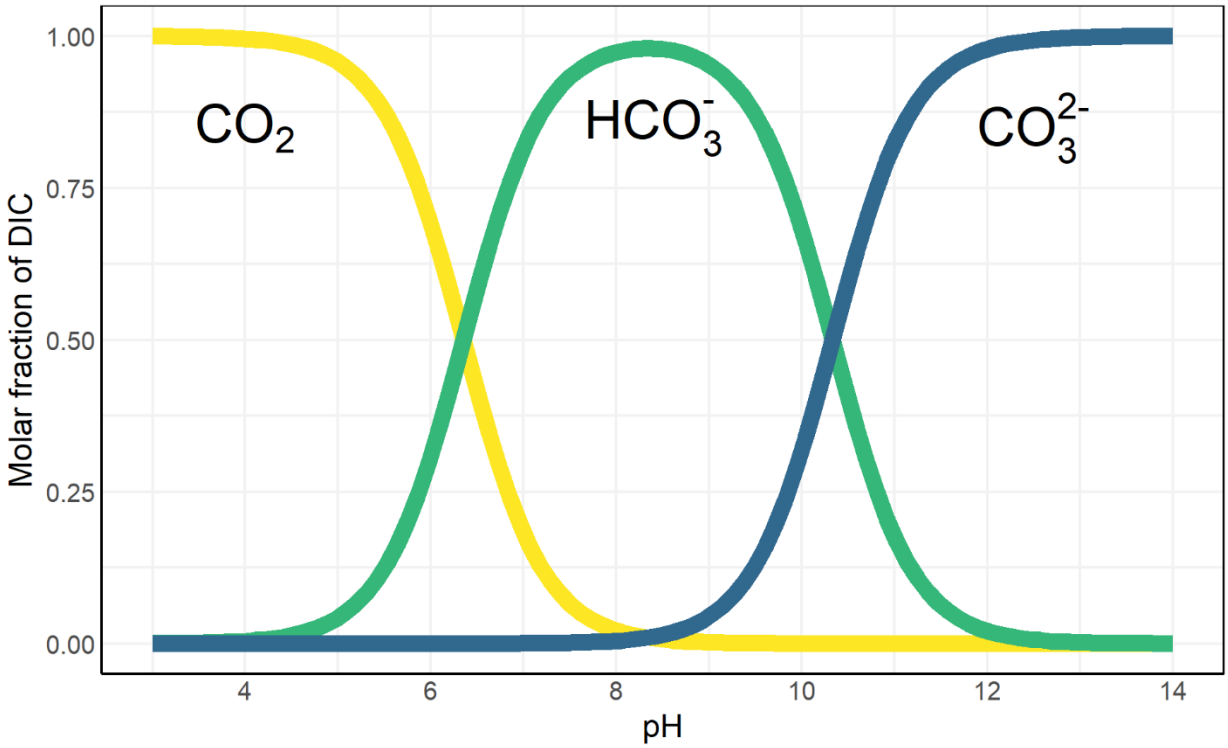

Figure 1.2: Distribution of the three dissolved carbonate species along a pH gradient at standard temperature and pressure.

The carbonate system protects against environmentally hazardous pH swings by providing buffering capacity. HCO_3^- and CO_3^{2-} neutralize acids by accepting protons (Wetzel, 2001). Carbonate alkalinity is the sum of the concentrations of these ions and OH^-, minus the concentration of H^+ (Equation 1.3; Stumm & Morgan, 1996). Researchers measure carbonate alkalinity to determine the maximum amount

of acid that a system can neutralize before a substantial drop in pH. Systems with high carbonate alkalinity have a higher buffering capacity and can neutralize more acid.

$$[Carbonate\ alkalinity] = [HCO_3^-] + 2[CO_3^{2-}] + [OH^-] - [H^+] \quad (1.3)$$

Increasing or decreasing $[CO_2]_{(aq)}$ does not explicitly affect carbonate alkalinity, because CO_2 does not change the net charge balance in Equation 1.3. However, changes in $[CO_2]_{(aq)}$ tend to occur simultaneously with other reactions that do impact alkalinity. For example, photosynthesis consumes $CO_{2(aq)}$, but also NO_3^-, NH_4^+, and HPO_4^{2-}; while the change in $[CO_2]$ does not consume H^+ or OH^-, the assimilation of the other ions does (Stumm & Morgan, 1996).

HCO_3^- and CO_3^{2-} predominantly come from carbonate rocks that slowly dissolve in water. Hard water lakes are underlain by carbonate rocks like limestone, have high concentrations of HCO_3^- and CO_3^{2-}, a high buffering capacity, and are resistant to changes in pH when acid enters the system. Soft water lakes are underlain by silicate rocks like granite, and have a lower alkalinity and a lower buffering capacity (Wetzel, 2001); pH is sensitive to small changes in [DIC] in these systems (Figure 1.3).

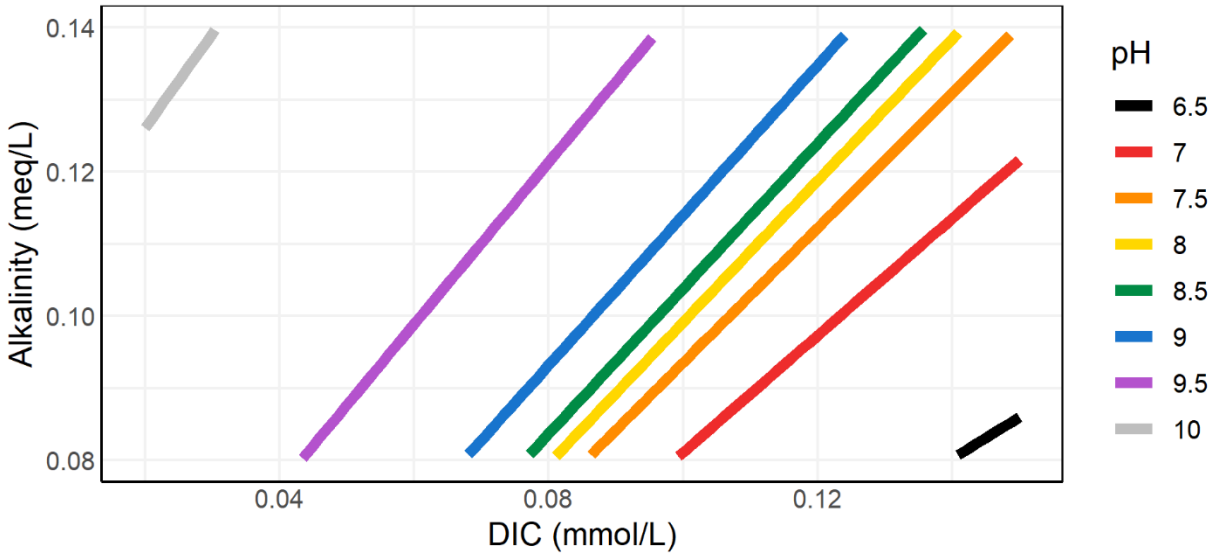

Figure 1.3: pH values at low alkalinity and low [DIC] values, similar to a soft water eutrophic lake (based on Figure 4.10 in Stumm and Morgan, 1996).

Methane in the aquatic carbon cycle

There is growing interest in aquatic methane (CH_4) production as a source of CH_4 to the atmosphere (DelSontro et al., 2018; Sanches et al., 2019). CH_4 that does not escape to the atmosphere can also be a source of dissolved CO_2 in lakes. Bacteria ferment organic matter under anoxic conditions, producing CH_4 and CO_2 in the anoxic hypolimnion and at the sediment-water interface (Equation 1.4).

$$CH_3COOH \rightarrow CH_4 + CO_2 \quad (1.4)$$

In the oxygenated water column, anoxic CH_4 oxidation converts CH_4 to CO_2 (Equation 1.5).

$$CH_4 + 2O_2 \rightarrow CO_2 + 2H_2O \quad (1.5)$$

CH_4 production in eutrophic lakes is low compared to primary production (Rudd & Hamilton, 1978). I will focus on ER and gas exchange with the atmosphere as the dominant sources of CO_2 in this work.

1.3 Environmental Stable Isotopes

Analysis of environmental stable isotopes is a technique to study the movement and transformations of nutrients through ecosystems. Isotopes are atoms of an element that have the same number of protons but differ in the number of neutrons. One isotope of an element may be predominant, with one or more isotopes occurring less abundantly. For example, 98.9 % of carbon atoms have an atomic mass of 12, 1.1 % have an atomic mass of 13, and < 0.0001 % have an atomic mass of 14. To differentiate between isotopes, the sum of protons and neutrons is indicated with a superscript (e.g. ^{13}C).

Isotopes may be radioactive or stable. Radioactive isotopes decay over time to different elements, while stable isotopes do not decay. A stable environmental isotope is any stable isotope involved in biogeochemical cycling in the natural environment, including hydrogen, carbon, nitrogen, oxygen, silicon, sulfur, iron and strontium (Sulzman, 2007). The natural abundance of these isotopes can be measured in gas, water, and solid phases by isotope ratio mass spectrometry (IRMS). The sample is first ionized, and the resulting ion beam then travels along a curved track bent by a magnetic field. Heavier isotopes will separate from the lighter isotopes along the track, and the isotopes are sorted into Faraday cups according to their mass-to-charge ratio (Sulzman, 2007).

Researchers measure the ratio of two stable isotopes and report the value relative to an international standard. The reporting convention for isotope values is to express the ratio as a delta value (δ) in units of per mil (‰). $\delta^{13}C$ is reported relative to the standard Pee Dee Belmnite (VPDB), a Cretaceous fossil (Equation 1.6; Brugnoli & Farquhar, 2000). The ^{13}C:^{12}C ratio of PDB is high relative to the natural range, and with the exception of carbonate rocks, most $\delta^{13}C$ values are negative (Falkowski & Raven, 2007).

$$\delta^{13}C = \frac{(^{13}C/^{12}C)_{sample}}{(^{13}C/^{12}C)_{standard}} - 1 \quad (1.6)$$

There are measurable differences in δ values across environmental pools. Both heavy and light isotopes are involved in physical, biological, and chemical processes, but they are transformed at different rates.

This phenomenon is an isotope effect (Brugnoli & Farquhar, 2000). If a reaction does not go to completion, one or more isotope effects cause one pool to contain more of the heavy isotope relative to the other. The isotopic fractionation factor, α, is the ratio of the heavy to light isotope ratio (R) for each pool (Equation 1.7; Farquhar et al., 1989). In the case of carbon, Equation 1.7 could represent a phase change between gaseous and dissolved CO_2, the conversion of dissolved CO_2 to HCO_3^-, or assimilation of dissolved CO_2 through photosynthetic fixation.

$$\alpha_{A/B} = \frac{R_A}{R_B} = \frac{1+\delta_A}{1+\delta_B} \quad (1.7)$$

α values tend to be very close to 1, so in this work I present them as a deviation from 1, ε, in units of per mil (‰; Equation 1.8; Farquhar & Richards, 1984).

$$\varepsilon_{A/B} = \alpha_{A/B} - 1 \quad (1.8)$$

There are two types of isotope effects that cause isotopic fractionation: equilibrium and kinetic isotope effects. Equilibrium isotope effects are temperature-dependent and occur during reversible reactions (Brugnoli & Farquhar, 2000). The substance with the higher oxidation state, molar mass, or density tends to be associated with a higher δ value in reactions at equilibrium, and ε increases with decreasing temperature. $^{13}CO_2$ is an exception to this pattern, as $\delta^{13}C\text{-}CO_{2(g)}$ is higher than $\delta^{13}C\text{-}CO_{2(aq)}$ in equilibrium with the atmosphere (Falkowski & Raven, 2007).

Kinetic isotope effects arise from reactions that occur in one direction, where a substrate is converted into a new product (Brugnoli & Farquhar, 2000). The δ value of the product tends to be lower, as lighter isotopes have a higher molecular collision frequency than their heavier counterparts and will react more quickly (Falkowski & Raven, 2007). Fixation of CO_2 by RuBisCO in phytoplankton cells is associated with a kinetic isotope effect of up to -28 ‰ (Sharkey & Berry, 1985).

Researchers commonly measure stable carbon isotopes of dissolved CO_2, DIC, DOC, CH_4, and particulate organic carbon (POC) in lakes to determine where the carbon originated, the fate of carbon in aquatic ecosystems, and how carbon moves through the aquatic food web. Predictable amounts of isotopic fractionation occur during reactions that transform carbon in aquatic ecosystems, and many of the sources and sinks of carbon have a distinct isotopic value that researchers can measure. From these measurements and known isotopic fractionation factors, researchers can infer the sources and transformations of carbon in an aquatic ecosystem.

1.4 IISD Experimental Lakes Area

I conducted my research at the International Institute for Sustainable Development Experimental Lakes Area (IISD-ELA) in northwestern Ontario, 90 km east of Kenora. This research station, comprised of 58 small boreal lakes and their watersheds, is "the world's freshwater laboratory". In the 1960s, concerns about freshwater pollution led to the Fisheries Research Board of Canada founding the Experimental Lakes Area (Schindler, 2009). Researchers perform physical and chemical manipulations on several small lakes to study whole-ecosystem responses to change, allowing for interactions that could not take place in a laboratory experiment. Other pristine lakes are monitored as part of a Long-Term Ecological Research program (LTER), which allows researchers to investigate how lakes are changing without direct human influence, and to compare the conditions in experimental lakes to a control lake.

History of Lake 227

Lake 227 (L227) is the site of the longest-running experiment at IISD-ELA. Since 1969, each week during the ice-free season researchers have added nutrients to the lake to promote the growth of phytoplankton. L227 was initially chosen for this experiment because its DIC concentration was very low, and researchers wanted to test whether phytoplankton blooms could grow with abundant access to N and P, but very little carbon (Schindler, 2012). The lake quickly became eutrophic, demonstrating that

the atmosphere provided sufficient CO_2 to allow for the excess growth of phytoplankton (Schindler et al., 1972).

The initial fertilization regime in L227 was a molar N:P ratio of 29:1, similar to loading in the Great Lakes. Researchers decreased the ratio in 1975 to 11:1, and from 1990 onwards they only added P (Hendzel et al., 1994). Reductions in N additions led to increases in N-fixing cyanobacteria, which now comprise the majority of the phytoplankton biomass (Schindler et al., 2008).

In addition to the eutrophication experiment, L227 has been the site of a food web manipulation study (Elser et al., 2000). Researchers added pike to the lake in 1993 to consume all other fish, and then fished out the pike in 1996. There have been no fish in L227 since the food web manipulation study.

After more than 50 years, L227 continues to be an important site for phytoplankton bloom research. Ongoing work includes studying the role of iron in bloom formation and phytoplankton community composition; the utility of floating wetlands for P removal; monitoring the response of phytoplankton to N removal; and continuing to study the impact of phytoplankton on the aquatic carbon, nitrogen, and phosphorus cycles.

Chapter 2: Site Description and Sample Analysis

L227 was the principle study site for the research presented in this thesis. There is a wealth of geochemical, meteorological, and limnological data available from IISD-ELA from a sampling regime that began in 1969. The University of Waterloo Environmental Geochemistry Lab (EGL) has supplemented this dataset with dissolved and particulate carbon isotope data since 2010. The sample collection and analysis techniques shared by the subsequent chapters are summarized in this section.

2.1 Site Description

L227 (49°42'N, 93°42'W) is a 5 ha, bowl-shaped boreal headwater lake with a maximum depth of 10 m (Figure A1). The lake is underlain by granitic bedrock and has no known groundwater inputs. Ephemeral streams can flow into the lake during snowmelt or following periods of prolonged rain, but otherwise hydrologic inputs come from rain and overland flow from the catchment. There is one outflow point on the north side of the lake that drains into a wetland.

Fertilization experiments

L227 has been the site of an on-going eutrophication experiment since 1969 (Schindler et al., 2008). Researchers fertilize the lake by adding nutrients to the epilimnion on a weekly basis from ice-off until fall turnover, increasing the total dissolved P concentration to approximately 6-10 µg L^{-1} during the ice-free season. Initially, researchers added N and P at a molar ratio of 29:1; this was decreased to 11:1 starting in 1975, and since 1990 L227 has been fertilized with P only (Hendzel et al., 1994). Researchers reduced N inputs in 1975 to test whether low N:P would favour N-fixing species of phytoplankton, and then ceased N fertilization in 1990 to test whether reducing N inputs to a lake is an effective strategy to control phytoplankton blooms (Higgins et al., 2018; Schindler et al., 2008).

The current fertilization regime promotes the growth of two annual phytoplankton blooms with predictable community compositions (Higgins et al., 2018). N-fixing cyanobacteria dominate the first

bloom, which tends to peak in the epilimnion and metalimnion in late June. Following the first bloom, phytoplankton biomass declines sharply at both depths, and the second bloom builds gradually from mid-July until mid-September. The phytoplankton density of the second bloom is lower than the first, and dominated by cyanobacteria and chlorophytes. L227 is an ideal site to study biogeochemical relationships under two different phytoplankton community compositions, but otherwise similar physical conditions and nutrient loads.

Ice dates and thermal stratification

IISD-ELA records ice-off and ice-on dates from Rawson Lake, a 54-hectare lake adjacent to the field station. Ice-off is the date when no significant ice remains on the lake, and ice-on is the date when Rawson Lake is approximately 80% covered by ice. Ice-off typically occurs between mid-April and early May, and the ice-free season typically lasts until early November. Smaller, shallower lakes nearby, such as L227, tend to have ice-off and ice-on dates approximately one week earlier than Rawson Lake.

Following ice-off, the surface of L227 warms quickly and the lake becomes thermally stratified by early- to mid-May. The thermocline, where the water temperature changes by more than 0.25 °C/0.25 m, marks the bottom of the epilimnion (Spence et al., 2018); for most of late spring and summer, the epilimnion depth is 0.5-1.5 m. The metalimnion starts below the epilimnion, and ends at the depth where 1 % surface PAR is reached, typically 3-4m (Sandilands, 2018). In early to late fall the surface of the lake cools, which leads to mixing. Since 2010, autumn mixing in L227 has typically begun between in early- to mid-September, but as late as early November.

2.2 Sample Collection

Researchers collected all samples relevant to this thesis from the L227 centre buoy (CB), a permanent buoy marking the deepest point in the lake. IISD-ELA collects depth-integrated samples from the epilimnion and metalimnion with an integrated sampling device. A standard L227 profile for most

geochemical parameters consists of integrated epilimnion and metalimnion samples, and discrete samples from 4, 6, 8 and 10 m depths. Instead of integrated epilimnion and metalimnion samples, I collected discrete samples for isotopic analysis from 1 m and 3 m depths, as well as the standard 4, 6, 8, and 10 m depths, with a gear pump and a weighted line of calibrated tubing. I flushed the tubing with lake water from the chosen depth and pumped water directly into sample bottles, then stored the samples on ice in the dark before bringing them back to the IISD-ELA field station for processing.

All researchers collected samples from L227 in mid-morning, between 08:00 and 11:00 CST. In productive lakes, where photosynthetic activity during the day causes diel cycles in various geochemical parameters, mid-morning samples do not represent the maximum or minimum values in a diel cycle (Dubois et al., 2009; Bogard & del Giorgio, 2016).

Historical geochemical data

IISD-ELA researchers have sampled L227 monthly or bi-weekly for a suite of physical and geochemical parameters during the ice-free season since 1969. Of particular relevance to this study are temperature, DIC, chlorophyll a (Chl a), and pH data. Schindler et al., 2008 and Stainton et al., 1977 have described detailed fertilization, sample collection and analysis methods.

Stable carbon isotopes

I collected samples for $\delta^{13}C$ analysis of DIC and POC weekly as water column profiles during the ice-free season in 2017 and 2018. Researchers from IISD-ELA and the EGL also collected these samples approximately monthly during the ice-free season from 2010-2016, collecting additional sporadic isotope samples in December and March of some years.

All researchers collected $\delta^{13}C$-DIC samples in duplicate in 60 mL glass serum bottles with no headspace, and we preserved each sample with at least 5 uL of 100% w/v $ZnCl_2$ solution per 1 mL of water. The University of Waterloo Environmental Isotope Lab (EIL) injected the samples with a helium headspace,

shook the samples for 90 minutes, and analysed the equilibrated gas for $\delta^{13}C$ by GC-CF-IRMS with an Agilent 6890 gas chromatograph coupled to a MicroGas-IsoPrime mass spectrometer (Agilent, Santa Clara, CA; Elementar UK Ltd., Manchester, UK) or MAT-253 gas isotope ratio mass spectrometer (Thermo Fisher Scientific, Waltham, MA).

All researchers collected 1L of water for $\delta^{13}C$-POC analysis and filtered it through a Whatman QM-A filter (Sigma-Aldrich, St. Louis, MI) using a vacuum pump at the IISD-ELA field station. We baked the QM-A filters at 550 °C prior to filtering to remove any organic material, and then dried the filters in a desiccator overnight after filtering. The EIL packed approximately 1/8 of each filter into an Elemental Microanalysis D1002 tin sample cup (Elemental Microanalysis Ltd., UK) and analysed the samples by EA-IRMS on a Carlo Erba 1108 EA coupled to a Delta^{PlusXL} continuous flow IRMS (Carlo Erba, Milan, Italy; Thermo Fisher Scientific, Waltham, MA). $\delta^{13}C$-DIC and $\delta^{13}C$-POC values are reported relative to VPBD with a precision of ± 0.2 ‰.

Instrumentation

I deployed a HOBO RX3000 weather station (Onset Computer Corp., Bourne, MA) with instruments at 1 m above the lake surface on a raft stationed several metres southeast of CB. The weather station recorded air temperature, pressure, relative humidity, PAR, and wind speed at 10-minute intervals from July-September 2018. IISD-ELA supplied additional local climate data, including temperature, windspeed at 10 m, air pressure, and relative humidity from the Rawson Lake meteorological station located 2 km west of L227 (Environment Canada Climate ID 6036904).

I deployed a YSI EXO2 sonde (YSI Inc., Yellow Springs, OH) at 1 m on CB from July-September in 2017 and 2018 and from May-October in 2019. Every 15 minutes the sonde recorded temperature, pH, specific conductivity, and concentrations of dissolved oxygen (DO), Chl a, and phycocyanin, a pigment indicating the presence of freshwater cyanobacteria (Kasinak et al., 2014). I collected weekly profiles of the same

parameters with it at 0.25-0.5 m intervals from surface to bottom. I also deployed a U26 HOBO logger (Onset Computer Corp., Bourne, MA) at 2.5 m on CB from June-September in 2018 and 2019. The logger recorded water temperature and DO concentration at 10-minute intervals in the metalimnion, where DO is supersaturated for most of the summer.

Chapter 3: Ecosystem respiration controls DIC return in a eutrophic boreal lake

3.1 Introduction

Lakes are widely recognized as significant sites of carbon processing, sequestration, and emissions in the global carbon cycle (Cole et al., 2007). Supersaturation of CO_2 in the majority of lakes causes global net CO_2 emissions of approximately 0.53 Pg C-CO_2 annually, a flux equivalent to 74% of the net annual anthropogenic greenhouse gas emissions of Canada (Environment and Climate Change Canada, 2019; Tranvik et al., 2009). Estimating the flux of CO_2 from lakes to the atmosphere requires a detailed understanding of aquatic carbon budgets: the balance of autochthonous and allochthonous carbon inputs to lakes and subsequent transport to the atmosphere, sediments, or downstream (Chapin et al., 2006).

Considerable work has been done to quantify the relative contributions of allochthonous and autochthonous carbon to aquatic food webs (Bade et al., 2004; Karlsson et al., 2007; Soloman et al., 2011). This is appropriate for oligotrophic lakes, where the dominant source of carbon can be the surrounding catchment (Wilkinson et al., 2013), but not for eutrophic lakes, where the high amount of phytoplankton biomass is more active in autochthonous production and cycling of DIC (Balmer & Downing, 2011; Pacheco et al., 2014). As climate change and nutrient pollution are projected to increase aquatic primary productivity (Paerl and Huisman, 2009), understanding the role of phytoplankton blooms in aquatic carbon budgets is necessary to estimate the global flux of CO_2 from lakes (DelSontro et al., 2018).

The aquatic carbon cycle is dynamic, and sources of DIC change on diel, seasonal, and decadal scales (Hanson et al., 2006). Gas exchange with atmospheric CO_2 and respiration by aquatic organisms and microbes are abundant sources of DIC to the epilimnion of stratified eutrophic lakes, with diffusion of DIC from the hypolimnion, DIC inputs from streamflow and groundwater, oxidation of methane from lake sediments, and photolysis of DOC serving as additional minor sources (Molot & Dillon, 1997;

Schindler & Fee, 1973; Whiticar, 1999). The relative contributions of atmospheric CO_2 and ER to the epilimnetic and metalimnetic DIC pools, where phytoplankton are most abundant, are the focus of this chapter.

Gas exchange is the dominant source of atmospheric CO_2 in natural waters with a pH below 8 (Stumm & Morgan, 1996; Wanninkhof, 1985). The rate of gas exchange is dependent on the CO_2 concentration gradient between the air and water, and a modelled temperature-dependent gas exchange coefficient, k_{CO2} (Raymond et al., 1997; Wanninkhof, 1993). Chemically enhanced diffusion (CED), an increase in the rate of CO_2 diffusion by the factor β, can occur in eutrophic lakes during periods of low wind and high pH as a result of the reaction between CO_2 and excess OH^- (Equation 3.1; Bade & Cole., 2006; Emerson, 1975). By transforming CO_2 into HCO_3^-, this reaction maintains a very high concentration gradient between atmospheric and dissolved CO_2.

$$CO_2 + OH^- \leftrightarrow HCO_3^- \quad (3.1)$$

ER in the water column encompasses CO_2 production by aquatic organisms in the surface mixed layer of a lake (Equation 3.2; Williams & del Giorgio, 2005; Woodwell & Whittaker, 1968). Researchers estimate ER in the water column and from sediments using bottle experiments with an added ^{14}C or ^{18}O tracer, whole-lake carbon budget analysis, or high-frequency DO or CO_2 measurements (Peeters et al., 2016). Bottle experiments with added ^{14}C do not capture high rates of primary productivity when samples are collected during periods of low DIC concentration (Schindler and Fee, 1973). Continuous DO measurements do not account for anaerobic processes such as fermentation that can contribute significantly to the CO_2 pool, leading to an over-estimation in carbon sequestration (Bogard and del Giorgio, 2016). Changes in dissolved CO_2 concentration can be easily measured with modern CO_2 probes (Peeters et al., 2016), however the sources of CO_2 are not evident from these measurements.

$$C_6H_{12}O_2 + 6O_2 \rightarrow 6CO_2 + 6H_2O \quad (3.2)$$

Carbon stable isotope values of DIC (δ^{13}C-DIC) reflect the relative contributions of dissolved CO_2 sources to a lake. δ^{13}C values of two major CO_2 sources, the atmosphere and ER, can be directly measured from air and particulate organic matter (POM), respectively. The chemical reactions involved in gas exchange, CED, and ER are associated with equilibrium and kinetic isotope effects that cause a known amount of isotopic fractionation, predictably changing the source δ^{13}C value. DIC in the water column is a mixture of CO_2 sources, and the δ^{13}C-DIC value reflects the relative contributions of each source. Because photosynthesis does not occur at night, the changes in δ^{13}C-DIC during the period between sunset to sunrise are indicative of the relative contributions of the major DIC sources to replenishing the DIC pool. Measuring δ^{13}C-DIC values between sunset and sunrise provides an opportunity to exploit diel changes in δ^{13}C-DIC to learn about the sources of DIC to the epilimnion and metalimnion.

There are very few studies that measure diel δ^{13}C-DIC values, likely due to the inconvenience of accessing field sites overnight or the assumption that diel variability is negligible. Studies investigating diel cycles in productive rivers found that δ^{13}C-DIC values decreased overnight and increased during the day by 1.5-5 ‰: variations that researchers attributed to biological processes rather than gas exchange of CO_2 (Parker et al., 2005; Gammons et al., 2011). In eutrophic Lake Taihu, researchers found that diel δ^{13}C-DIC variability was far greater than weekly variability (Van Dam et al., 2018). They attributed the fluctuations to isotope effects of GPP and ER, but they did not explore gas exchange as a cause of these changes despite high pH values. In oligotrophic and mesotrophic lakes in Quebec, Dubois et al. (2009) determined that groundwater anaerobic respiration of littoral sediments was a source of excess CO_2 that caused supersaturation. They analysed weekly early-morning DIC concentrations and δ^{13}C-DIC samples, and suggested that kinetic isotope fractionation during CO_2 degassing to the atmosphere led to higher δ^{13}C-DIC values. These studies demonstrate that there is variability in values of δ^{13}C-DIC on a diel timescale due to the different fractionation factors of multiple processes that increase or decrease [DIC]. Variability in δ^{13}C-DIC values on short timescales can provide insight into the sources of DIC to aquatic

systems, and how these sources set the measured value of δ^{13}C-DIC. In this chapter, I interpret overnight pH, [DIC], and δ^{13}C-DIC values in a eutrophic lake to (1) estimate the relative contributions of atmospheric and respired carbon to determine what sets the morning δ^{13}C-DIC value of this lake, and to (2) evaluate if those estimates agree with existing techniques to model DIC inputs to lakes.

3.2 Materials and Methods

See Chapter 2 for a detailed description of the field site, sampling regime, and analysis techniques.

Overnight sampling

To measure δ^{13}C-DIC values and assess the sources of DIC without the influence of photosynthesis, I collected samples at night from L227 on three occasions: July 10-11, 2018, September 5-6, 2018, and June 26-27, 2019. These dates reflect overnight conditions in the epilimnion during one period of biomass decline, and two periods of high biomass with different phytoplankton community compositions, respectively. In June and July the phytoplankton community was dominated by cyanobacteria, and in September the community was composed of a more diverse group of phytoplankton, including cyanobacteria and chlorophytes.

During each sampling event I measured temperature, pH, and concentrations of DO, Chl a, and phycocyanin with a YSI EXO2 sonde, and I collected samples for analysis of DIC concentration and δ^{13}C-DIC. I collected all measurements and samples hourly from CB between sunset and sunrise, from both 1 m and 3 m depths to target high biomass zones in the epilimnion and metalimnion. To allow for immediate δ^{13}C-DIC sample preservation, I collected all samples manually as described in Chapter 2 from a boat stationed at CB. While in the field I stored the samples on ice in the dark, and upon return to the field station I transferred the samples into a refrigerator until analysis.

3.3 Calculations and Modelling

CO_2 flux and chemical enhancement

For all calculations I set the concentration of CO_2 in the atmosphere to 410 ppm, the average concentration at the Mauna Loa Observatory for May-September in 2018 and 2019 (Tans & Keeling, 2020). I modeled the hourly rate of diffusive flux (F) of atmospheric CO_2 to L227 with Fick's law (Equation3.3). I calculated the equilibrium concentration of CO_2 from the temperature-dependent Henry constant, k_H (Sander, 2015), and measured values of air pressure; and the concentration of aqueous CO_2 from pH, [DIC], and temperature-dependent dissociation constants (Harned & Davies, 1943; Harned & Scholes, 1941). To calculate gas exchange (k_{600}) and the gas- and temperature-specific transfer velocity (k_{CO2}) I used the *k.cole* and *k600.2.kGAS* functions of *LakeMetabolizer* version 1.5.0 in R version 3.6.1 (R Core Team, 2019; Winslow et al., 2016) with 10 m wind speed data from the IISD-ELA meteorological station 2 km west of L227.

$$F = k_{CO_2}\beta\left(CO_{2_{aq}} - k_H \times pCO_2\right) \tag{3.3}$$

The chemical enhancement factor, β, in Equation 3.3 is the additional flux due to chemical enhancement: the reaction between CO_2 and OH^- (Equation 3.4; Bade & Cole, 2006). If no chemical enhancement occurs, $\beta = 1$ and all flux is attributed to atmospheric exchange. Under high-pH and low-wind conditions $\beta > 1$, increasing F by a factor of β. Values of β vary with pH, water temperature, and wind speed, but for summer bloom conditions at L227 (water temperature 20-23 °C, pH up to 9.7, low wind) the anticipated range of β is 1-4 (Bade & Cole, 2006).

I calculated β from values of wind speed at 10 m and water temperature and pH at a depth of 1 m following the method of Hoover and Berkshire (1969) as presented by Bade and Cole (2006). The authors calculated diffusivity (D) according to Jähne et al. (1987); defined the boundary layer (z) as D/k_{CO2} (Lewis and Whitman, 1924); and defined τ with dissociation constants for $CO_2 \rightarrow {HCO_3}^-$ and

$HCO_3^- \rightarrow CO_3^{2-}$ by Harned and Davis (1943) and Harned and Scholes (1941), respectively. Following Bade and Cole (2006), I defined <*r*> as the combined rate of the reactions $CO_2 + H_2O \rightarrow H_2CO_3$ and $CO_2 + OH^- \rightarrow HCO_3^-$ with rate constants from Wang et al. (2010) that I corrected for temperature with the Eyring equation.

$$\beta = \frac{\tau}{(\tau-1)+\{tanh[(\langle r\rangle \tau D^{-1})^{1/2} z]/[(\langle r\rangle \tau D^{-1})^{1/2} z]\}} \quad (3.4)$$

Lake metabolism

I calculated rates of GPP, NEP, and ER in R (R Core Team, 2019) as mg O_2 L^{-1} d^{-1} using the *metab.kal* function in the *LakeMetabolizer* package (Winslow et al., 2016). I used 10 m wind speed data from the IISD-ELA meteorological station; the *k600.col* and *k600.2.kgas.base* functions to calculate the gas transfer coefficient (k) for O_2; and the *o2.at.sat.base* function and measured water temperature data to calculate the equilibrium DO concentration. Instead of using the *ts.meta.depths* function to estimate z, the bottom of the epilimnion, I applied the IISD-ELA definition of the bottom of the epilimnion: a change in temperature of more than 0.25 °C over 0.25 m (Spence et al., 2018).

Unit conversion

The values I calculated from Fick's law have units of mmol CO_2 m^{-2} h^{-1}, and the values I modelled with *LakeMetabolizer* have units of mg O_2 L^{-1} d^{-1}. To compare flux and ER values, I converted both into units of µmol CO_2 L^{-1} d^{-1}. To convert the rate of atmospheric CO_2 flux I divided the hourly rates by z, the bottom of the epilimnion, and summed the hourly rates for each day. I converted ER values from their original units to µmol O_2 L^{-1} d^{-1}, then multiplied the molar value by a respiratory quotient of 0.81 mol CO_2 produced/mol O_2 consumed. This respiratory quotient is suitable for freshwater phytoplankton in net autotrophic lakes (Berggren et al., 2012; see also Williams & del Giorgio, 2005).

Isotope end-member values

I calculated the $\delta^{13}C$ values of three DIC sources to L227: atmospheric gas exchange, CED, and ER. The amount of isotope fractionation during each process varies (Table 3.1). To calculate the $\delta^{13}C$ value of DIC originating from atmospheric CO_2, I added the values of equilibrium and kinetic isotope fractionation during the dissolution of CO_2 to the atmospheric $\delta^{13}C$-CO_2 value, then accounted for the equilibrium isotope effects of redistribution among the three carbonate species at the measured temperature and pH (Bade et al., 2004; Mook et al., 1974; Zhang et al., 1995). The $\delta^{13}C$ value of atmospheric CO_2 is approximately -8.5 ‰ (Morales-Williams et al., 2020; Scripps CO_2 Program, 2020), and passive diffusion of gaseous CO_2 across the lake surface causes combined kinetic and equilibrium isotopic fractionation of approximately -2 ‰, depending on the water temperature (Zhang et al., 1995). The $\delta^{13}C$ value of dissolved CO_2 originating from the atmosphere was therefore approximately -10.5 ‰. At a pH of 7-9.5 and a lake temperature of 20 °C, most of the dissolved CO_2 becomes HCO_3^-, increasing the value of $\delta^{13}C$-DIC.

When pH is higher than approximately 8, CED causes isotope fractionation between $CO_{2(aq)}$ and HCO_3^- in the reaction $CO_2 + OH^- \rightarrow HCO_3^-$ (Emerson, 1975; Herzceg, 1987). Researchers typically cite -15 ‰ as the value of kinetic isotopic fractionation during CED (Bade and Cole, 2006; Bontes et al., 2006; Lammers et al., 2017). Bade and Cole (2006) presented an alternate approach for modelling chemically enhanced fractionation (CEF), where β^{13} is the enhancement factor for the diffusion of $^{13}CO_2$ (Equation 3.5). I calculated β^{13} by multiplying the parameters in Equation 3.4 by relevant equilibrium and kinetic isotope fractionation factors given by Zhang et al. (1995) and described by Bade and Cole (2006). CEF is calculated as an isotopic fractionation factor (refer to the calculation of ε, Equation 1.5): the sum of CEF and the $\delta^{13}C$ value of dissolved CO_2 originating from the atmosphere is equal to the value of $\delta^{13}C$-HCO_3^- originating from CED. Because DIC is predominantly HCO_3^- when CED occurs, the $\delta^{13}C$-HCO_3^- value is the

end-member value for DIC originating form CED. pH, temperature, and wind speed affect the magnitude of CEF (Figure A2).

$$CEF = [(\beta^{13}/\beta) - 1] \quad (3.5)$$

I set the endmember for ER as the δ^{13}C-POC value on the day of sampling. In a eutrophic lake such as L227, where the majority of particles are phytoplankton, the δ^{13}C-POC value reflects the δ^{13}C value of phytoplankton (Higgins et al., 2018). ER is associated with very little isotopic fractionation of carbon, causing the production of DIC with a δ^{13}C value close to that of the POC (Finlay, 2003; Venkiteswaran et al., 2013).

Table 3.1: Summary of the values of isotope fractionation ($\varepsilon_{A/B}$) between two pools of carbon, A and B, for three processes contributing dissolved inorganic carbon (DIC) to L227: gas exchange, chemically enhanced diffusion, and respiration. Values for $\varepsilon_{A/B}$ during gas exchange are for 21 °C as listed in Table 1 in Zhang et al., 1995. I calculated the values of chemically enhanced fractionation as outlined in Bade and Cole, 2006: -12.2 ‰ is the lowest value given the maximum pH and water temperatures and minimum wind speed for L227.

Process	**Type of isotope fractionation**	**A**	**B**	**Isotope fractionation ($\varepsilon_{A/B}$)**
Gas exchange	Equilibrium	Atmospheric CO_2	Dissolved CO_2	-1.1 ‰
	Kinetic			-1.0 ‰
Chemically enhanced diffusion	Kinetic (chemically enhanced fractionation)	Dissolved CO_2	HCO_3^-	0 ‰ to -12.2 ‰
Respiration	N/A	Phytoplankton	DIC	0 ‰

3.4 Results

Three overnight sampling events represented overnight geochemical changes that can occur during three stages of the annual phytoplankton blooms in L227 (Figure 3.1; vertical dashed lines highlight the overnight sampling events in figures throughout). I postponed the first planned sampling event in late June 2018 due to heavy rain, and instead sampled during the cyanobacteria-dominated bloom on June 26-27, 2019. Although the June 2019 sampling event is a proxy for the same period in June 2018, Chl a in the epilimnion was lower during the June 2019 sampling event than it was the previous year (Figure A3). The concentration of phycocyanin in the epilimnion was similar for the same period in both years (not shown). The second event, July 10-11, 2018, occurred when phytoplankton biomass was declining after the first seasonal cyanobacteria bloom. The last event, September 5-6, 2018, occurred during the sustained high-biomass period toward the end of the summer.

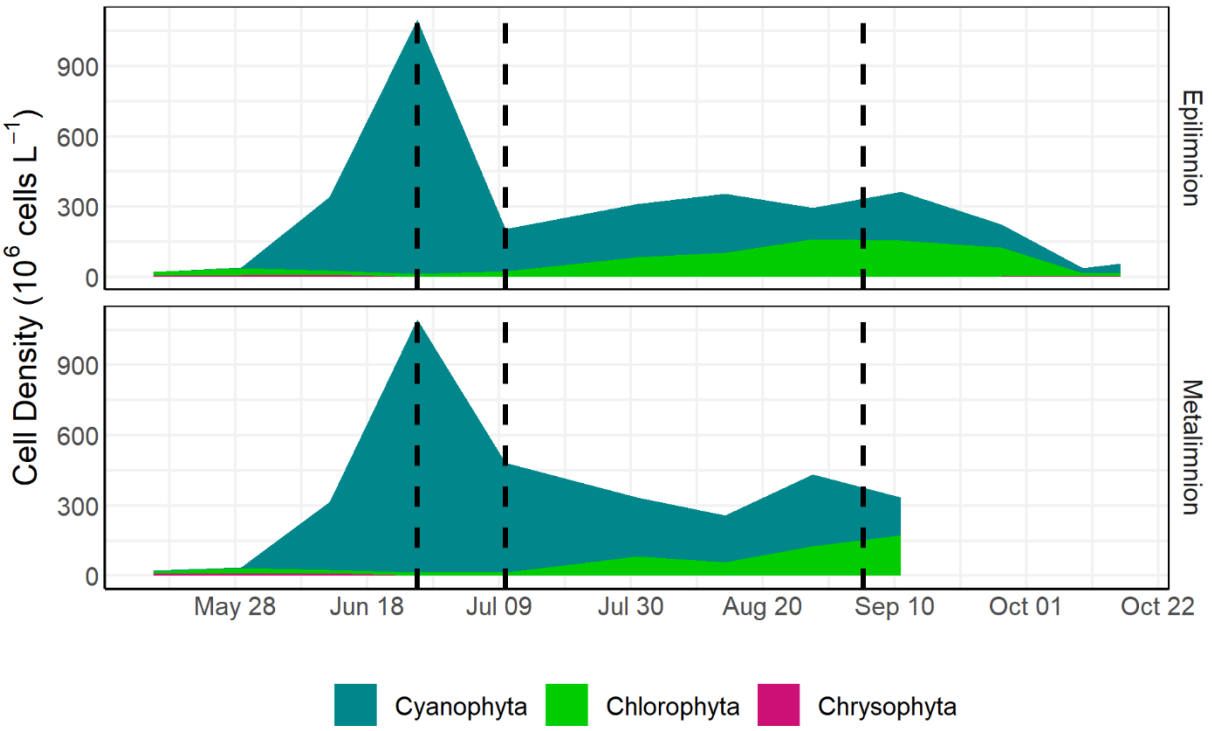

Figure 3.1: Phytoplankton cell density by phylum in L227 during the 2018 ice-free season. Dashed lines mark overnight sampling events. Note that the June sampling event took place in 2019 under similar conditions.

Lake profiles during diel sampling events

The thermal, chemical, and biological structure of L227 differed between the three sampling events (Figure 3.2). The lake was thermally stratified for each sampling event, with a well-mixed epilimnion, and peaks in pH, DO, and pigments indicating biomass (Chl a and phycocyanin) at or near the thermocline.

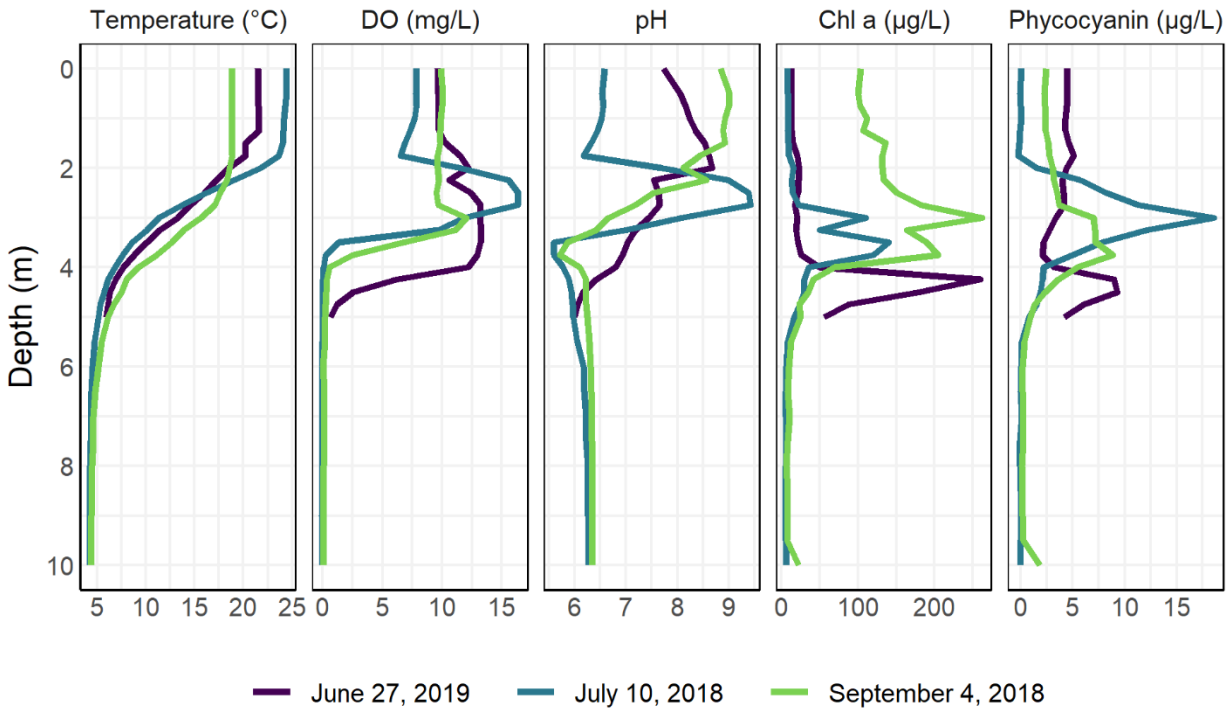

Figure 3.2: Summary of daytime temperature, dissolved oxygen, pH, Chl a, and phycocyanin values in L227 prior to or during the overnight sampling events. I measured all values from the centre buoy with a YSI EXO2 sonde.

The concentration of phycocyanin was highest at 1 m during the June 2019 sampling event, and highest at 3 m during the July 2018 sampling event. The July diel sampling event followed a decline in 1 m phycocyanin and Chl a concentration (Figures A3 and A4), and a decline in phytoplankton cell density in the epilimnion and metalimnion (Figure 3.1). The peak in cyanobacteria shifted down in the water column to a depth of 3-3.5 m, where the phycocyanin concentration increased for several weeks before reaching a peak in mid-July (Figure A4). The concentration of biomass at 3 m continued to exceed biomass at 1 m until the end of August 2018.

The concentration of Chl a at 1 m was highest during the September 2018 sampling event, when a greater proportion of chlorophytes were present in the epilimnion. Like phycocyanin, Chl a was lowest in the epilimnion during the July sampling event. For both July and September, Chl a was higher at 3 m than it was in the epilimnion.

Overnight trends in pH, [DIC], and δ^{13}C-DIC

The daytime profiles of L227 did not reflect the conditions of the lake during a 24-hour period (Figure 3.3). There was diel variation in pH, [DIC], and δ^{13}C-DIC throughout the summer, but the overnight trend in each parameter was not consistent across the three sampling events.

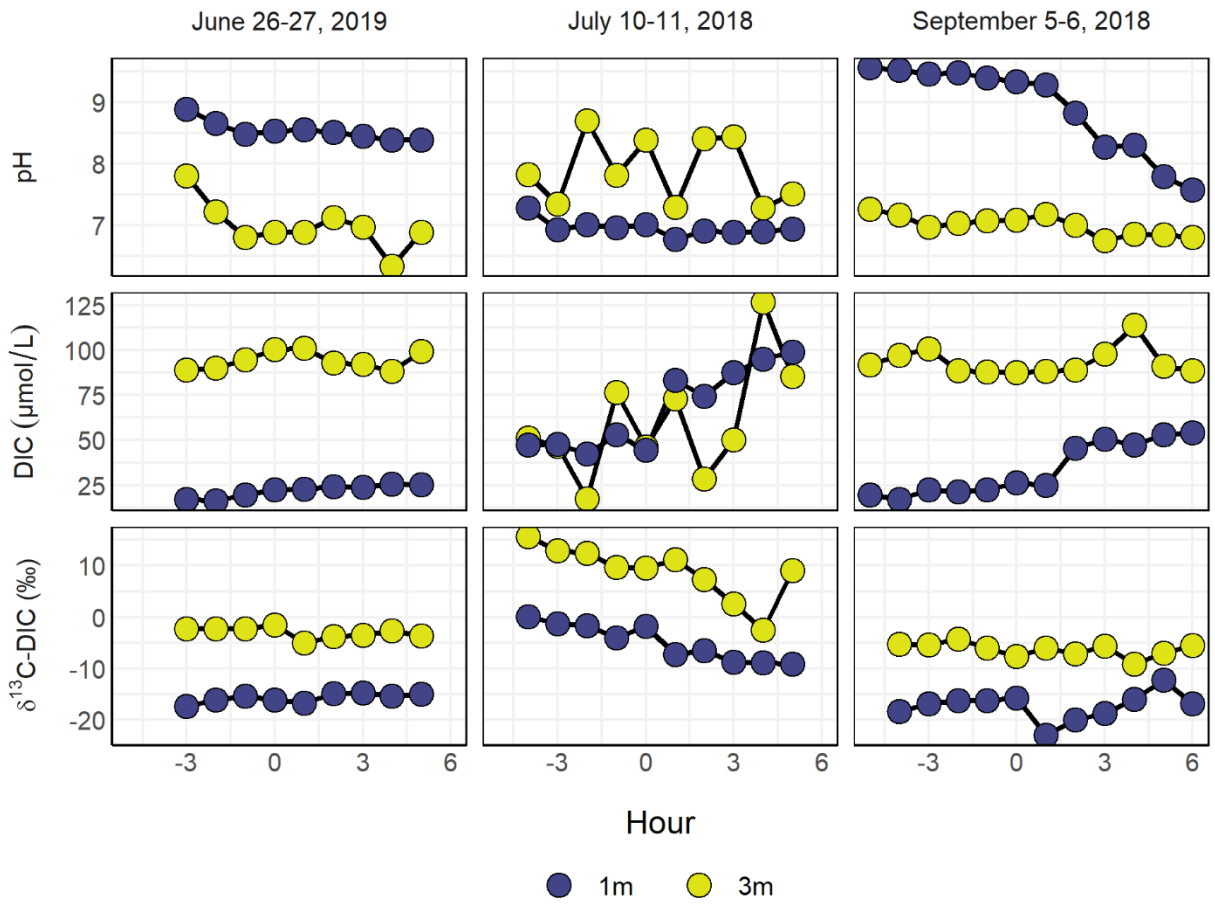

Figure 3.3: Summary of overnight pH, DIC concentration and δ^{13}C-DIC values in L227 during three half-diel sampling events. Hour 0 is midnight CST.

The magnitude of pH change over a 24-hour cycle varied on a daily timescale (Figures A5 and A6). pH at 1 m was relatively stable overnight during the June and July sampling events, decreasing by < 0.5 pH units between sunset and sunrise. The average overnight pH was 8.5 for the June event and 7.0 in July, a difference that affected the distribution of carbonate species. Less than 1% of the DIC pool was CO_2 at sunrise in June, while 18% of the DIC pool was CO_2 at sunrise in July. During the September sampling event pH decreased from 9.5 to 7.5 overnight, causing the proportion of dissolved CO_2 in the DIC pool to increase from < 1% at sunset to 6.6% by sunrise.

The DIC concentration increased overnight at 1 m during all diel sampling events. Unlike the observations of Schindler and Fee (1973), who measured consistent overnight increases in [DIC] of approximately 35-40 µmol L^{-1} in L227 over two months, the magnitude of [DIC] increase at 1 m was variable during our 2018 and 2019 diel sampling events. The DIC concentration was highest and increased the most, from 50 µmol L^{-1} to 100 µmol L^{-1}, during the lower epilimnetic biomass period in July. During the higher biomass periods in June and September, [DIC] was < 20 µmol L^{-1} in the evening and increased to 25 µmol L^{-1} and 54 µmol L^{-1}, respectively, by sunrise (Figure 3.3). There was a negative linear relationship between [DIC] and pH measurements at 1 m during the higher epilimnetic biomass sampling events only (June $r^2 = 0.62$ and September $r^2 = 0.91$; $p < 0.05$).

Both pH and [DIC] remained relatively stable at 3 m in June and September, with similar values during each sampling event: average overnight [DIC] was 94 µmol L^{-1} and pH was approximately 7. In July, when biomass at 3 m was highest, pH and [DIC] were highly variable overnight. Although the values did not steadily increase or decrease overnight, there was a negative linear relationship between [DIC] and pH at 3 m during the July sampling event only ($r^2 = 0.50$, $p < 0.05$).

Trends in δ^{13}C-DIC tended to mirror those in [DIC]. As [DIC] increased overnight during the July sampling event at 1 m and 3 m, δ^{13}C-DIC decreased. In June at 1 m and 3 m and in September at 3 m, when [DIC]

was relatively constant overnight, there was also very little overnight change in the δ^{13}C-DIC values (Figures 3.3, 3.4, A7). The exception to this trend was at 1 m during the September sampling event; prior to 01:00, [DIC] and δ^{13}C-DIC remained relatively constant, but as [DIC] increased after 01:00, δ^{13}C-DIC increased.

δ^{13}C-DIC values were lower at 1 m than at 3 m for each sampling event. The highest values of δ^{13}C-DIC for both depths and the greatest magnitude of overnight change in δ^{13}C-DIC occurred during the July sampling event. During the two blooms, δ^{13}C-DIC was relatively constant overnight at both depths.

Overnight δ^{13}C-DIC values in relation to end-member δ^{13}C-DIC values

For the range of pH values during the three overnight sampling events and a water temperature of 20 °C, the range of isotope end-member values for DIC originating from gas exchange was -1.9 ‰ to +0.7 ‰. The range of δ^{13}C values for DIC originating from CED at a water temperature of 20 °C and wind speed of 0.17 m/s, the lowest wind speed at 10 m above the lake surface, was -10.5 ‰ to -22.6 ‰ (Figure 3.4). The ER end-member values at 1m were -22.2 ‰ and -24.2 ‰ during the overnight sampling events in June and September, respectively, and -27.7 ‰ during the July overnight sampling event. The 3 m δ^{13}C-POC values were lower than the corresponding 1 m values by -2.5 ‰ to -7.1 ‰ (Figure A7).

The 1 m δ^{13}C-DIC values at 1m fell within the end-member values for gas exchange and ER (Figure 3.4). In June and September, the 1 m δ^{13}C-DIC values also fell between the ER and CED end-members. The δ^{13}C-DIC values were highest in the evening during the July sampling event, reaching equilibrium with atmospheric δ^{13}C-CO_2 values. During the July and September sampling events, the measured δ^{13}C-DIC values were much closer to the values of δ^{13}C-DIC respired by phytoplankton or δ^{13}C-DIC originating from CED. Most of the δ^{13}C-DIC values were 15-20 ‰ lower than the gas exchange end-member values.

The 3 m δ^{13}C-DIC values for all three sampling events were higher than the ER end-members by 18-46 ‰ (Figure A7). While the ER end-member was relatively consistent between sampling events, δ^{13}C-DIC was

much higher during the July 2018 sampling event, when biomass and pH were highest. Refer to Chapter 4 for additional results pertaining to isotopic fractionation between DIC and POC in L227.

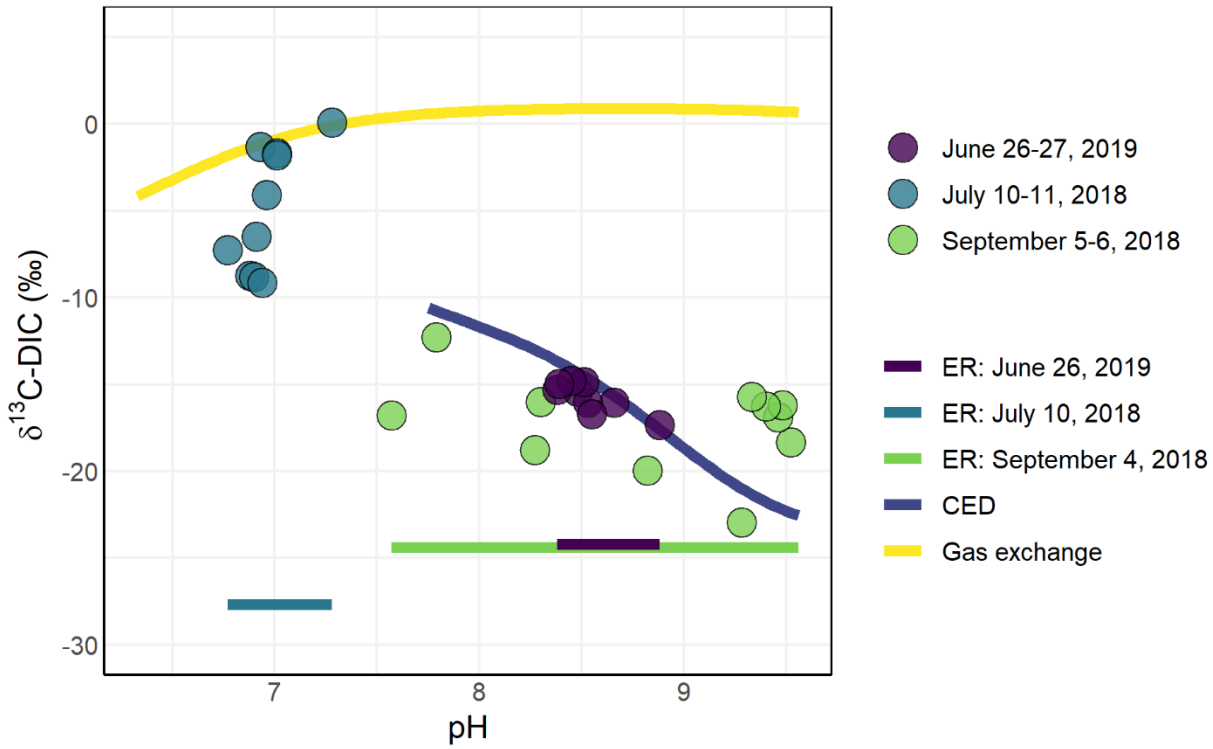

Figure 3.4: Summary of overnight δ^{13}C-DIC and pH values from 1 m at the L227 centre buoy (points), and δ^{13}C-DIC end-member values for atmospheric gas exchange, chemically enhanced diffusion (CED), and ecosystem respiration (ER). Refer to the text for descriptions of calculations to determine end-member values.

L227 as a CO_2 source and sink

L227 was a sink of atmospheric CO_2 during the overnight sampling events in June and September, and changed from a sink to a source of atmospheric CO_2 during the overnight sampling event in July (Figure 3.5). The hourly rate of CO_2 flux into L227 was highest during the June and September sampling events, but decreased between sunset and sunrise during all three sampling events. The flux of CO_2 into the lake decreased overnight as [CO_2] increased and approached equilibrium with the atmosphere.

The concentration of dissolved CO_2 was closest to equilibrium with the atmosphere during the July overnight sampling event, when the concentration of phytoplankton in the epilimnion was declining.

Before midnight the average flux was 0.1 mmol m^{-2} h^{-1} and the lake acted as a CO_2 sink. After midnight the lake began emitting CO_2, and the average flux was -0.2 mmol m^{-2} h^{-1}. DIC in the epilimnion increased by 3.32 mol between sunset and sunrise, but net DIC emissions from the epilimnion were 0.02 mol.

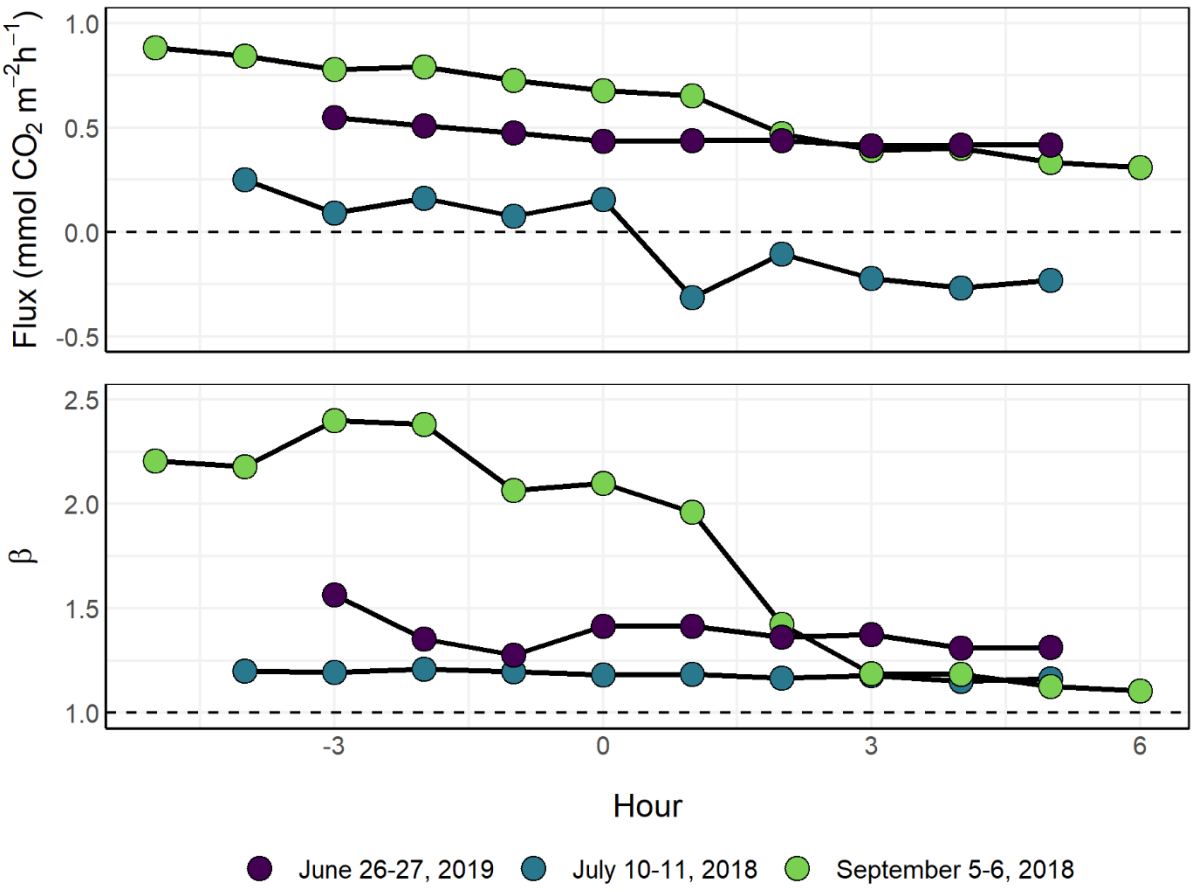

Figure 3.5: Overnight values of *β* (the chemical enhancement factor) and atmospheric CO_2 flux in the surface of L227 during three diel sampling events. Positive values indicate a flux of CO_2 into the lake from the atmosphere. Hour 0 is midnight CST.

During the higher-biomass sampling events, [CO_2] was consistently below equilibrium with the atmosphere. pH and [DIC] were relatively constant overnight during the June sampling event, causing the gradient between surface water and atmospheric CO_2 to also remain relatively constant; CO_2 flux into the lake was approximately 0.5 mmol m^{-2} h^{-1} all night (Figure 3.5). Total DIC in the epilimnion increased by 0.45 mol between sunset and sunrise, and based on the hourly rate of flux, gas exchange

accounted for 40% of this increase. In September, as [DIC] increased and pH decreased overnight, the flux of atmospheric CO_2 decreased from 0.9 mmol m^{-2} h^{-1} to 0.3 mmol m^{-2} h^{-1} (Figure 3.5). DIC in the epilimnion increased by 2.54 mol between sunset and sunrise, and gas exchange accounted for 12% of the increase.

The hourly rates of gas exchange overnight were not equal to the mid-morning rate of gas exchange based on the 09:00 value of [DIC] and pH. Calculating the average daily rate of atmospheric CO_2 flux into L227 based on the average overnight rate of flux and the hourly flux at 09:00 CST gave different results (Table 3.2). For the June and July sampling events, the daily rates I calculated from the 09:00 sampling event were greater than the rates based on hourly sampling points at night.

Table 3.2: Summary of average daily flux of CO_2 from the surface of L227 reported in units of mmol m^{-2} d^{-1} and µmol L^{-1} d^{-1}. The average daily flux is calculated using two methods: the average of all overnight flux measurements (*n* = 10-12), and from a single measurement at 09:00 CST. Flux values are based on the depth of the bottom of the epilimnion: 1.25 m on June 26, 2019; 1.5 m on July 10, 2018, and 1.75 m on September 5, 2018.

Sampling Event	Daily rate of atmospheric CO_2 flux			
	Average overnight hourly flux		Hourly flux at 09:00 CST	
	mmol m^{-2} d^{-1}	µmol L^{-1} d^{-1}	mmol m^{-2} d^{-1}	µmol L^{-1} d^{-1}
June	10.9	8.7	17.4	14.0
July	-0.97	-0.65	-13.0	-8.7
September	13.9	8.0	14.6	8.3

The overnight sampling events were the only occasions I collected DIC samples at a high temporal resolution. However, assuming a relatively constant alkalinity, I calculated CO_2 concentration at 1 m from continuous 2018 pH data (Figure A8). Alkalinity in the epilimnion of L227 was 76-137 µeq L^{-1} during the ice-free season in 2018 (not shown). From late July until mid-September, [CO_2] followed a daily pattern: the highest [CO_2] value occurred between 05:00 and 10:00, and the lowest [CO_2] value occurred between 15:00 and 20:00. The concentration of CO_2 was often below equilibrium with the atmosphere for the whole day, at times approaching 0 µmol L^{-1}, and the daily rate of CO_2 flux into L227 was 8.8-22 mmol m^{-2} d^{-1} (5.8-13.2 µmol L^{-1} d^{-1}; Figure A9). Even the highest daily rates of atmospheric invasion that I calculated during the blooms were lower than the rates Schindler and Fee (1973) calculated during their

diel studies of L227: between 24-60 mmol m^{-2} d^{-1}. Near the beginning and end of the second bloom, [CO_2] approached or exceeded equilibrium in the morning only. By the end of September, [CO_2] in L227 was consistently greater than the atmosphere, and the lake served as a source of CO_2 to the atmosphere.

Chemical enhancement in L227

CED, which increases the rate of CO_2 flux into a lake when pH is high (Equation 3.3), occurred to some degree while L227 was thermally stratified: the CED model rarely predicted a β value of 1 (Figure A6). β is sensitive to changes in pH, and therefore shifted throughout the day as pH increased or decreased. When pH was 7.0-8.5 during the June and July sampling events, β was consistently 1.2-1.5. During the September sampling event, when pH was 7.5-9.5, β decreased from 2.2 to 1.2 as pH declined overnight (Figure 3.5). There was very low to no wind during each sampling event, which allowed for a thicker boundary layer, but the pH conditions were only high enough for chemical enhancement > 1.5 from 21:00 on September 5 until 01:00 on September 6. As pH declined overnight, so did β and the rate of atmospheric CO_2 flux into the lake.

The average wind speed at 1 m above the surface of L227 was typically between 0.5 and 1.5 m/s in 2018, with overnight wind speeds generally lower than during the day. The daily maximum pH was always > 9.4 during the phytoplankton blooms, but the daily minimum pH varied by up to 2.5 pH units, 6.7-9.2 (Figure A5). Daily periods of high pH allowed for the conditions promoting CED to occur during the afternoon and evening when pH was highest, potentially increasing the flux of CO_2 for several hours. The range of possible β values between late July and early September 2018 was 1-2.9 (Figure A6). pH, and therefore β values, were highest during the blooms in the late afternoon and overnight.

Primary productivity and ecosystem respiration

Biological activity in L227 contributed DIC at a higher rate than gas exchange. Daily rates of GPP and ER in L227 during the ice-free season in 2018 and 2019 ranged from 18-228 µmol O_2 L^{-1} d^{-1} and 6-163 µmol CO_2 L^{-1} d^{-1}, respectively (Figures A9, A10), while the daily rates of gas exchange with the atmosphere were 5.8-13.2 µmol CO_2 L^{-1} d^{-1} (Figure A9). These values of ER are comparable to measurements researchers have previously made in L227: 2.4-122 µmol DIC L^{-1} d^{-1} (Schindler & Fee, 1973). GPP tended to be higher than ER in 2018: daily rates of NEP were 0-31 µmol O_2 L^{-1} d^{-1}. L227 was net autotrophic, as the phytoplankton consumed more CO_2 than the ecosystem respired. In 2019, L227 was net autotrophic during the cyanobacteria-dominated bloom, but a second bloom did not occur; the lake was predominantly net heterotrophic following the decline of phytoplankton in the epilimnion. Daily rates of NEP were between 101.5 and -155.8 µmol O_2 L^{-1} d^{-1} (Figure A10).

Based on the rates of ER that *LakeMetabolizer* generated for the June 2019 and September 2018 overnight sampling events, the majority of DIC added to the epilimnion of L227 between sunset and sunrise originated from ER. The rates of ER during the blooms were 13 µmol CO_2 L^{-1} d^{-1} on June 27, 2019, and 53.1 µmol CO_2 L^{-1} d^{-1} on September 6, 2018. ER generated 53% of the DIC increase overnight during the June sampling event, and 70% of the DIC increase during the September sampling event. No ER rate is available for the July 2018 overnight sampling event.

GPP and ER were linearly positively related both years for the time periods displayed in Figure 3.6 (r^2 = 0.75, r^2 = 0.87, respectively; $p << 0.05$). The ranges of GPP and ER were smaller during the cyanobacteria and chlorophyte-dominated bloom in August 2018 than during the cyanobacteria-dominated bloom in June 2019. The concentration of biomass as phycocyanin was lower during the August 2018 bloom than the June 2019 bloom, and more evenly distributed over the range of GPP and ER values. During the June 2019 bloom, the concentration of phycocyanin was highest at relatively lower rates of GPP and ER.

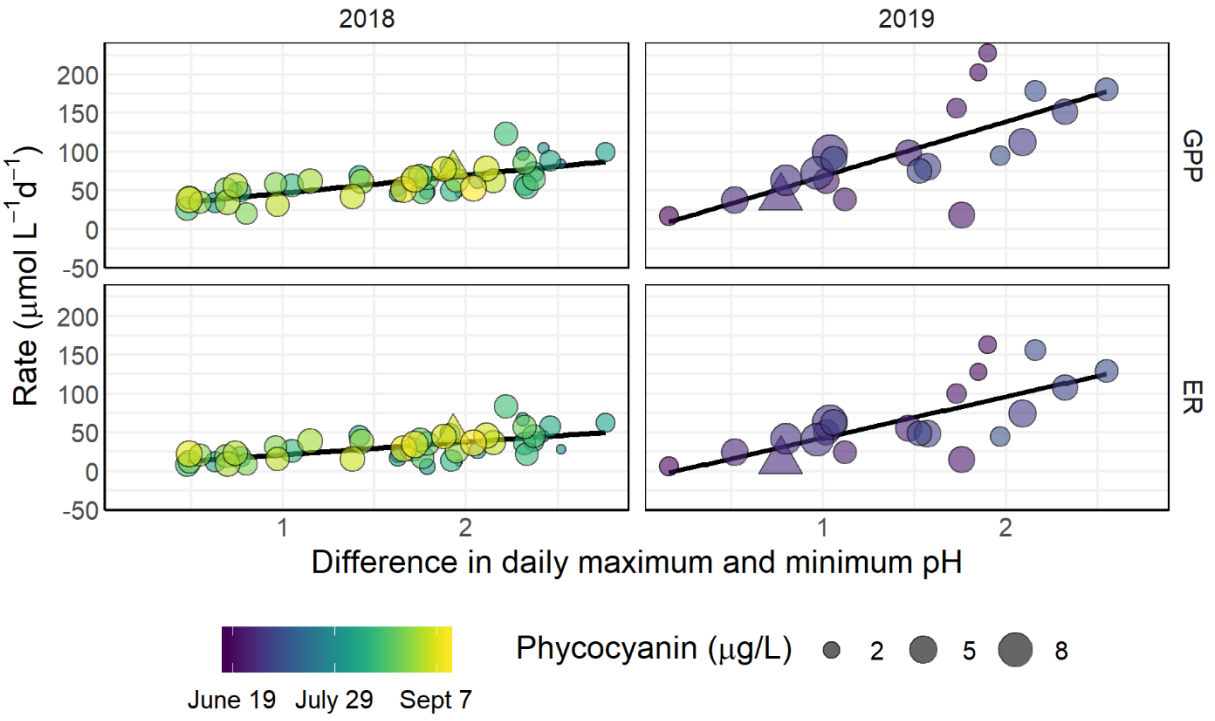

Figure 3.6: The relationship between gross primary productivity (GPP), ecosystem respiration (ER), and daily pH change (r^2 values range from 0.39-0.52, $p << 0.01$). Values of GPP are in µmol O_2 L^{-1} d^{-1}, and values of ER are in µmol CO_2 L^{-1} d^{-1}. The two triangles represent the September 6, 2018 and June 27, 2019 values (no productivity data is available for the July sampling event), and the size of the points reflects the daily maximum concentration of phycocyanin. The 2019 values span June 15-July 7, and the 2018 values span July 26-September 11. Only a single cyanobacteria-dominated bloom occurred in 2019, and a sensor malfunction prevented data recording prior to July 26, 2018.

The daily rates of GPP and ER were linearly related to the net daily pH change (Figure 3.6). Daytime pH was 8-9.5 throughout the epilimnion and metalimnion during periods of higher biomass, and 6-7 during periods of lower biomass (Figure A4). Maximum daily pH at 1 m was typically highest in the evening before sundown, reaching 9.5 during the blooms in August 2018 and June 2019, and decreased overnight by 0.5-2.5 pH units (Figure A5). The minimum daily pH occurred between 05:00 and 07:00 each day. There was no relationship between the daily change in pH and the daily rate of GPP or ER on the previous or subsequent day.

3.5 Discussion

Ecosystem respiration controls DIC recharge and sets the morning δ^{13}C-DIC value during phytoplankton blooms in the epilimnion

I chose the timing of the diel sampling events to capture the geochemical conditions in L227 during three different stages of the epilimnetic phytoplankton blooms: a cyanobacteria-dominated bloom in early summer, a mid-summer decline in epilimnetic biomass, and a late-summer bloom dominated by cyanobacteria and chlorophytes (Figure 3.1). However, the high-frequency pH measurements revealed that the geochemical conditions during any one of these stages were not consistent from day to day (Figure A5). I captured three distinct combinations of overnight pH and DIC conditions in the epilimnion instead: a strong decline in pH with a moderate [DIC] increase (September 2018); steady, moderate pH with very little [DIC] increase (June 2019); and steady, low pH with a relatively high[DIC] increase (July 2018). Similar geochemical conditions can arise in the epilimnion throughout the ice-free season while the lake is thermally stratified.

The pH value was an indicator of a [DIC] increase in L227. At a constant alkalinity, an increase in [DIC] causes pH to decline (Figure 1.3). According to Le Chatelier's principle, an increase of CO_2 on the left side of the reaction $CO_2 + H_2O \leftrightarrow HCO_3^- + H^+$ leads to an increase in H^+ on the right side, and therefore a decline in pH. At night, when there is no removal of DIC by primary productivity, CO_2 increases and pH decreases. High rates of CO_2 return should lead the pH to drop overnight, while low rates of CO_2 return would leave the pH value high. The role of GPP and ER in depleting and replenishing the DIC pool has been noted in eutrophic lakes (Balmer & Downing, 2011; Van Dam et al., 2018; Wang et al., 2016), heterotrophic lakes (Bade et al., 2004; Bogard & del Giorgio, 2016), and in other freshwater environments such as streams (Rocher-Ros et al., 2019). To investigate the connection between GPP, R, and the DIC pool in L227, I used the magnitude of daily pH change as a proxy for CO_2 production or consumption.

The overnight decline in pH was as large as 2.5 pH units: during blooms the pH at 1 m reached 9.5-9.7 by the late afternoon, but pH did not consistently return to neutral (Figure A5). During the June overnight sampling event, low DIC inputs led to almost no change in pH at 1 m, while during the September diel sampling event, higher DIC inputs caused pH to drop overnight (Figure 3.3). On days when the pH did not return to neutral, there was likely an insufficient increase in [DIC] to cause a pH decline.

The 1 m pH was low and stable during the July overnight sampling event despite the increase in [DIC] (Figure 3.3). At a constant, low alkalinity, a small change in [DIC] shifts the pH between 7-9; outside of this pH range, a greater change in [DIC] is necessary to shift the pH. The combination of low alkalinity and low [DIC] values that I measured in L227 constrain the range of possible pH values to be approximately 7-9.5 (Figure 1.3). During the July overnight sampling event, the daytime pH was already at the bottom of this range; the overnight inputs of DIC were not sufficient to cause a decrease in pH from 7 (Figure A4). In September, when daytime productivity and pH were higher than in July, a smaller overnight increase in [DIC] caused the pH to decline rapidly from 9.5 to 7.5.

Low-alkalinity, low-DIC lakes are more susceptible to diel changes in pH. Prior to 1990, additions of $NaNO_3$ kept alkalinity in the epilimnion of L227 between 150-300 μeq L^{-1} from May-October, relatively higher than the range of 50-150 μeq L^{-1} that has occurred from May-October since the late 1990s (Flinn, 2012). In contrast to the findings of this study, Schindler and Fee (1973) measured consistent epilimnion pH values of 10 overnight in the summer of 1972. Diel pH changes such as those I observed in this study have likely occurred in the epilimnion of L227 since the 1990s, when N fertilization with $NaNO_3$ stopped.

The positive linear relationships between the difference in maximum and minimum pH and the daily rates of both GPP and ER during blooms in 2018 and 2019 (Figure 3.6) suggest that lake metabolism controls diel cycles of [DIC] decline and increase in L227. These relationships could arise because pH drops overnight when a high rate of ER increases the amount of DIC in the lake, or because the rate of

carbon fixation increases if the morning pH is lower and [DIC] is higher. Since GPP and ER are daily rates, and there is a positive linear relationship between the daily rates of GPP and ER, it is difficult to discern from sensor data whether the rate of GPP influences the rate of ER or vice versa.

The low daily rates of gas exchange and CED provide additional evidence that lake metabolism controls DIC recharge. The rates of gas exchange that I calculated for the overnight sampling events and estimated from pH and alkalinity measurements were up to 8.4 times less than the corresponding daily rate of ER (Figure A9). The daily rate of gas exchange was relatively consistent compared to the fluctuations in ER; on days when the rates of gas exchange and ER were comparable, both rates were low. I included the chemical enhancement factor when calculating the rates of gas exchange, as CED occurred daily during the phytoplankton blooms when pH was relatively high (Figures A6, A9). Despite the occurrence of CED, diel pH fluctuations limited the number of hours that CED could occur to the late afternoon and evening (Figure A6), and the chemical enhancement factor and rate of CO_2 flux were too low for CED to contribute a high percentage of DIC. Since CED accounts for a small proportion of the daily DIC increase, the large kinetic isotope fractionation associated with CED has a negligible effect on the overall δ^{13}C-DIC value of L227. ER controls the length of time CED can occur by causing a decline in pH overnight.

The amount of DIC recharge and the relative contributions of each DIC source affected the magnitude and direction of δ^{13}C-DIC change overnight. Of the three overnight sampling events, the smallest overnight change in [DIC] and δ^{13}C value occurred during the June 2019 sampling event (Figure 3.3). The total input of DIC on this night was lower compared to the other two sampling events due to the low rate of ER. Without this source, the [DIC] increase and change in the δ^{13}C-DIC value were both low. CED did not increase the rate of gas exchange sufficiently to increase [DIC]; the increase in δ^{13}C-DIC values along the CED end-member line overnight is likely coincidental (Figures 3.4, 3.5). Conversely, the relatively high DIC inputs during the July overnight sampling event led to a greater change in the

δ^{13}C-DIC value. There was sufficient ER to cause the lake to become a source of CO_2 to the atmosphere overnight and to cause the δ^{13}C-DIC value to decline.

There was a general trend in δ^{13}C-DIC values overnight and between the three overnight sampling events: δ^{13}C-DIC was closer to the ER end-member value during the blooms, and closer to the gas exchange end-member value between the blooms (Figure 3.4). These δ^{13}C-DIC values reflected the probable dominant source of DIC during the three sampling events, but did not reflect photosynthetic fractionation that should have caused δ^{13}C-DIC values to increase during the day leading up to the sampling event (see Van Dam et al., 2018). The preferential fixation of ^{12}C-CO_2 during photosynthesis and subsequent leakage of relatively more unfixed ^{13}C-CO_2 caused δ^{13}C-DIC to increase from -9.8 ‰ at 09:00 to 0 ‰ at 20:00 on July 10, 2018. The high concentration of phytoplankton biomass during the blooms drew down the daytime [DIC] to a lower value than during the lower-biomass period, but there was no corresponding increase in the δ^{13}C-DIC value (Figure 3.3). Because the concentration of aqueous CO_2 approached 0 µmol L^{-1} during the bloom events, the lower amount of photosynthetic fractionation could be due to fixation of HCO_3^-. Although there is little fractionation involved in either the passive uptake of CO_2 or the active uptake of CO_2 or HCO_3^-, researchers have observed less fractionation between DIC and phytoplankton when phytoplankton fix HCO_3^- (Morales-Williams et al., 2017). Cyanobacteria readily take up HCO_3^- and can convert HCO_3^- to CO_2 in carboxysomes with very little leakage out of the cell (Badger & Price, 2003; Sharkey & Berry, 1985; Wang et al., 2016). If nearly all of the HCO_3^- taken up was converted to CO_2 and fixed, $^{13}CO_2$ would be fixed instead of accumulating in the cell or leaking out (Fielding et al., 1998). This would have the effect of minimizing the difference between δ^{13}C-DIC and δ^{13}C-POC in the evening, which occurred on June 26, 2019 and September 5, 2018. See Chapter 4 for a discussion of phytoplankton carbon concentrating mechanisms and seasonal changes in photosynthetic fractionation in L227.

Microstratification can prevent gas exchange on diel timescales

With greater amounts of DIC recharge, [DIC] and $\delta^{13}C$ values did not always change incrementally or in the expected direction between sunset and sunrise. The concentration of DIC doubled overnight and the $\delta^{13}C$-DIC values spanned 10 ‰ during the July and September 2018 sampling events (Figure 3.3). Rather than a steady hourly change, the greatest shift in each parameter during both sampling events happened between midnight and 02:00 CST. These changes could be the result of microstratification developing at the surface of the water column during the day and collapsing as air temperature decreased at night. Under sunny, low-wind conditions, a thin layer of warm water at the surface of a lake can become thermally stratified, separating it from the rest of the epilimnion (Hanson et al., 2008). As the surface water cools and becomes denser at night, it sinks and mixes with the warmer water below it, increasing the CO_2 concentration throughout the epilimnion (Åberg et al., 2004).

Microstratification could explain the sudden increase in [DIC] shortly after midnight on July 11 and September 6, 2018 (Figure 3.3). On both nights, the air cooled by more than 10 °C between the highest afternoon and lowest morning measurements, while the water temperature at 1 m depth decreased by less than 2 °C over the same time period (not shown). As the surface water cooled, it might have mixed with the rest of the warmer water in the epilimnion and introduced accumulating CO_2 from atmospheric gas exchange. Detailed water temperature measurements throughout the top 1 m of the water column would be necessary to confirm the presence and degree of microstratification (see Hanson et al., 2008), but the YSI profile I collected on August 14, 2018 suggested that microstratification occurs in L227 (Figure A4). By 09:00 CST at a depth of 0.25 m the temperature was 22.8 °C, while the temperature from 0.5 m to 1.5 m was 23.5 °C. The pH was also slightly lower at the surface, suggesting that there was some separation between the surface layer and the rest of the epilimnion.

The unusual pattern of δ^{13}C-DIC change overnight in September could also be explained by microstratification. If microstratification was established while the pH was above 9, CED likely occurred in the surface layer and caused δ^{13}C-DIC to decrease. The influx of DIC with a lower δ^{13}C value between midnight and 01:00 could be the result of the surface layer mixing with the epilimnion water beneath it. Following 01:00, the increasing values of δ^{13}C-DIC suggest that gas exchange continued to be the dominant source of DIC (Figures 3.3, 3.4). This trend is at odds with the modeled rates of ER and gas exchange, which indicate that ER was the dominant source of DIC. However, if significant microstratification developed for an extended period, neither method to estimate the rate of gas exchange with the atmosphere would be valid. For example, if a shallow mixing layer of 0.25 m developed at the top of an epilimnion 1.75 m deep, the rate of gas exchange for the evening of September 5, 2018 would be 3.6 µmol L^{-1} h^{-1} instead of 0.51 µmol L^{-1} h^{-1}

Daily variation in lake metabolism controls DIC increases and δ^{13}C values at discrete depths in the metalimnion

The thermal structure of the water column created different DIC consumption and recharge conditions at 3 m compared to the well-mixed epilimnion. 3 m was typically near the bottom of the metalimnion, where gas exchange with the atmosphere would not occur, and diffusion of DIC from the hypolimnion was negligible (Schindler & Fee, 1973). This depth was also approximately 1 m above the anoxic boundary during the sampling period, making CH_4 oxidation an unlikely source of CO_2. Since biomass was abundant at 3 m during the overnight sampling events, ER was the only likely DIC source.

The vertical movement of phytoplankton in the water column over the season made the three nights difficult to compare. Based on the concentration of phycocyanin, in June the cyanobacteria peak was above 3 m, in July the peak was at 3 m, and in September the peak was below 3 m. Unlike in June and September, the high concentration of phycocyanin and Chl a at 3 m on July 10, 2018 likely contributed to a high ER rate. The DIC concentration increased overnight, and δ^{13}C-DIC decreased from the highest

value of the summer: +15.6 ‰. The elevated δ^{13}C-DIC values at 3 m can be explained by photosynthetic fractionation alone. The metalimnion is not a closed system because ER serves as a continuous source of DIC, but assuming a closed system makes the Rayleigh equation applicable. If the photosynthetic fractionation factor was -20 ‰, phytoplankton would need to fix 65% of the available DIC to cause an increase in δ^{13}C-DIC from -5.3 ‰ to +15.6 ‰: the values I measured at 09:00 and 20:00 CST on July 10, 2018. There was a 54% decrease in [DIC] over the same time period.

While δ^{13}C-DIC decreased relatively steadily during the July overnight sampling event, mixing in the thermocline obscured the trend in increasing [DIC]. On the morning of July 10, 2018, 3 m was near the steep bottom of the thermocline. The change in temperature between 2.75 m and 3.25 m was 3.6 °C, and the change in pH was 2.4 pH units. Mixing with water 0.25 m above or below 3 m likely caused shifts in temperature and pH values within this range. 0.25 m gradations were labelled on the sampling line and sonde, so human error was not responsible for the shifts. Since δ^{13}C-DIC did not fluctuate, the value was similar above and below 3 m. While [DIC] was not stable, the source of DIC return was likely the same throughout this part of the metalimnion. Vertical shifts in the thermocline and phytoplankton biomass make it more challenging to model geochemical processes at depths below the epilimnion, and are responsible for fluctuations in [DIC] and δ^{13}C values at hourly, daily, and seasonal timescales.

Carbon balance calculations for productive lakes require high-resolution data

These results demonstrate the value in collecting high-resolution sensor and isotope data in L227. By sampling hourly at two different depths I captured changes in pH, [DIC], and δ^{13}C-DIC values that were not apparent from weekly or even daily sampling events. High-frequency sampling also revealed potential diel changes in the thermal structure of the lake, which can influence estimates of ER and gas exchange rates by over-estimating the depth of the mixing layer that interacts with the atmosphere (Coloso et al., 2011). Because the changes in δ^{13}C-DIC values reflected the input of the actual DIC

sources rather than theoretical rates, isotope values were useful in interpreting the extent that both ER and gas exchange contributed to the DIC pool overnight in the well-mixed epilimnion, and the extent that ER contributed to the DIC pool overnight at 3 m.

Single measurements of [DIC] do not scale up to an accurate daily rate of CO_2 flux in productive lakes. A single mid-morning sample could lead to an over-estimation of daily CO_2 flux into the lake if [DIC] was low from carbon fixation, or an over-estimation of CO_2 flux out of the lake if [DIC] remained high until later in the day. A single calculation of β could have a similar effect in lakes with pH values that increase sufficiently to promote CED on short timescales. Poor estimates of the daily rate of atmospheric gas exchange cannot be compared to daily rates of ER. *LakeMetabolizer* requires regular DO and water temperature measurements from automatic loggers to calculate daily rates of GPP, NEP, and ER in units of mg O_2 L^{-1} d^{-1}, assuming that the rate of ER is constant over 24 hours (Winslow et al., 2016). To compare the daily rates of ER and gas exchange, both should be a daily rate. The increasing availability of automated sensors for measuring dissolved [CO_2] will allow for more accurate daily flux measurements in freshwater systems.

In addition to high-frequency sampling, recording water temperature at a higher spatial resolution is necessary for modelling in-lake processes affecting CO_2. Models that estimate the rates of lake metabolism and gas exchange are based on physical and geochemical measurements at a discrete depth in the surface mixed layer, and apply the rate over the volume of the whole layer. These models make two tenuous assumptions about the surface mixed layer: that it is a relatively constant depth over short timescales, and that it is open to the atmosphere (e.g. Bade & Cole, 2006; Winslow et al., 2016). The depth of the surface mixing layer can change at an hourly timescale, affecting the conversion between areal and volumetric rates of lake metabolism and gas exchange (Coloso et al., 2011). Warm, low-wind conditions can cause microstratification at the surface that confines gas exchange to a shallower depth than the mixing depth, also rendering the calculated rate of flux into the lake inaccurate (Coloso et al.,

2011; Hanson et al., 2008). These issues can be better accounted for by deploying thermistor chains to identify the depth of the surface mixing layer and periods of surface microstratification.

The high-resolution sensor data also provided context for interpreting the overnight δ^{13}C-DIC data. Since the daily rate of gas exchange with the atmosphere was typically much lower than the rate of ER, I was able to eliminate CED as a major DIC source. The continuous pH measurements revealed that the long periods of high pH necessary for prolonged, high rates of CED did not occur. The dissolution of carbonate minerals in hard water lakes allows for higher alkalinity and [DIC] at pH values of 10-11, leading to chemical enhancement factors of 10-15 (Kragh & Sand-Jensen, 2018). The amount of isotope fractionation during CED can be up to -15 ‰, leading to potentially low δ^{13}C-DIC values (Bade & Cole, 2006). In this low-alkalinity system with variable, moderate pH, the low δ^{13}C-DIC values during the blooms were more likely due to ER or HCO_3^- uptake than CED.

The high-frequency δ^{13}C-DIC samples were laborious to collect, but demonstrated that δ^{13}C-DIC values can change on hourly timescales in productive, soft water lakes. Seasonal trends, such as a decrease in DIC or increase in δ^{13}C-DIC during periods of intense phytoplankton growth, appear at lower temporal resolution, but hide potential diel changes in these parameters. Like diel variability in [DIC], the potential for diel cycles in δ^{13}C-DIC can impact the interpretation of mid-morning values. For example, modelling photosynthetic fractionation from a single δ^{13}C-DIC value is ineffective if δ^{13}C-DIC changes by 10 ‰ over a day. Sampling at a daily, weekly, or greater timescales may not offer sufficient temporal resolution to interpret the dynamic role of DIC in the aquatic carbon cycle in this type of lake.

3.6 Conclusions

In this study, I examined three different field situations where [DIC] increased overnight in the epilimnion of a eutrophic lake: a small increase at moderately high pH, a high increase at neutral pH, and a moderate increase as pH declined from high to neutral. The magnitude of [DIC] increase and the amount of pH change overnight differed at daily timescales during two seasonal phytoplankton blooms with different phytoplankton community compositions. Weekly mid-morning sampling did not capture the daily [DIC] decline or the overnight [DIC] increase that occurred in the epilimnion, or the potential for the lake to act as a temporary source of CO_2 to the atmosphere.

During the two phytoplankton blooms, lake metabolism regulated the amount of DIC in the epilimnion of L227 to a greater extent than gas exchange with the atmosphere. Overnight δ^{13}C-DIC values and modelled daily rates of ER and gas exchange both indicated that a greater proportion of DIC inputs originated from ER during the phytoplankton blooms. The high-pH, low-wind conditions in L227 allowed for periods of CED, but low rates of gas exchange and a limited number of hours when CED could occur did not support CED as a major source of DIC to L227. Microstratification in the epilimnion may have further reduced the capacity for gas exchange by limiting the depth that DIC originating from gas exchange could diffuse into the lake.

Diel variation in pH, [DIC], and δ^{13}C-DIC values in the epilimnion of L227 was common during the summer months. Continuous measurements of pH and [CO_2] would allow for a robust understanding of diel variation in the carbonate system and atmospheric gas exchange. In lieu of a probe with the capability to measure [CO_2], the sensitivity of pH to changes in DIC makes continuous pH measurements a good proxy for overnight DIC recharge in low-alkalinity, low-DIC lakes. A combined dataset of continuous pH, [CO_2], DO, temperature, and windspeed measurements allows for convenient modelling of gas exchange with the atmosphere, lake metabolism, and CED. Monitoring water temperature at a

higher spatial resolution near the top of the epilimnion could clarify the role of microstratification in hindering DIC recharge on a diel timescale.

Collecting δ^{13}C-DIC samples at a high temporal resolution is time-consuming, expensive, and laborious. While overnight δ^{13}C-DIC samples can support the identification of sources to the DIC pool, using automated sensors to collect data for common models is a more practical solution. Diel δ^{13}C-DIC measurements are uncommon in the literature, and the range of overnight fluctuation that I reported is higher than the ranges measured in previous studies. Understanding that diel variability in δ^{13}C-DIC can arise in eutrophic lakes at a magnitude similar to seasonal variation is important for designing studies that rely on δ^{13}C-DIC measurements.

Lakes that are highly productive during summer months may alternate between acting as a CO_2 source or sink. At a daily timescale, there may be a flux of CO_2 out of the lake overnight during periods of lower biomass, while at a seasonal timescale, the lake may only serve as a sink of CO_2 during summer phytoplankton blooms. Data collected at high temporal resolution, including overnight, is necessary to avoid over- or under-estimating the capacity of eutrophic lakes to serve as sources or sinks of CO_2 in regional carbon budgets.

Chapter 4: Biomass concentration drives seasonal variability in δ^{13}C-DIC and δ^{13}C-POC

4.1 Introduction

Lakes are a globally significant source, sink, and conduit of carbon (Cole et al., 2007; Tranvik et al., 2009). To develop small- and large-scale carbon budgets, there is interest in quantifying the amount of carbon that lakes emit and sequester. Measuring stable isotope values of carbon is a popular but complex method for interpreting how carbon moves through the aquatic carbon cycle. In particular, temporal variability in δ^{13}C values of DIC and phytoplankton occurs at different timescales with a number of causes. We need to understand how temporal variability in δ^{13}C arises to better interpret carbon stable isotope data.

DIC is the sum of all dissolved CO_2, HCO_3^-, and CO_3^{2-} in a body of water, the distribution of which is dependent on pH (Figure 1.2). In a lake with a low concentration of DIC, δ^{13}C-DIC can vary on a diel timescale as primary productivity consumes DIC during the day, and [DIC] increases overnight (Chapter 3). Seasonal variability in δ^{13}C-DIC occurs as phytoplankton blooms grow and consume DIC, or if the sources of DIC change over time. The magnitude of diel variability in δ^{13}C-DIC can be greater than the magnitude of seasonal variability (Van Dam et al., 2018).

Phytoplankton produce, store, and transform carbon as part of the aquatic carbon cycle. In eutrophic lakes, where particles are predominantly phytoplankton, the value of δ^{13}C-POC depends on the concentration and δ^{13}C value of DIC, the isotopic fractionation during DIC uptake and fixation, and the changes in these values as POC accumulates and settles out of the water column over time (Gu & Schelske, 2006; Hayes, 1993; Lehmann et al., 2004). Temporal variability of δ^{13}C-POC occurs over longer timescales than δ^{13}C-DIC because phytoplankton cells assimilate DIC over days to weeks, incorporating DIC of different δ^{13}C values.

The isotopic fractionation between the carbon source and phytoplankton cell during carbon uptake and fixation (ε_p) varies by species and by lake (Bade et al., 2006; Falkowski, 1991). Isotopic fractionation by RuBisCo is approximately -29 ‰ in green algae and -22 ‰ to -25 ‰ in cyanobacteria, but among autotrophs the known range in ε_p is -11 to -29 ‰ (Falkowski & Raven, 2007; Thomas et al., 2019). ε_p would be approximately equal to the fractionation by RuBisCO if CO_2 only diffused into the phytoplankton cell, but most freshwater phytoplankton employ carbon concentrating mechanisms (CCMs) to actively take up CO_2 or HCO_3^- (Kaplan & Reinhold, 1999; Giordano et al., 2005). CCMs can reduce net isotopic fractionation and result in a higher $\delta^{13}C$ value of phytoplankton (Hayes, 1993; Sharkey & Berry, 1985). The $\delta^{13}C$ of cyanobacteria, in particular, tends to be higher than other phytoplankton taxa (Bontes et al., 2006; Lammers et al., 2017; Pel, 2003; Vuorio et al., 2006).

CCMs include the production of the enzyme carbonic anhydrase (CA) to convert HCO_3^- into CO_2 outside or inside the cell, and the active uptake of HCO_3^- or CO_2 (Giordano et al., 2005). As phytoplankton lower [DIC] during blooms, CCMs may "turn on", resulting in lower ε_p and higher $\delta^{13}C$-POC values (Hoins, 2016; Morales-Williams et al., 2017). This reduction can occur because cells take up HCO_3^-, or because external CA converts HCO_3^- to CO_2 outside the cell for CO_2 uptake. The equilibrium isotope fractionation between CO_2 and HCO_3^- is approximately 8 ‰ (Mook et al., 1974), and the kinetic isotope fractionation in the CA-mediated conversion of HCO_3^- to CO_2 is 10 ‰ (Paneth & O'Learly, 1985). The similar values of fractionation in these reactions means that a higher $\delta^{13}C$-POC value of phytoplankton does not specifically indicate whether cells are taking up CO_2 or CA-mediated HCO_3^- (Reibesell and Wolf-Gladrow, 1995; Takahashi et al., 1990).

While intense primary productivity and CCMs leads to higher $\delta^{13}C$-POC values when [DIC] is low, DIC drawdown in unbuffered waters also causes high pH values and chemically enhanced diffusion (CED). CED is the reaction of CO_2 with OH^- to form HCO_3^-, where the newly formed HCO_3^- has a lower $\delta^{13}C$ values, and results in CEF up to -12.2 ‰ in L227 (see section 3.2; Bade & Cole, 2006; Herzceg, 1987).

Takahashi et al. (1990) and Lammers et al. (2017) suggested that CED contributed to lower δ^{13}C-DIC values mid-summer in their respective eutrophic study lakes, but also measured the highest δ^{13}C-POC values at this time.

Changes in the value of δ^{13}C-DIC on different timescales, succession of dominant phytoplankton taxa, fluctuating [DIC] and pH, use of CCMs, and the rate of phytoplankton turnover can all contribute to variability in δ^{13}C-POC, making it difficult to interpret individual measured values, let alone to predict what seasonal variability will be. The objectives of this chapter are (1) to identify the causes of recurring seasonal trends in δ^{13}C-DIC and δ^{13}C-POC in a eutrophic lake, and (2) to evaluate how temporal variability of δ^{13}C-POC affects interpretations of δ^{13}C values of lake seston and sediments.

4.2 Materials and Methods

See Chapter 2 for a detailed description of L227, sample collection procedures, and analysis techniques.

Stable carbon isotopes

In 2017 and 2018, I collected weekly samples for δ^{13}C-DIC and δ^{13}C-POC analysis from 1 m and 3 m depths in L227. 1 m samples represented the well-mixed epilimnion, while 3 m samples targeted higher biomass that accrues at the bottom of the metalimnion during the ice-free season. Researchers from the EGL collected monthly 1 m samples from L227 in 2010 and 2011 (see Flinn, 2012) and intermittent samples from 2012-2016.

I started weekly sampling in early May of 2017 and 2018, shortly after ice-off, and ended sampling in early September, shortly before fall turnover and before the end of the second bloom. In 2018 and 2019 I also conducted three half-diel sampling events to investigate how δ^{13}C values change overnight. I targeted the cyanobacteria-dominated bloom on June 26-27, 2019; the cyanobacteria and chlorophyte bloom on September 5-6, 2018, and the declining biomass period between the two blooms on July 10-11, 2018. I measured δ^{13}C-DIC hourly at 1 m and 3 m between sunset and sunrise for all three sampling events, and during the June 2019 sampling event I also collected δ^{13}C-POC samples at 21:00, 1:00, and 5:00. Refer to Chapter 3 for the detailed results of the half-diel sampling events.

Geochemical analysis

As part of the IISD-ELA LTER program, researchers collected routine geochemical samples biweekly or monthly from L227 over the same sampling period. For this chapter, I supplemented my stable isotope data with biomass counts, Chl a measurements, and concentrations of suspended C. N, and P from the IISD-ELA database. I assumed a well-mixed epilimnion and matched the integrated epilimnion samples from the IISD-ELA database with 1 m stable isotope measurements for 2010-2016. If sampling by IISD-ELA and the EGL did not occur on the same day, I matched samples from within the same week. In

2017 and 2018, I submitted discrete samples from 1 m and 3 m for analysis of Chl a and suspended C, N, and P concentrations to the IISD-ELA chemistry lab.

No data is available for some geochemical parameters for the 2013 and 2014 field seasons due to a federal government-imposed funding cut and shutdown of the field station. In this chapter I focus on 2010, 2011, 2017, and 2018, where the most complete datasets exist for stable isotope values, nutrient concentrations, and biomass counts.

4.3 Calculations

Stoichiometry and nutrient deficiency

I calculated the molar ratios of particulate C:N, C:P, and N:P from suspended C, N, and P data. I assumed that all particles were phytoplankton, as L227 has high phytoplankton biomass for most of the ice-free season (Higgins et al., 2018). This is a common assumption for eutrophic lakes (Bade et al., 2006; Van Dam et al., 2018). Particulate nutrient ratios of freshwater phytoplankton are an indicator of the degree of N or P deficiency (Table 4.1; Healey & Hendzel, 1980).

Table 4.1: Thresholds for nitrogen (N) and phosphorus (P) deficiency in freshwater phytoplankton (µmol/µmol). This table is a modified version originally presented by Hecky et al. (1993), based on data from Healey & Hendzel (1980).

Molar ratio	Deficient nutrient	Threshold for nutrient deficiency		
		None	Moderate	Severe
C:N	N	< 8.3	8.3-14.6	> 14.6
C:P	P	< 129	129-258	> 258
N:P	P	< 22	N/A	> 22

Photosynthetic fractionation

There are several methods for approximating ε_p (see Morales-Williams et al., 2017, Van Dam et al., 2018, Wang et al., 2016). The simplest method is to measure both δ^{13}C-DIC and δ^{13}C-POC, and calculate the difference (Equation 4.1). In lakes that are saturated in CO_2, the difference between δ^{13}C-CO_2 and δ^{13}C-POC or a simple model can approximate ε_p (e.g. Bade et al., 2006; Gu et al., 2006). Due to equilibrium fractionation, δ^{13}C-CO_2 is 8-10 ‰ lower than δ^{13}C-HCO_3^-, and consequently also lower than δ^{13}C-DIC when pH > 5 (Mook et al, 1974).

$$\varepsilon_p \approx \Delta\delta^{13}C_{POC-DIC} = \delta^{13}C_{DIC} - \delta^{13}C_{POC} \quad (4.1)$$

In a lake with a higher pH, where most of the DIC is HCO_3^-, the difference between δ^{13}C-DIC and δ^{13}C-POC is more representative of ε_p (Lehmann et al., 2004; Van Dam et al., 2018). If nearly all DIC is HCO_3^-, δ^{13}C-DIC and δ^{13}C-HCO_3^- are approximately equal. The pH in L227 was > 9 during the day for most

of the sampling period, and ~90% of DIC was HCO_3^-. For this reason, I approximated ε_p as in Equation 4.1. These values are the apparent photosynthetic fractionation, ε_{app}. This approximation is limited by changes in δ^{13}C-DIC and δ^{13}C-POC values on different timescales. While the value of δ^{13}C-DIC can change on a diel timescale (see Chapter 3), the value of δ^{13}C-POC is the average value for phytoplankton growing over days or weeks (Bade et al., 2006).

4.4 Results

Seasonal trends in particulate nutrient stoichiometry

Chl a in L227 was consistently much higher than in nearby unfertilized lakes. In oligotrophic L442, a reference lake 13 km northwest of L227, Chl a in the integrated epilimnion did not exceed 2 µg L^{-1} in the summer of 2018 (not shown). Immediately following ice-off in 2018, Chl a in L227 was 10 µg L^{-1} at 1 m. The concentration of Chl a changed on a weekly timescale, increasing at 1 m from 13 µg L^{-1}on June 4 to 60.7 µg L^{-1} on June 26; by July 10, Chl a fell to 14 µg L^{-1} (Figure 4.1). Chl a at 1 m then increased at a slower rate until sampling stopped on September 4, reaching 59.7 µg L^{-1} before fall turnover.

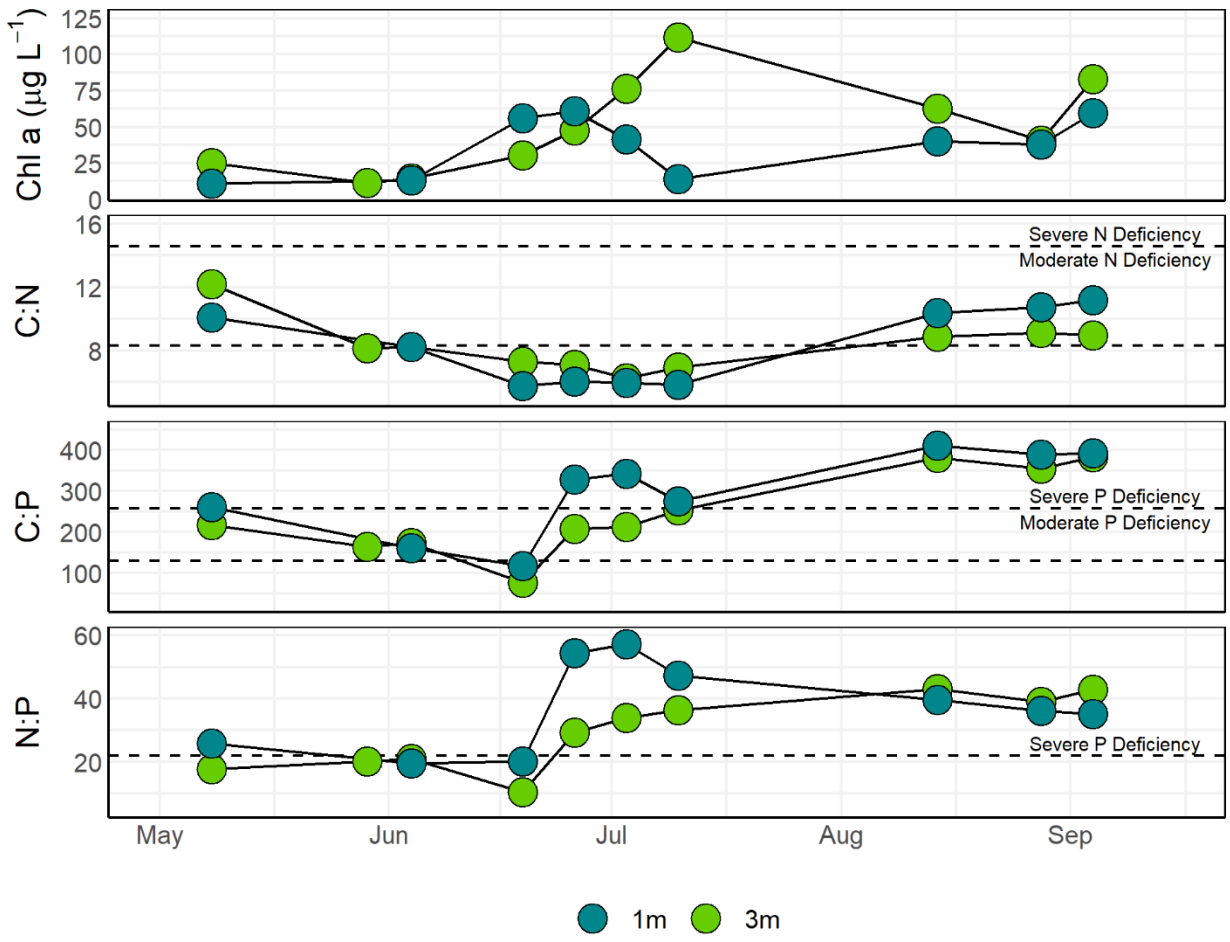

Figure 4.1: Summary of 2018 Chl a and suspended molar nutrient ratios from 1 m and 3 m in L227. The dashed lines indicate thresholds for moderate and severe nutrient deficiency (Hecky et al., 1993). Values below the bottom-most dashed line indicate no deficiency.

As the first epilimnetic bloom migrated down in the water column in early July 2018, Chl a at 3 m increased above the concentration at 1 m. On July 10, Chl a at 3 m reached a peak of 115 µg L^{-1}, exceeding all other measurements. For most of the summer the metalimnion ended at 3 m, where Chl a was highest and light levels reached 1% of surface PAR.

Temporal variability in suspended C:N:P occurred with shifts in Chl a at discrete depths (Figure 4.1). During the first bloom, when Chl a was highest at both depths, C:N remained low. N-fixing cyanobacteria were most prevalent during the first bloom (Figure 3.1), and were able to fix N_2 from the atmosphere to avoid N deficiency (Table 4.1; Healey & Hendzel, 1980; Hecky et al., 1993). High C:N prior to the first bloom and during the second bloom indicated moderate N deficiency at all depths.

C:P and N:P values indicated there was P deficiency in phytoplankton for most of the ice-free season. Prior to the first bloom, there was moderate P deficiency at both depths (Figure 4.1). One week after June 19, the date by which Chl a increased in the epilimnion and metalimnion, C:P and N:P increased above the threshold for severe P deficiency (Table 4.1; Healey & Hendzel, 1980; Hecky et al., 1993). Higgins et al. (2018) observed similar trends in temporal variability of Chl a and particulate nutrient stoichiometry in their analysis of 2011 data from L227.

Inter-annual trends in chlorophyll a concentrations and $\delta^{13}C$ values

Temporal variation in the concentration and $\delta^{13}C$ values of particulate carbon in L227 were related to temporal variation in Chl a and [DIC] (Figure 4.2). Corresponding Chl a, [DIC], and $\delta^{13}C$-POC data was available for five field seasons: 2010, 2011, and 2016-2018. For these five years of data, $\delta^{13}C$-POC values at 1 m ranged from approximately -35 ‰ to -23 ‰ (Figures 4.2, 4.3). The lowest $\delta^{13}C$-POC values occurred before ice-off and after fall mixing, and increased as the lake thermally stratified, phytoplankton density increased, and [DIC] decreased at the beginning of the ice-free season (Figure

4.3). The highest δ^{13}-POC values occurred during the early-summer bloom dominated by cyanobacteria, but δ^{13}C-POC tended to remain relatively high while Chl a was highest and [DIC] was lowest (Figure 4.2).

The relationship between δ^{13}C-POC and Chl a was positive, but not linear (Figure 4.2). At lower Chl a, the range of observed δ^{13}C-POC value was greater than 10 ‰; above 30 µg L^{-1} of Chl a, the range of observed δ^{13}C-POC values was less than 3 ‰. As Chl a increased above 25 µg L^{-1}, values of δ^{13}C-POC approached an asymptote of approximately -22.5 ‰. This pattern repeated for the four years with weekly to monthly sampling points: 2010, 2011, 2017, and 2018. There was a negative relationship between daytime [DIC] and δ^{13}C-POC (r^2 = 0.75, p < 0.01). The highest δ^{13}C-POC values occurred when [DIC] was below 50 µmol L^{-1}.

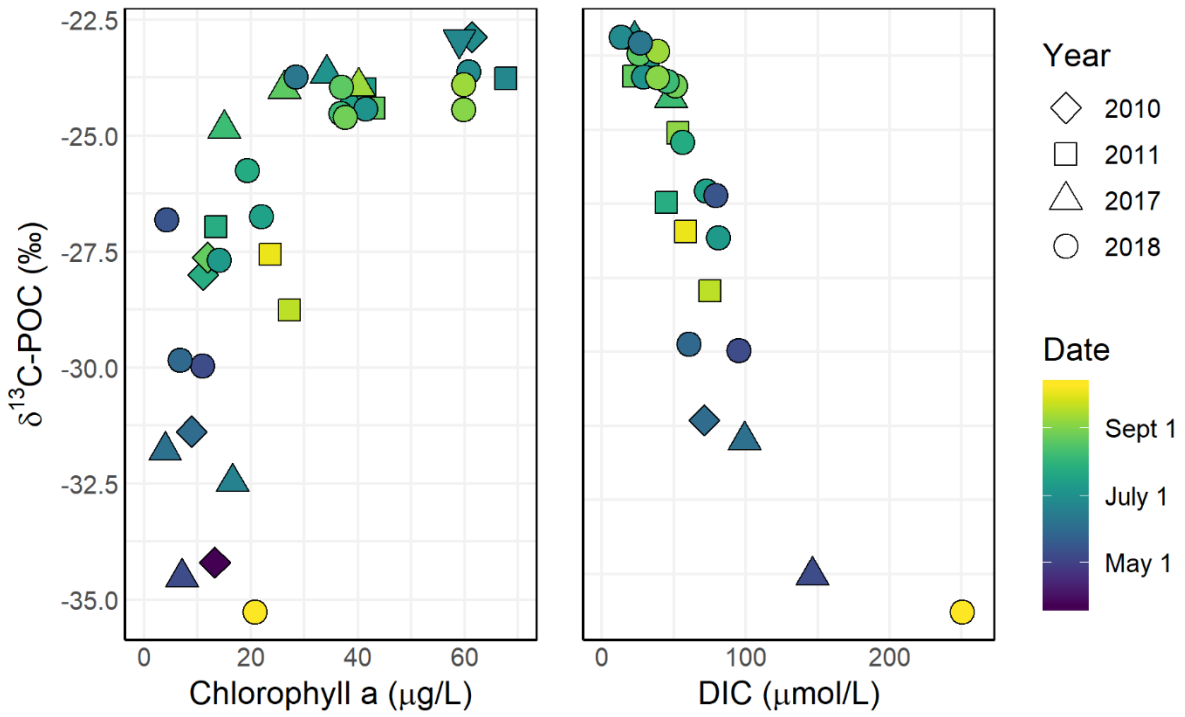

Figure 4.2: The relationship between δ^{13}C-POC, Chl a, and [DIC] in the surface mixed layer of L227 from 2010-2018. Researchers collected all δ^{13}C-POC samples from a depth of 1 m at CB. [DIC] and Chl a samples in 2010-2016 are from the integrated epilimnion, while samples in 2017-2018 are from 1 m.

There was no relationship between δ^{13}C-POC and Chl a at 3 m over multiple seasons (Figure A11). However, in 2017 and 2018, years with a full suite of 3 m samples, there was a similar pattern between the progression of the phytoplankton bloom and the δ^{13}C-POC values (Figure 4.3). During the first bloom, δ^{13}C-POC increased from the low values prior to thermal stratification. As Chl a in the surface mixed layer decreased between the two blooms, there was a period of up to three weeks where δ^{13}C-POC at 3 m decreased by approximately 5 ‰. When the concentration of Chl a increased at 3 m over July and August, δ^{13}C-POC values increased again and were higher than during the first bloom. Although there are incomplete datasets for other years, the existing data for 2012, 2014 and 2016 followed the same trend.

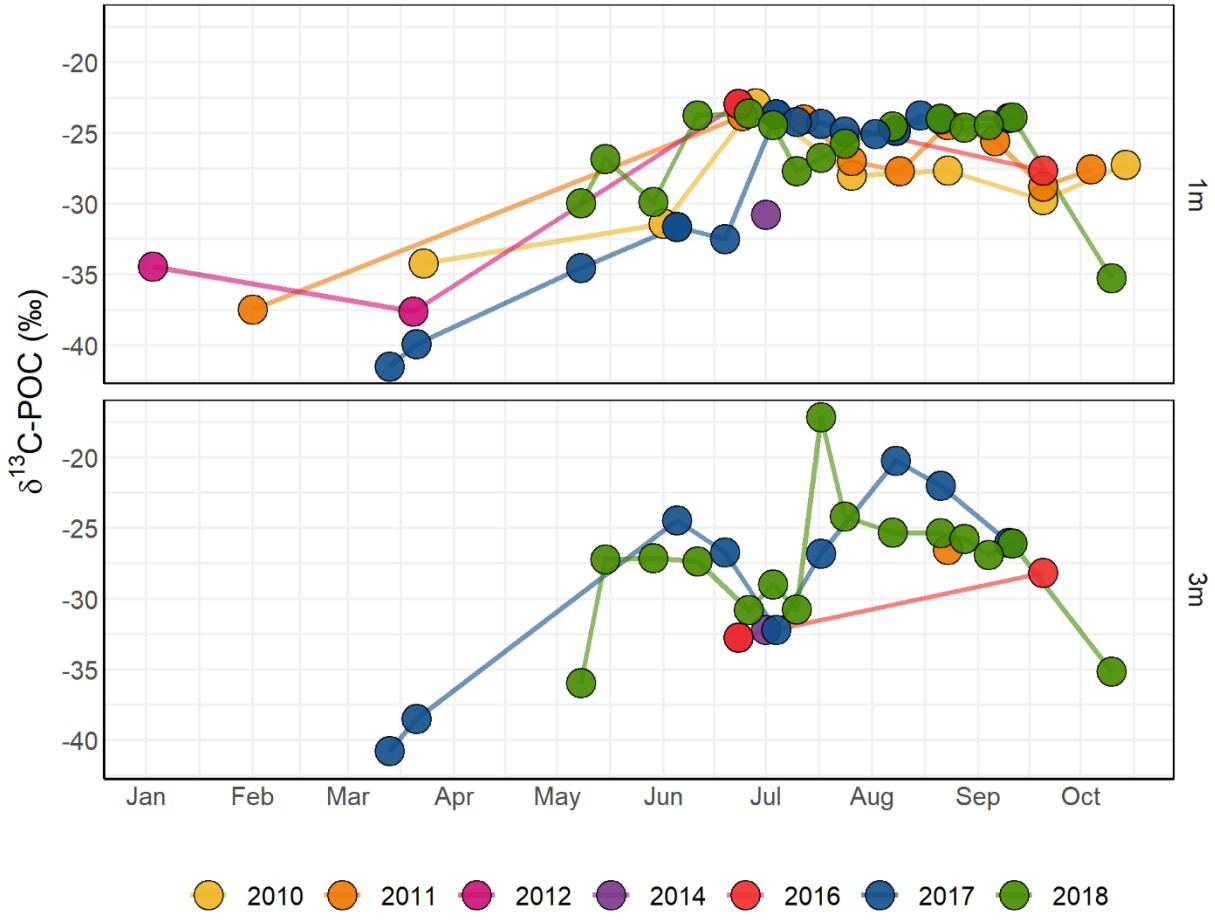

Figure 4.3: Seasonal values of δ13C-POC in L227 from 2010-2018. Researchers collected all δ13C-POC samples from a depth of 1 m or 3 m at CB, or from under-ice for January-March sampling events.

There was also a significant negative linear relationship between [DIC] and δ^{13}C-POC at 3 m in 2018 only (Figure A11; $r^2 = 0.62$, $p < 0.01$). The majority of the δ^{13}C-POC values were -25 ‰ to -27.5 ‰, and mid-morning [DIC] ranged from 40-100 µmol L^{-1}.

Seasonal dynamics of stable carbon isotope values and apparent photosynthetic fractionation

Between May and September of 2018, δ^{13}C-POC at 1 m in L227 ranged from -30.0 ‰ to -23.6 ‰ (Figure 4.4). During the bloom peaks δ^{13}C-POC was -25.0 ‰ to -23.6 ‰, and week-to-week variation was < 2 ‰. δ^{13}C-POC was lowest in May and as biomass declined in July.

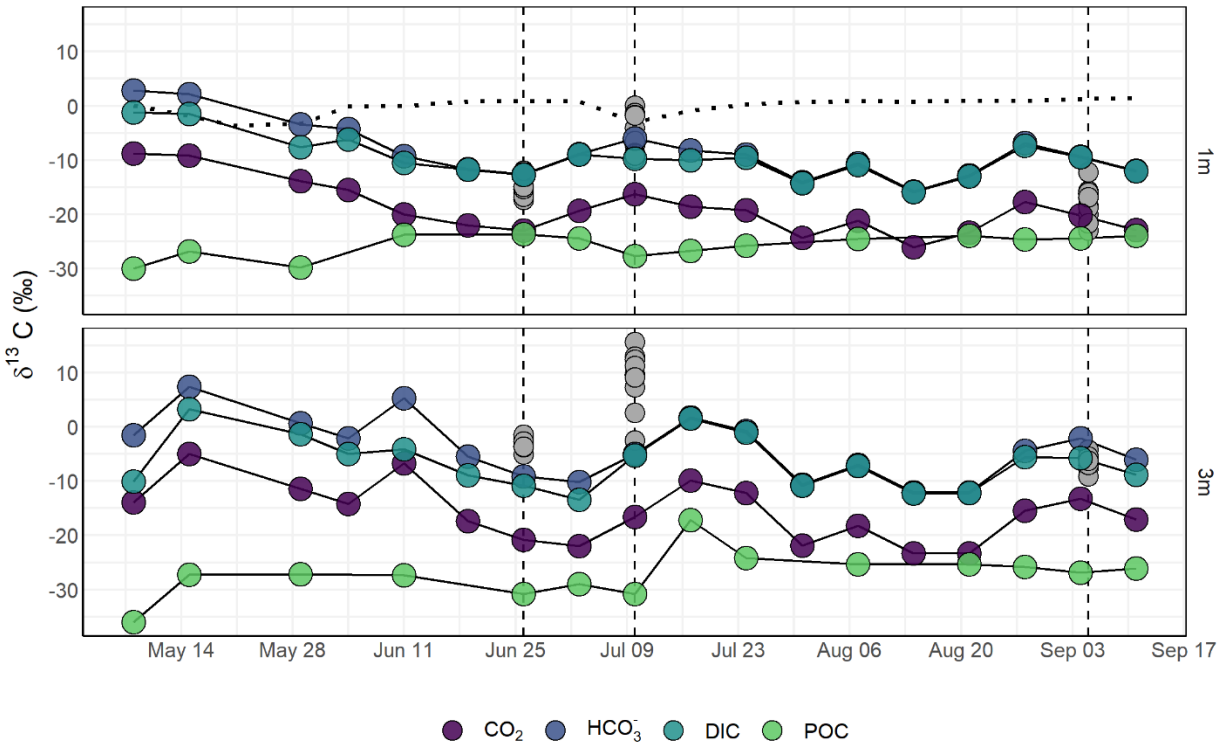

Figure 4.4: Weekly measured values of δ^{13}C-DIC and δ^{13}C-POC and calculated values of δ^{13}C-CO_2 and HCO_3^- at 1 m and 3 m in L227 over the 2018 ice-free season. The black dotted line is the δ^{13}C-DIC value in equilibrium with atmospheric δ^{13}C-CO_2 at the measured daytime pH and temperature values (Zhang et al., 1995). Dashed lines highlight the three overnight sampling events, and grey circles are the hourly δ^{13}C-DIC measurements made between sunset and sunrise on these nights. Note that the June 26-27, 2019 sampling event is superimposed on June 26, 2018 for reference. The 1 m δ^{13}C-DIC value on June 27, 2019 was -11.9 ‰ at 09:00; I could not collect a 3 m sample, but based on the diel values it was likely similar to or higher than the 2018 value.

At 3 m, δ^{13}C-POC values ranged from -36.0 ‰ to -17.1 ‰, but for most of the sampling period δ^{13}C-POC values were between -30.8 ‰ and -25.3 ‰ (Figure 4.4). On June 26, 2018, during the peak of the cyano-dominated bloom in the epilimnion and metalimnion, δ^{13}C-POC at 1 m was -23.6 ‰ while δ^{13}C-POC at 3 m was -30.0 ‰. As the phycocyanin peak shifted down to 3 m in mid-July (Figure A4), δ^{13}C-POC quickly increased from -30.8 ‰ to -17.1 ‰ between July 10 and July 17 (Figure 4.4). δ^{13}C-POC declined to -24.1 ‰ by July 24, and for the rest of the sampling period week-to-week variation remained low. Average δ^{13}C-POC before July 17 was -28.7 ‰, and -25.6 ‰ after July 17.

There was no diel variability in the samples I collected for δ^{13}C-POC analysis during the June 2019 overnight sampling event. Variation between the three nighttime sampling points for each depth was < 1.

Like δ^{13}C-POC values, δ^{13}C-DIC values at 1 m and 3 m appeared to be relatively stable while the lake was thermally stratified (Figure 4.4). However, the range in measured δ^{13}C-DIC values during the diel sampling events was greater than the range of weekly 09:00 values. In July 2018 the daytime 1 m and 3 m δ^{13}C-DIC values were lower than the overnight values, while in June 2019 and September 2018 the daytime δ^{13}C-DIC values were closer to or higher than the average overnight value.

The range of daytime δ^{13}C-DIC values over the 2018 sampling period was -15 ‰ to 0 ‰ at 1 m, and -14 ‰ to +5 ‰ at 3 m (Figure 4.4). During the day, δ^{13}C-DIC values at 1 m were consistently lower than equilibrium with the atmosphere. The only sampling event where δ^{13}C-DIC was in equilibrium with the atmosphere was the evening of the lower-biomass diel sampling event in July; by sunrise, δ^{13}C-DIC was lower and returned to below equilibrium.

For most of the ice-free season, the pH in L227 was high enough that the majority of DIC was HCO_3^- (Figure A3). Although pH decreased overnight, several hours after sunrise the pH was elevated, [DIC] was low, and DIC was predominantly comprised of HCO_3^- (Figures A3, A6). During the blooms, the

calculated values of $\delta^{13}C\text{-}HCO_3^-$ at both depths were approximately equal to $\delta^{13}C$-DIC (Figure 4.4). Leading up to the blooms and during the period between the blooms, $\delta^{13}C\text{-}HCO_3^-$ was up to 9 ‰ higher than $\delta^{13}C$-DIC; $\delta^{13}C\text{-}CO_2$ was typically 5-9 ‰ lower than $\delta^{13}C$-DIC.

The range of ε_{app} was 11-29 ‰ at 1 m, and 13-36 ‰ at 3 m (Figure 4.5). Once the lake was thermally stratified, ε_{app} at 1 m was consistently lower than ε_{app} at 3 m. There was a positive correlation between ε_{app} and [DIC] at 1 m ($r^2 = 0.71$, $p << 0.01$), but not at 3 m.

Throughout June, August, and September, when biomass was elevated at 1 m, the apparent photosynthetic fractionation between $\delta^{13}C\text{-}CO_2$ and $\delta^{13}C$-POC ($\varepsilon_{app\text{-}CO2}$) at 1 m was very low during mid-morning sampling (Figure 4.4). At 3 m, $\varepsilon_{app\text{-}CO2}$ approached 0 in early August as the concentration of biomass increased at this depth. ε_{app} at 1 m and 3 m was highest before the first bloom began and Chl a began to increase in early June.

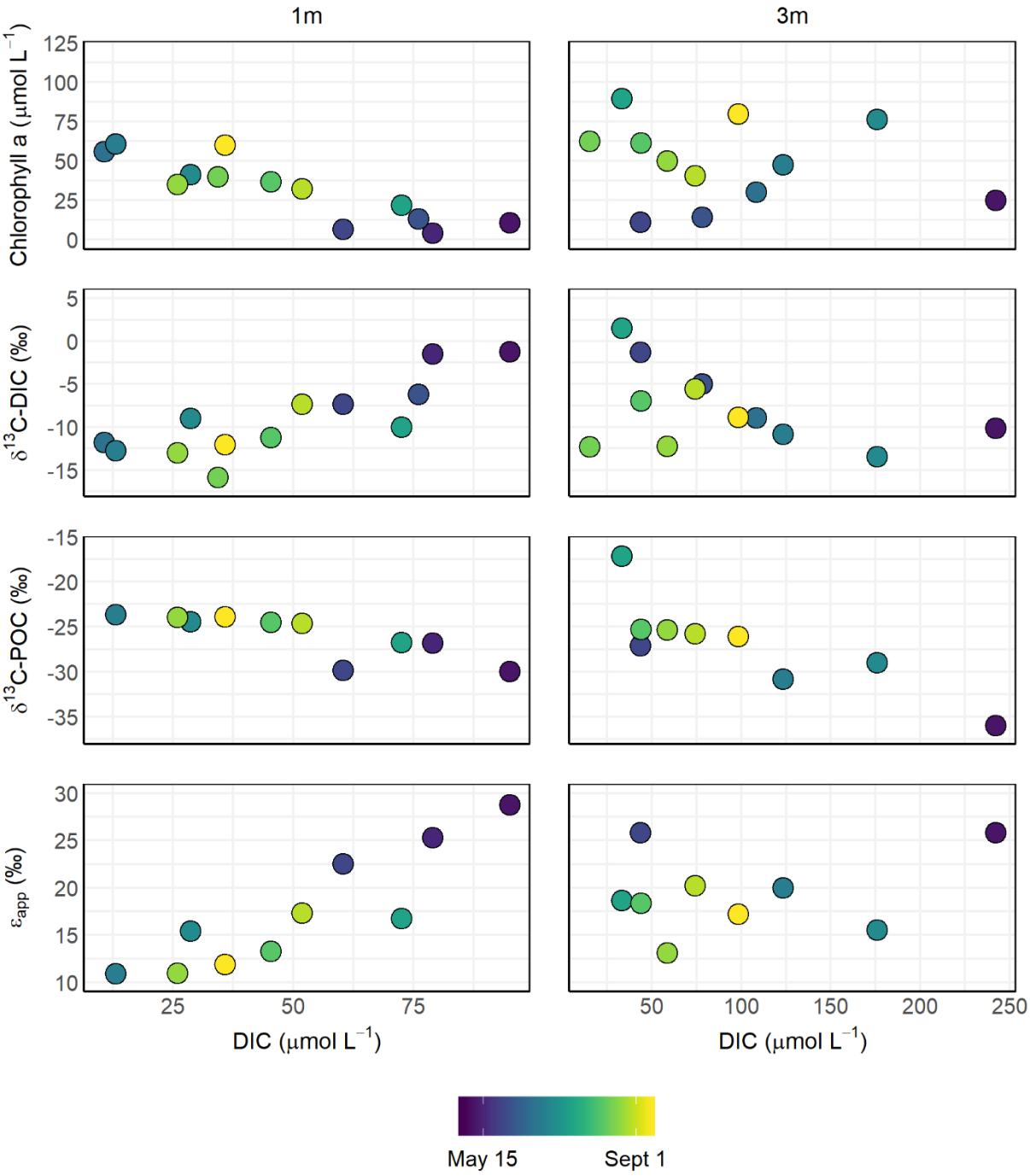

Figure 4.5: Summary of the relationships between [DIC] and Chl a, δ^{13}C-DIC, δ^{13}C-POC, and ε_{app} in L227 at 1 m and 3 m from May-September, 2018.

4.5 Discussion

Biomass increases drive temporal variability in δ^{13}C-POC by lowering [DIC]

The diel, weekly, and historical geochemical and isotope dataset for L227 show that while geochemical parameters such as pH and [DIC] vary on short timescales, seasonal patterns in δ^{13}C-POC repeat over multiple years. The recurring phytoplankton blooms drive changes in δ^{13}C-POC while the lake is thermally stratified by lowering [DIC] (Figure 4.5). δ^{13}C-POC and [DIC] are related by photosynthetic fractionation: if δ^{13}C-DIC increases, ε_p decreases, or both values change as a result of phytoplankton fixing DIC and decreasing the overall concentration, there should be an increase in the δ^{13}C-POC value. There is isotopic fractionation of up to -29 ‰ during the RuBisCO step of CO_2 fixation, as ^{12}C-CO_2 reacts more quickly than ^{13}C-CO_2; excess ^{13}C-CO_2 leaks from the cell, and δ^{13}C-DIC of the lake increases over time (Falkowski & Raven, 2007; Sharkey & Berry, 1985). When there is less DIC available to fix, phytoplankton fix relatively more ^{13}C-DIC and ε_p decreases.

The concentration of biomass in L227 is limited by the amount of P added to the lake. The particulate nutrient ratios indicated P limitation in the epilimnion and metalimnion nearly every week while the lake was thermally stratified (Figure 4.1). Because the P load is relatively consistent each year, so is the biomass concentration; interannual variation in average annual Chl a has been low since the P-only fertilization regime began in 1990 (Schindler et al., 2008). Phytoplankton have sufficient access to atmospheric CO_2 and cyanobacteria have sufficient access to N through N fixation to maintain high concentrations of biomass, so access to P controls the amount of biomass growth (Higgins et al., 2018; Schindler et al., 1972). While phytoplankton growth is not limited by [DIC], the decline in [DIC] as the bloom develops leads to changes in δ^{13}C-DIC and δ^{13}C-POC values that reflect shifts in DIC sources and speciation.

The concentration of biomass was a strong influence on [DIC] at 1 m in L227, and [DIC] was related to the values of δ^{13}C-DIC, δ^{13}C-POC, and ε_p at this depth (Figure 4.5). I measured the lowest δ^{13}C-DIC values when [DIC] was low (Figure 4.5). The same pattern occurred during the overnight sampling events: I measured the lowest δ^{13}C-DIC values on the evenings of the sampling events when epilimnion biomass was highest (see Chapter 3, Figure 3.3). This relationship does not demonstrate an increase in δ^{13}C-DIC with high rates of fixation (e.g. Lehmann et al., 2004). Since [DIC] did not increase substantially during the high-biomass overnight sampling events, input from DIC sources with low δ^{13}C values was likely not responsible for the low measured values of δ^{13}C-DIC. Instead, low [DIC] and δ^{13}C-DIC values in conjunction with high δ^{13}C-POC values could be evidence of HCO_3^- serving as the dominant substrate for carbon fixation. The cyanobacteria CCM allows for active uptake of HCO_3^- and CO_2, both of which are stored as HCO_3^- in the cytosol (Giordano et al., 2005). HCO_3^- is less prone to leakage than CO_2 and CO_2 leakage may be reduced when [DIC] is low (Fogel & Cifuentes, 1993; Sharkey & Berry, 1985). A reduction in CO_2 leakage could promote fixation of relatively more ^{13}C-CO_2, leading to an increase in δ^{13}C-POC values, a decrease in δ^{13}C-DIC values, and a decrease in ε_{app} when [DIC] is lowest.

Active uptake of HCO_3^- when [DIC] is low might also explain why δ^{13}C-POC values reached a maximum of approximately -23 ‰ at 1 m over multiple summers. When the biomass concentration is high enough to draw down [DIC] and increase pH sufficiently for HCO_3^- to be the dominant DIC species, ε_p should be lowest and δ^{13}C-POC should increase. δ^{13}C-POC was highest and ε_{app} was lowest during both blooms in the epilimnion. The upper limit of δ^{13}C-POC at 1 m might occur because the concentration of biomass does not fix a sufficient amount of DIC to lower ε_p further. The epilimnion is well-mixed and exposed to the atmosphere, providing a constant but insufficient source of DIC. Seasonal shifts in [DIC] driven by the concentration of phytoplankton in L227 control the pH, and therefore the relative amounts of CO_2 and HCO_3^-.

Photosynthetic fixation caused δ^{13}C-DIC values to increase when the biomass concentration in the epilimnion was at a summer low, but also when the biomass concentration reached a peak at 3 m. Evening δ^{13}C-DIC values reached some of the highest observed values of the summer during the July 10, 2018 diel sampling event. There was no subsequent increase in the value of δ^{13}C-POC at 1 m, possibly because the higher supply of DIC allowed ε_p to remain high. At 3 m, where [DIC] was lower, phytoplankton fixed DIC with a high δ^{13}C value and caused the value of δ^{13}C-POC to increase by 13.7 ‰ in up to one week (Figures 3.3, 4.4). This was the highest value I measured for any depth that season. At 3 m on the evening of July 10, ε_{app} was 42 ‰, while on the morning of July 11 ε_{app} was 29 ‰. Likely ε_p was lower than both values. With the possibility for a wide range of δ^{13}C-DIC values on an hourly timescale, and the time lag of up to a week for δ^{13}C-POC to reflect the higher δ^{13}C-DIC values, it is difficult to estimate what the value of ε_p was and if it was consistent when the biomass concentration was highest at 3 m.

The concentration of biomass and DIC has a greater effect on δ^{13}C-POC in L227 than seasonal succession of phytoplankton taxa. The value of ε_p for carbon fixation by cyanobacteria is lower than other phytoplankton taxa (Bontes et al., 2006; Lammers et al., 2017; Pel, 2003; Vuorio et al., 2006). If seasonal succession affects ε_p in L227, the magnitude of ε_{app} should be greater and the value of δ^{13}C-POC could be lower during the late-summer cyanobacteria- and chlorophyte-dominated bloom than during the early-summer cyanobacteria-dominated bloom. I found the opposite: δ^{13}C-POC was nearly identical during both blooms at 1 m in 2011, 2017, and 2018, and δ^{13}C-POC was higher during the second bloom in 2017 and 2018 (Figure 4.3). The changes in 1 m δ^{13}C-POC values tracked the three stages of the phytoplankton bloom in L227, with higher δ^{13}C-POC values during the blooms than during the lower-biomass period between the blooms. If ε_{app} was not similar between the two blooms, the difference was not apparent from δ^{13}C-POC values alone. The concentrations of biomass and DIC appeared to drive the shifts in δ^{13}C-POC.

Temporal variability in δ^{13}C-POC is minimized over seasonal timescales

Weekly variability in δ^{13}C-POC values was low in L227 compared to diel or weekly variability in δ^{13}C-DIC (Figure 4.4). The low weekly variability masked complex changes in the aquatic C cycle driven by ER and pH changes (see Chapter 3). The weekly δ^{13}C-POC values remained relatively constant at both 1 m and 3 m when the lake was thermally stratified and the concentration of phytoplankton was high, and the summer ranges between years were similar. Organic matter deposited as sediments during the summer phytoplankton blooms should reflect a relatively representative δ^{13}C-POC value for the season, as the greatest accumulation of sediments in L227 occurs during the productive summer months (Wolfe et al., 1994).

The δ^{13}C-POC values at 1 m were similar between weeks and between years during the phytoplankton blooms (Figures 4.3, 4.4). The range of measured δ^{13}C-POC values at 1 m was less than 3 ‰ when Chl a was greater than 30 µg L^{-1} and [DIC] was less than 50 µmol L^{-1} (Figure 4.2). These values are well below maximum Chl a, 60 µg L^{-1}, and minimum [DIC], 13 µmol L^{-1}, leading to the appearance of an asymptote approaching -23 ‰. The range in δ^{13}C-POC values was over 10 ‰ when Chl a was low, [DIC] was relatively high, and δ^{13}C-DIC values were more variable, but this range should have less of an impact on the δ^{13}C value of lake sediments as it represents a smaller amount of organic material.

The concentration of phytoplankton also influenced the δ^{13}C-POC values at 3 m, but there was no relationship between the two parameters over one or multiple years (Figure A11). This is likely because the depth of peak phytoplankton biomass changed over the course of each summer (see phycocyanin concentration in Figure A4). The highest δ^{13}C-POC value I measured at 3 m in 2018 was -17.1 ‰ on July 10, which corresponded with one of the highest Chl a measurement of the year (Figure A11). I measured a similar peak of -20.2 ‰ at 3 m on August 8, 2017, which followed a two-week period of high Chl a in the metalimnion. There could be a relationship between Chl a and δ^{13}C-POC at the Chl a peak, but since

the maximum concentration of peak phytoplankton biomass in the water column over the summer, I did not capture a relationship at the 3 m sampling depth. If a bloom shifts position in the water column, targeted sampling at the depth of highest phytoplankton biomass may be necessary to track how $\delta^{13}C$ of the bloom changes over time.

The vertical shift of cyanobacteria deeper in the water column led to the greatest rate of change in $\delta^{13}C$-POC. There was an increase of 13.7 ‰ at 3 m between July 10 and July 17: from -30.8 ‰ to -17.1 ‰ (Figure 4.4). July 10 was the first time the phycocyanin peak occurred at 3 m; prior to July 10 the peak was shallower (Figure A4). Intense productivity associated with higher biomass at 3 m likely increased the value of $\delta^{13}C$-DIC for a prolonged period; in particular, the evening $\delta^{13}C$-DIC values of up to +15 ‰ on July 10 demonstrate that phytoplankton were likely fixing DIC with a very high $\delta^{13}C$ value during this week (Figure 4.4).

Van Dam et al. (2018) suggested that diel variability in $\delta^{13}C$-POC should be considered in the context of sediment core $\delta^{13}C$-POC values. I only collected overnight $\delta^{13}C$-POC samples during the June 2019 sampling event. Although $\delta^{13}C$-POC was constant over this sampling event, so was $\delta^{13}C$-DIC (Figure 3.3). Based on these measurements, it is not conclusive that $\delta^{13}C$-POC is constant in L227 on a diel timescale. The lag in $\delta^{13}C$-POC change at 3 m between July 10 and July 17, 2018 suggests that changes in $\delta^{13}C$-DIC on diel timescales are not immediately reflected in $\delta^{13}C$-POC. The high $\delta^{13}C$-POC values did not persist for more than a week and would not be reflected in the sediment $\delta^{13}C$ value. Estimating $\delta^{13}C$-DIC or ε_p from the sediment $\delta^{13}C$ value would remain difficult, as diel variability in the speciation, concentration, and $\delta^{13}C$ value of DIC cause shifts in ε_p.

Understanding the contemporary drivers of temporal variability in $\delta^{13}C$-POC is necessary for interpreting sediment core $\delta^{13}C$ values. Flinn (2012) reported the most recent $\delta^{13}C$ values for a L227 sediment core. Since the $NaNO_3$ additions stopped in 1990, the $\delta^{13}C$ value of the sediments has decreased from

approximately -28.5 ‰ to pre-fertilization values of -31 ‰ (see Figure 4.11 in Flinn, 2012). The author suggested that the sediment $\delta^{13}C$ values reflect the change in alkalinity since N fertilization stopped, rather than any changes in productivity. The $\delta^{13}C$ value of surficial sediments in L227 was approximately -30 ‰ in July 2010, which reflected the $\delta^{13}C$-POC values of seston in the top 4 m of the water column that year (see Figure 4.4 in Flinn, 2012). 10 years have passed since $\delta^{13}C$-POC sampling began in earnest, and it would be valuable to confirm whether more recent sediment samples reflected the higher $\delta^{13}C$ values of seston that were prevalent during summer sampling events since 2010. If $\delta^{13}C$ values of late-summer surficial sediments or recent summer varves at the top of a sediment core are still approximately -30 ‰ instead of the higher values typical of the epilimnion, POC from the metalimnion, POC from another source, or diagenetic effects could be more important in setting the $\delta^{13}C$ value of the sediments.

4.6 Conclusions

Temporal variability in the dissolved and particulate carbon pools of L227 arises from change in the phytoplankton concentration when the lake is thermally stratified. As the phytoplankton blooms develop and Chl a increases, [DIC] decreases. Seasonal change in [DIC] drives changes in δ^{13}C-DIC and δ^{13}C-POC, which affects the magnitude of ε_{app}. Diel change in [DIC] and δ^{13}C-DIC does not have an observable effect on δ^{13}C-POC, which remains relatively constant at 1 m and 3 m throughout the summer.

Temporal variability in δ^{13}C-DIC is higher than δ^{13}C-POC on both hourly and weekly timescales, leading to short term variability in ε_{app}. Because δ^{13}C-POC is relatively constant during blooms, ε_{app} for a sampling event is dependent on δ^{13}C-DIC. In low-alkalinity eutrophic systems, infrequent sampling is likely insufficient to make strong interpretations about ε_p from δ^{13}C-DIC values. Weekly mid-morning sampling events still revealed significant relationships between [DIC] and Chl a, δ^{13}C-DIC, δ^{13}C-POC, ε_{app}, and pH, despite the potential for diel variability in [DIC].

Large increases in phytoplankton biomass, both as a result of phytoplankton growth and vertical migration of phytoplankton, cause the fastest increases in δ^{13}C-POC and the highest values of δ^{13}C-POC. While δ^{13}C-POC can change by up to 13.7 ‰ in a week, this magnitude of change is uncommon and short-lived. Since δ^{13}C-POC is relatively constant during periods of high biomass, organic matter that settles to the lake bottom from the top 3-4 m of the lake should reflect the high δ^{13}C-POC values observed during the phytoplankton blooms. Researchers have found that diel variability in δ^{13}C-POC can occur, and this should be investigated further to aid in interpreting the δ^{13}C-POC values of sediment cores.

The concentration of phytoplankton had a greater effect on δ^{13}C-POC than phytoplankton species composition. Constant access to DIC from the atmosphere might supply sufficient DIC to maintain a

higher value of ε_p in the epilimnion relative to 3 m. Lower [DIC] at 3 m in late summer forces phytoplankton to fix relatively more ^{13}C-DIC, increasing δ^{13}C-POC. A consistent supply of phosphorus leads to a similar biomass concentration each summer; these phytoplankton blooms create repeated seasonal patterns in epilimnion δ^{13}C-POC values, while vertical shifts of the biomass peak leads to variability in the measured δ^{13}C-POC values at 3 m. Understanding what sets the δ^{13}C-POC value on a seasonal timescale will aid in interpreting the δ^{13}C values of lake sediment.

Chapter 5: Conclusions

5.1 Tools for monitoring and modelling DIC in the aquatic carbon cycle

For this study, I deployed automated loggers, collected weekly geochemical and stable carbon isotope profiles, and collected hourly [DIC] and δ^{13}C-DIC samples on three occasions to investigate the sources of DIC and temporal variability in δ^{13}C-DIC and δ^{13}C-POC in L227. I combined my high-resolution data from 2018 with historical data from 2010-2017, and I analysed the geochemical and carbon stable isotope datasets with geochemical models, a two end-member isotope mixing model, and linear models.

Automatic loggers allowed for modeling the rates of GPP, ER, gas exchange, and CED with existing models in R. The 1 m GPP and ER rates I modeled with *LakeMetabolizer* revealed that both parameters vary on diel timescales, regardless of the density of the bloom. The rates were straightforward to model with readily available meteorological, temperature, and DO data, and were in the range of productivity estimates from previous bottle experiments. The rates of GPP and ER provided context for interpreting variability in δ^{13}C-DIC values and calculating the relative contributions of ER and gas exchange to the DIC pool.

The models for gas exchange and CED were also simple to reproduce in R. I estimated [DIC] at 15-minute intervals from continuous pH data and biweekly alkalinity data, and modelled the daily rates of CO_2 flux into or out of L227. I modeled β from pH, temperature, and windspeed data. Microstratification at the lake surface might have impacted my estimates of gas exchange, as I based my calculations on data recorded at 1 m. Additional temperature loggers deployed at the surface could confirm the presence and extent of microstratification, so that future research can model more accurate rates of gas exchange.

The continuous record of pH in L227 during the summer was valuable when analysing the δ^{13}C data. There was no indication from daytime values that pH could vary by up to 2.5 pH units over 24 hours, and

decreasing pH at night served as a useful proxy for an increase in [DIC]. From pH I was able to calculate the chemical enhancement factor and estimate values of gas exchange at regular intervals. Calculations such as DIC speciation and the chemical enhancement factor are sensitive to changes in pH, so care must be taken to monitor and re-calibrate pH probes deployed for long periods of time.

There was value in collecting sonde profiles at high spatial and temporal resolution. The weekly sonde profiles at 0.25 m intervals revealed that cyanobacteria migrate to the bottom of the metalimnion over the ice-free season. Integrated sampling methods can cause dilution of phytoplankton samples when phytoplankton are congregated at a narrower range in depth, leading to the perception of a population crash. Surface samples may not be indicative of bloom dynamics in lakes where the bloom is not contained near the surface.

The overnight sampling events showed that diel change in the values of δ^{13}C-DIC may or may not occur. The hourly overnight δ^{13}C-DIC measurements provided context for interpreting the mid-morning δ^{13}C-DIC values, which were not as high as expected given the potential for high photosynthetic fractionation when biomass is high. Less frequent sampling over a 24 period, including dawn, mid-day, and at night, is a more practical way to investigate the drivers of diel change in δ^{13}C-DIC values.

Geochemical models for gas exchange, CED, and lake metabolism are easy to use and require input from common data loggers. Future study of the aquatic carbon cycle at L227 should include continuous recording of temperature, DO, and pH at 1 m, and potentially at the depth of highest phytoplankton biomass. An automatic logger capable of recording [CO_2] would be beneficial for accurately measuring overnight change in DIC.

5.2 Relative contributions of DIC sources to L227

Gas exchange and ER are the main sources of DIC to L227, but the relative contributions of each source vary on daily timescales. Lake metabolism controls DIC in the epilimnion during the blooms, while gas

exchange is a more important source during the lower-biomass period. CED can double or triple the rate of gas exchange during the day when pH is above 9, but the rate of gas exchange remains low.

ER was the dominant source of DIC during the phytoplankton blooms, but the daily rate of ER is not consistent on a daily timescale. The positive linear relationship between ER and the magnitude of daily pH change indicates that the rate of ER drives an increase in [DIC], which causes pH to decrease overnight. The low values of δ^{13}C-DIC when the concentration of Chl a is highest could reflect higher rates of ER during phytoplankton blooms.

Gas exchange contributes a consistent, low daily amount of DIC to L227. Despite the potential for CED to double the rate of gas exchange with the atmosphere for an extended period on most summer days, the rate of gas exchange is low compared to ER. L227 tends to act as a sink for atmospheric CO_2, but during the lower-biomass period in the epilimnion the lake can serve as a CO_2 source to the atmosphere.

The concentration of DIC does not increase consistently between sunset and sunrise, despite photosynthesis stopping; there can be a relatively small or large increase overnight, and the increase can occur quickly. Microstratification at the surface could impede gas exchange with the atmosphere in L227, or the rate of ER could be low. When the overnight change in [DIC] is low, there is little change in the δ^{13}C-DIC value. The lack of change in [DIC] and δ^{13}C-DIC values overnight makes it difficult to interpret the low values.

5.3 Temporal and spatial variability in δ^{13}C-DIC and δ^{13}C-POC values

Values of δ^{13}C-DIC and δ^{13}C-POC vary at different timescales and by depth in L227. δ^{13}C-DIC values varied on hourly to weekly timescales, and changes were related to the daily amounts of primary productivity. Changes in δ^{13}C-POC occurred on weekly timescales or greater and were related to increases and decreases in phytoplankton biomass as blooms developed and shifted in the water column.

This study is one of very few that report overnight values of δ^{13}C-DIC in a lake. The potential range of δ^{13}C-DIC values on a diel timescale is higher than in existing studies. The value of δ^{13}C-DIC can remain relatively consistent overnight or decrease by up to 18 ‰ between sunset and sunrise. On a diel timescale, variation in [DIC] controls δ^{13}C-DIC. A high daytime rate of productivity and low [DIC] cause the value of δ^{13}C-DIC to increase as phytoplankton preferentially fix ^{12}C-CO_2. Strong diel fluctuations in the value of δ^{13}C-DIC could affect calculations of ε_{app}, as δ^{13}C-POC values change at a slower rate. During the epilimnion blooms, when pH is high enough during the day that most of the DIC pool is HCO_3^-, δ^{13}C-DIC remains low. Efficient CCMs that reduce CO_2 leakage and isotopic fractionation by RuBisCO when [DIC] is low could explain why δ^{13}C-DIC does not increase during epilimnion blooms.

This study is also one of few that reports δ^{13}C-POC samples for multiple seasons spanning 10 years. Understanding interannual variability in δ^{13}C-POC is of interest for interpreting sediment core δ^{13}C values. Interannual variability in δ^{13}C-POC is low during the ice-free season, with similar δ^{13}C-POC values and patterns in change at 1 m and 3 m. A consistent supply of P allows phytoplankton blooms to develop each year. On a seasonal timescale, the concentration of biomass drives increases and decreases in [DIC], which in turn controls the values of δ^{13}C-DIC, δ^{13}C-POC, and ε_{app}. The values of δ^{13}C-POC remain relatively consistent while L227 is thermally stratified; large changes in δ^{13}C-POC values at a discrete depth do not span multiple weeks. A consistent, high value of δ^{13}C-POC during summer phytoplankton blooms should result in high sediment δ^{13}C values, but this has not occurred in L227. Sediment δ^{13}C analysis of surficial sediment and a more recent core should be conducted to determine if the δ^{13}C value of seston is comparable to that of the sediments.

The spatial distribution of phytoplankton affects δ^{13}C-POC values at discrete depths. The greatest rate of change and highest δ^{13}C-POC value occurred when the phytoplankton bloom descended to 3 m. The high δ^{13}C-POC value did not persist for more than 2 weeks at this depth, but vertical migration could have led to higher δ^{13}C-POC at depths where I did not collect samples. Sampling at a higher spatial

resolution during the blooms or targeting discrete depths with the highest concentration of biomass would confirm whether the δ^{13}C-POC value of the most concentrated area of the bloom varies with time.

These results highlight the importance of choosing a monitoring regime or long-term dataset that best aligns with the research question. Eutrophic, soft water lakes are susceptible to diel fluctuations in [DIC] and may require higher temporal resolution for some monitoring parameters. Sampling at a higher spatial resolution or targeting the depth of the biomass peak over time may be necessary to study blooms situated below a well-mixed epilimnion.

Appendix A: Supplemental Figures

Figure A1: Bathymetric map of Lake 227. The centre buoy marks the deepest point in the lake, 10 m.

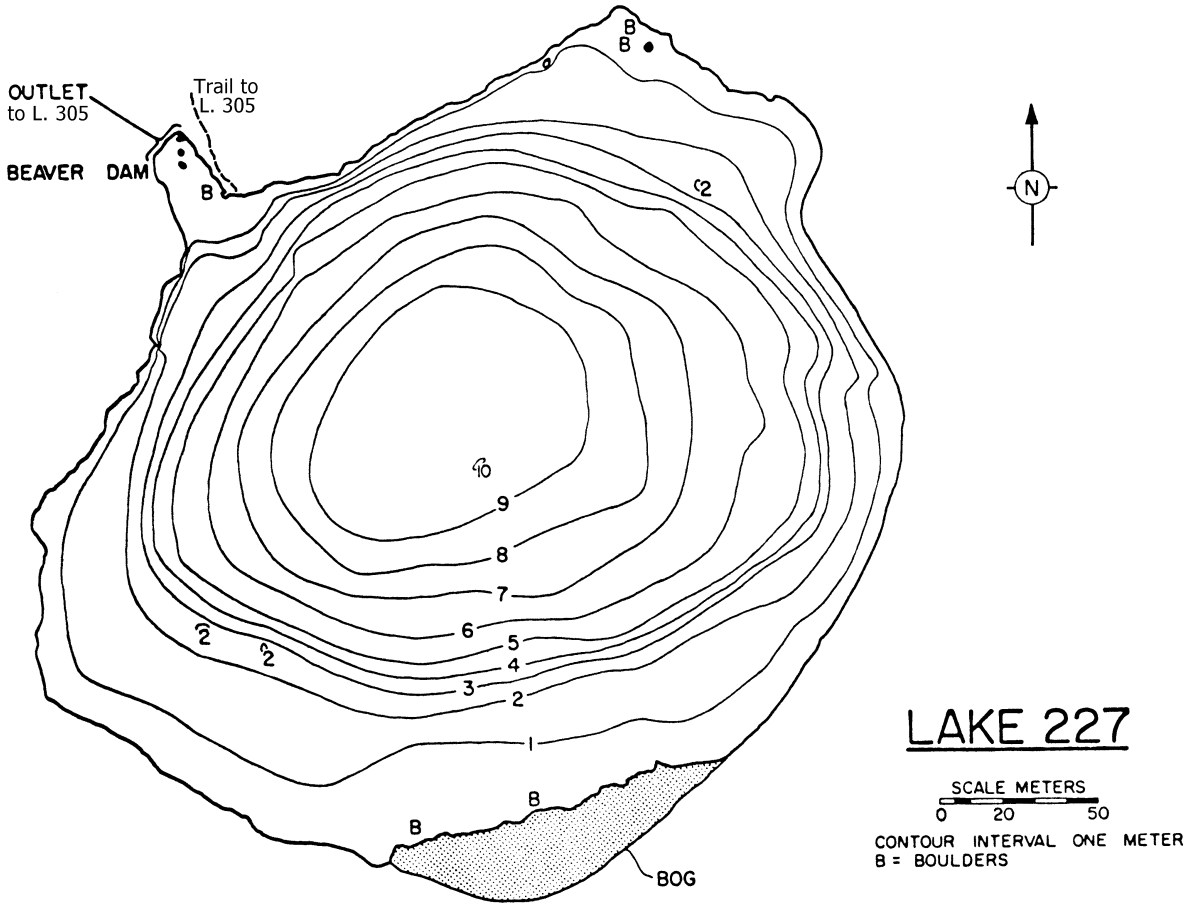

Figure A2: Theoretical values of chemically enhanced fractionation (CEF) over a range of pH values at six different wind speed and water temperature conditions. The darker colour in each group represents the modelled value of CEF at 25 °C, and the lighter colour at 10 °C. The three 10 m wind speeds represent the minimum, median, and maximum wind speeds at the IISD-ELA meteorological station from May 1-September 30, 2018.

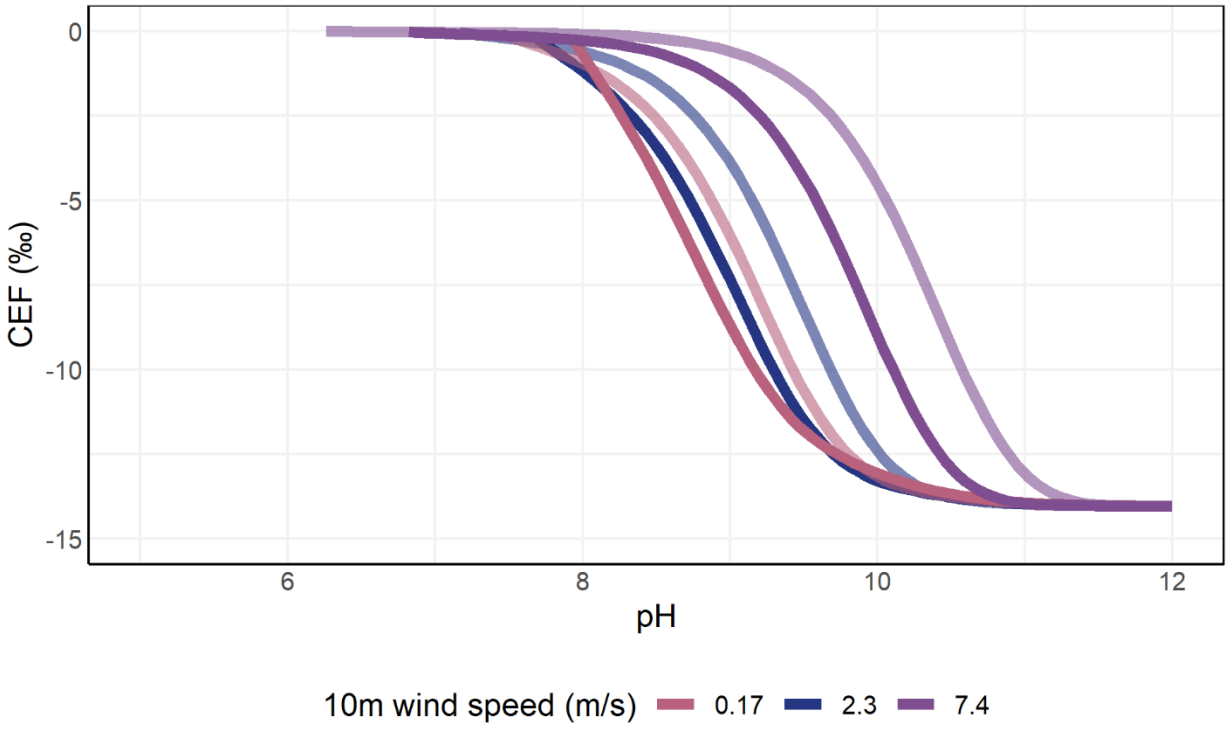

Figure A3: Weekly DIC and Chl a concentrations for 1 m and 3 m (2018) and the integrated epilimnion and metalimnion (2019) in L227. Dashed lines mark the overnight sampling events, and grey circles indicate the overnight values of [DIC]. In 2018 we sampled L227 weekly, while in 2019 IISD-ELA researchers sampled the lake monthly as part of their long-term ecological research (LTER) program.

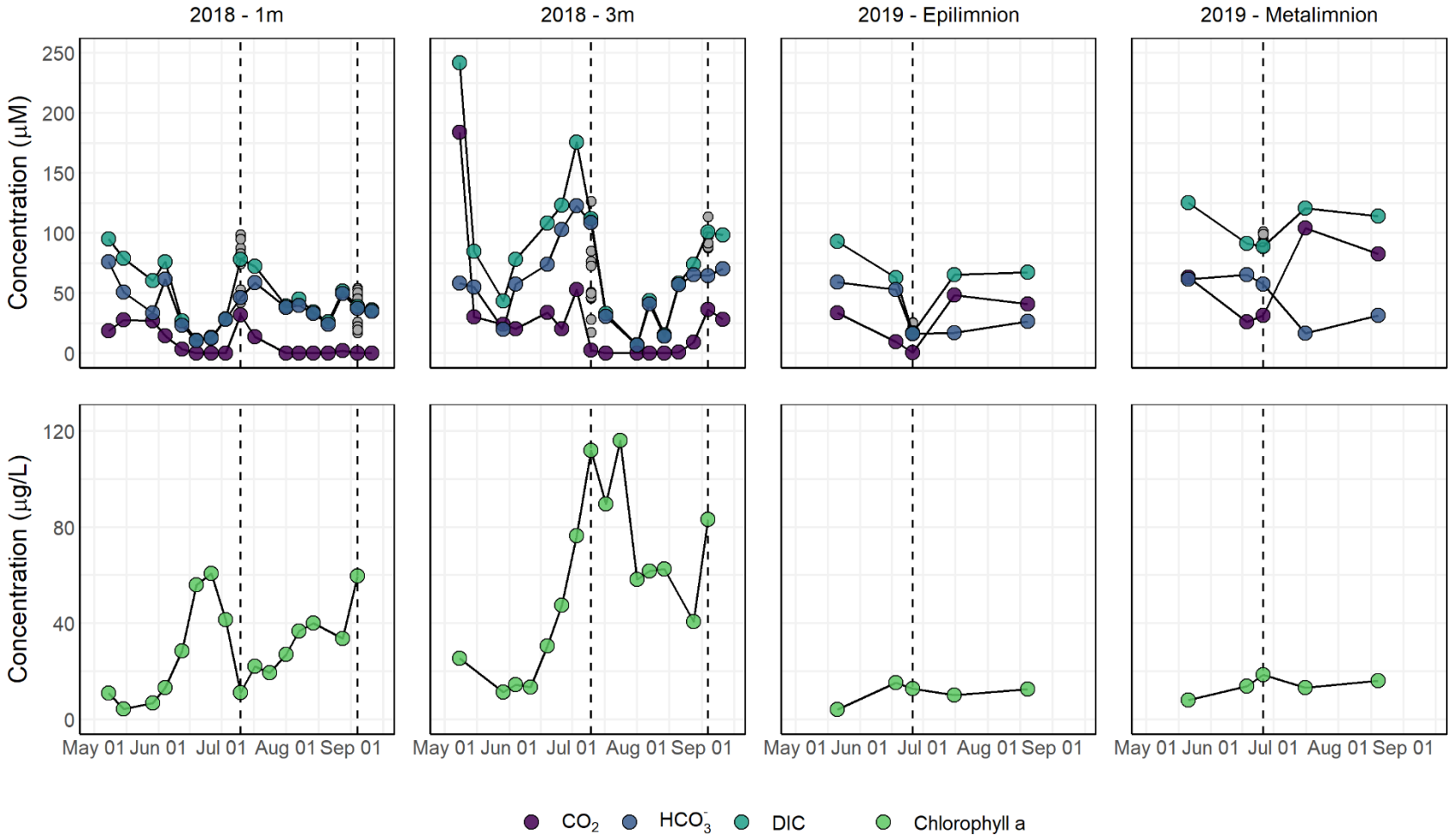

Figure A4: 2018 weekly concentration profiles of phycocyanin, a pigment indicating the concentration of cyanobacteria (BGA, µg L^{-1}); dissolved oxygen (DO, mg L^{-1}); and pH for the top 5 m of L227. Orange circles represent the bottom of the epilimnion (temperature change greater than 0.25 °C/0.25 m), and orange squares represent the bottom of the metalimnion (1% light). I took measurements at 0.25 m intervals at the deepest part of the lake (10 m). There is little change in these parameters below 5 m.

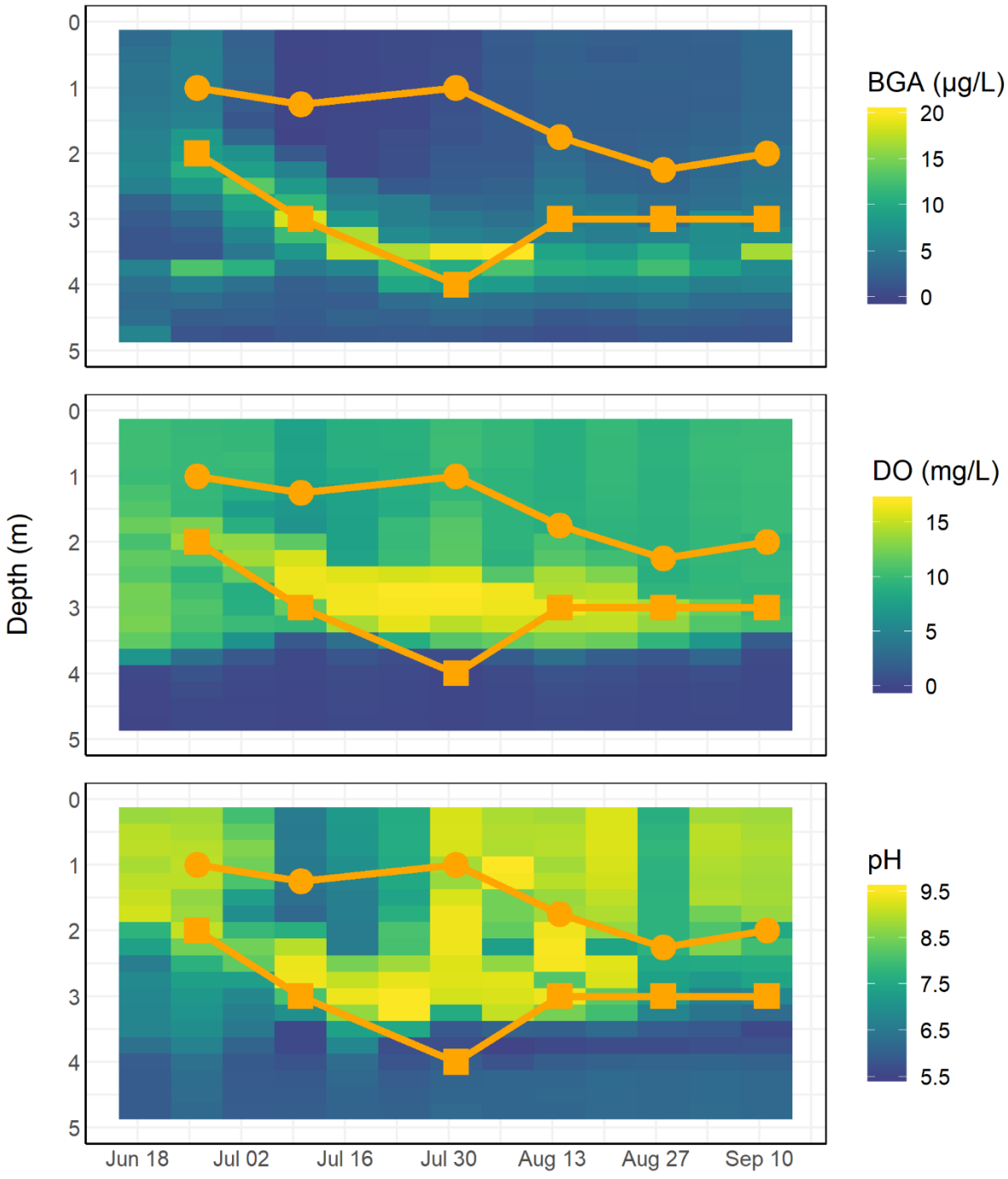

Figure A5: Daily maximum and minimum pH values for July 26-September 11, 2018 recorded from 1 m depth at the L227 centre buoy.

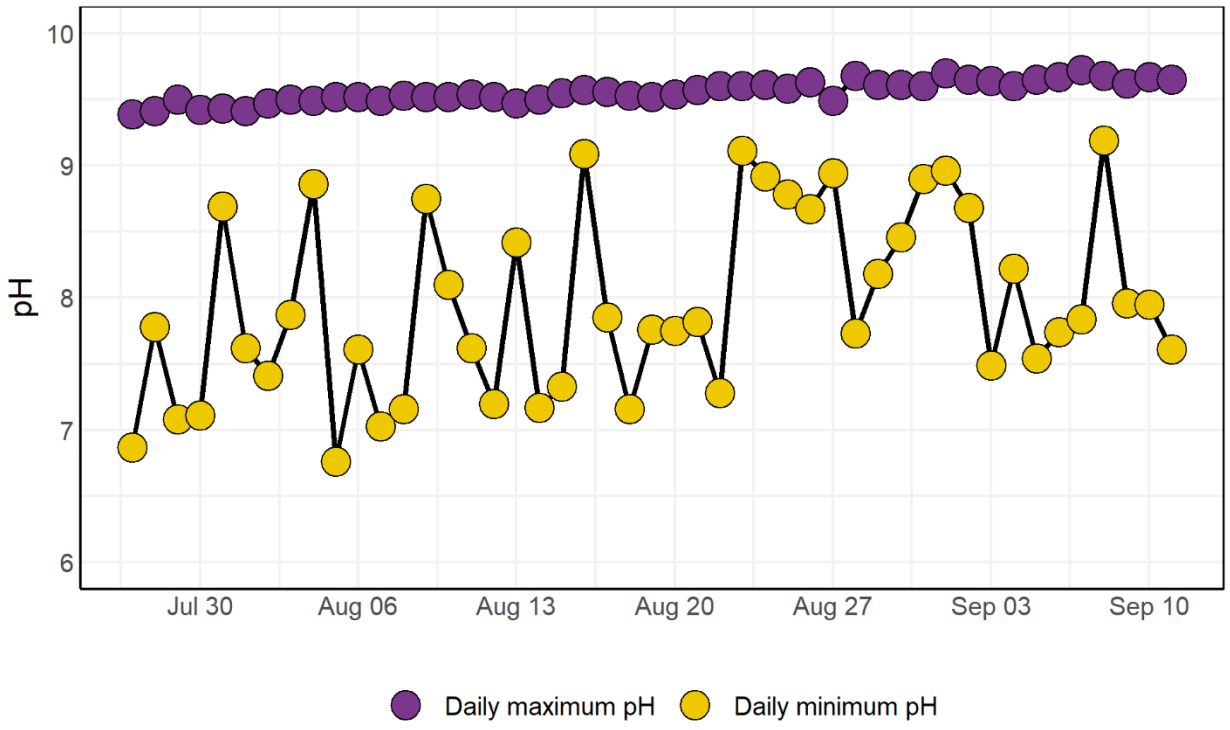

Figure A6: Measured pH values and calculated values of the chemical enhancement factor (*β*) and chemically enhanced fractionation (CEF) at 1 m every 6 hours in L227 during the summer of 2018. Prior to July 25 there was no continuous data recording, and we recorded manual pH measurements weekly at approximately 10:00 CST.

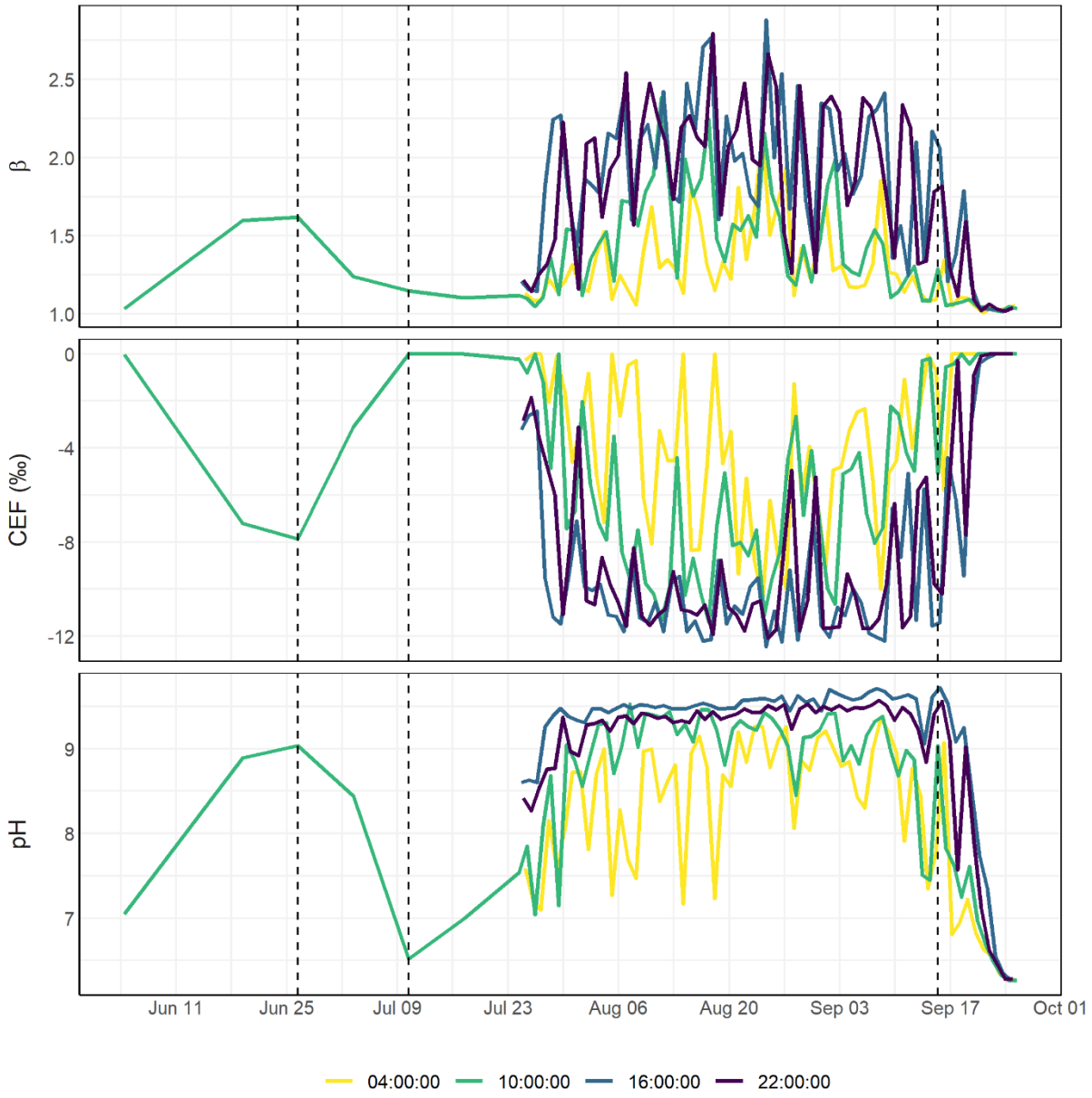

Figure A7: Summary of overnight δ^{13}C-DIC and pH values from a depth of 3 m at the L227 centre buoy (points), and δ^{13}C-DIC end-member values for ecosystem respiration (ER; lines). The δ^{13}C-DIC end-member for ER is equal to the δ^{13}C-POC value on the day of sampling.

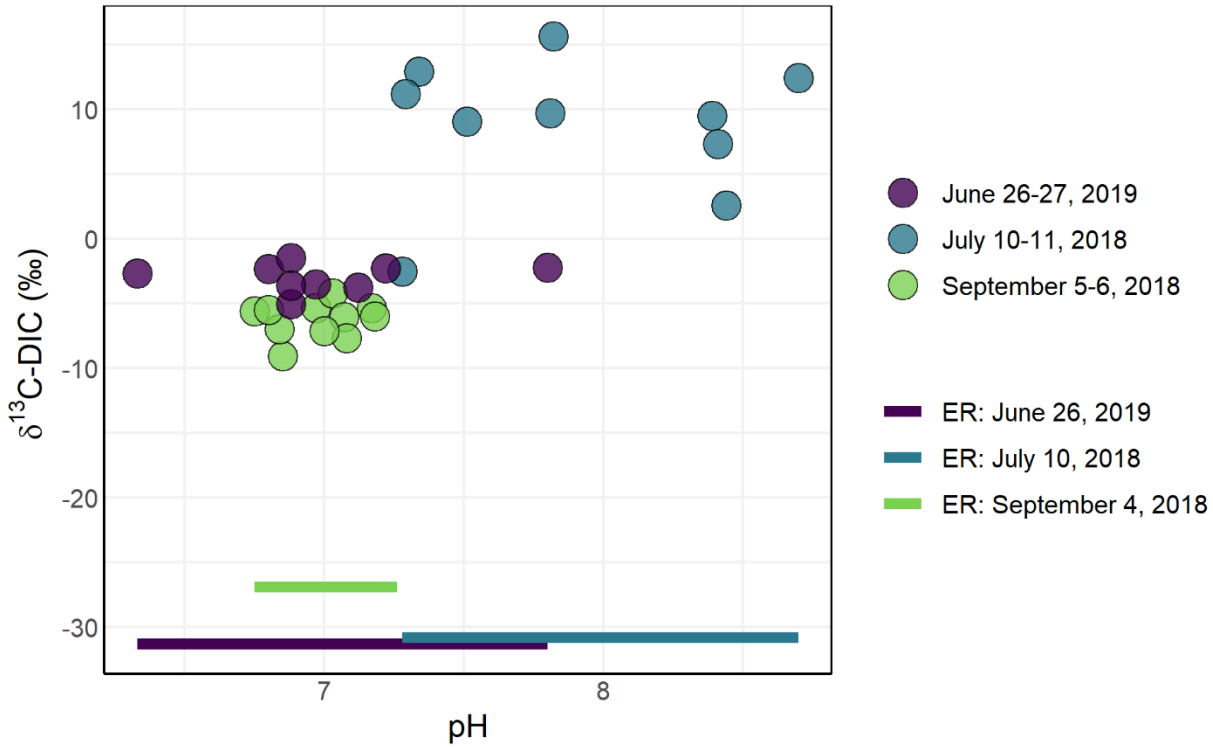

Figure A8: Dissolved CO_2 concentration at 1 m in L227 during the summer of 2018. I calculated [CO_2] from continuous pH and temperature measurements, and bi-weekly integrated epilimnion alkalinity values. I assumed that the epilimnion was well mixed, that alkalinity was constant on a diel timescale, and that change in alkalinity from day to day linear. I applied the function $\mathbf{geom\_smooth(method = 'loess', y \sim x)}$ to improve visibility of the diurnal pattern. The dashed line is 14 uM CO_2, the approximate value of dissolved CO_2 in equilibrium with the atmosphere. Note the logarithmic scale.

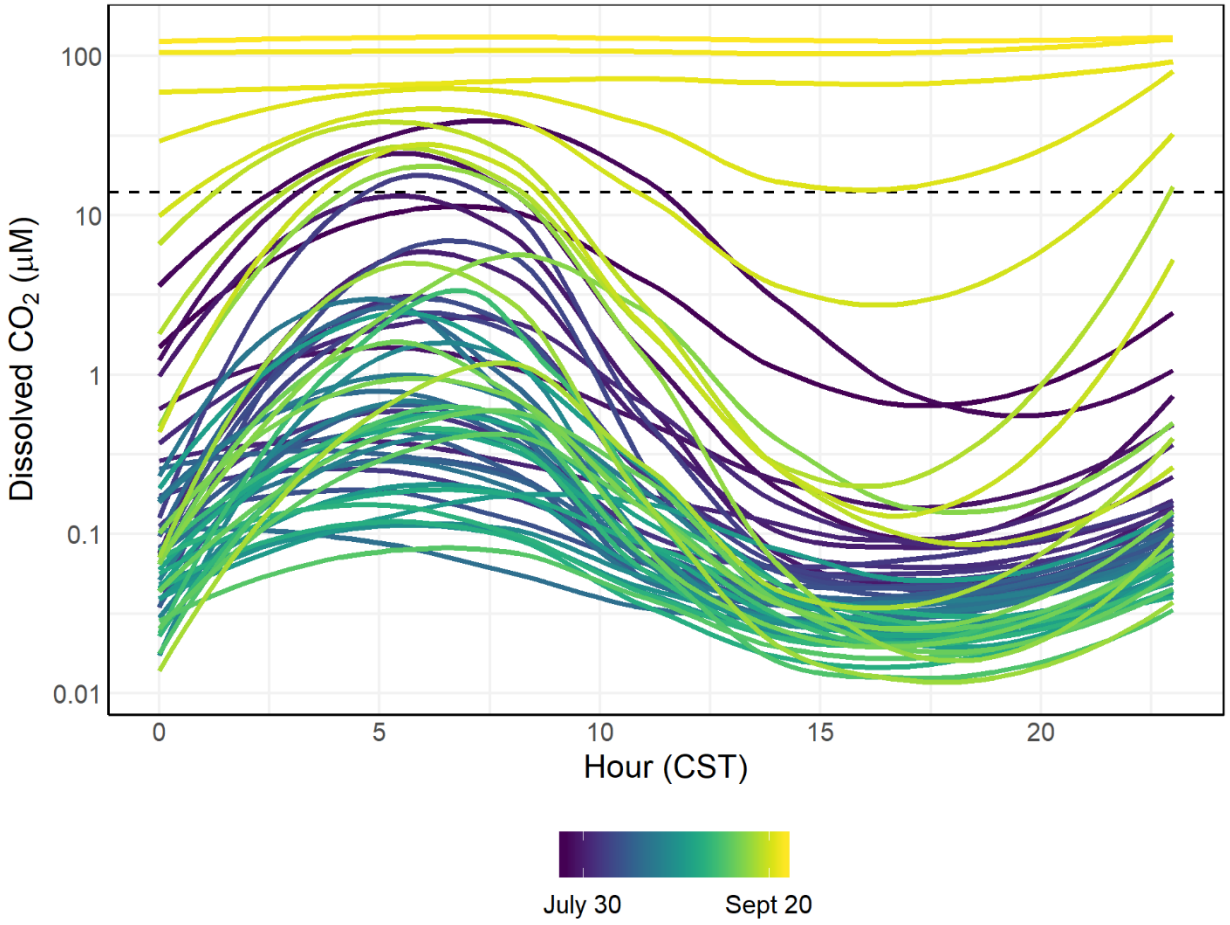

Figure A9: Daily rates of ecosystem respiration and gas exchange at 1m in L227 from July 27-September 11, 2018. I modelled ecosystem respiration values from continuous dissolved oxygen and temperature data with the R package *LakeMetabolizer* (Winslow et al., 2016). I estimated gas exchange values from alkalinity and pH measurements at different timescales (see section 3.4, *L227 as a CO_2 source and sink*, in the text). Gas exchange estimates account for chemically enhanced diffusion.

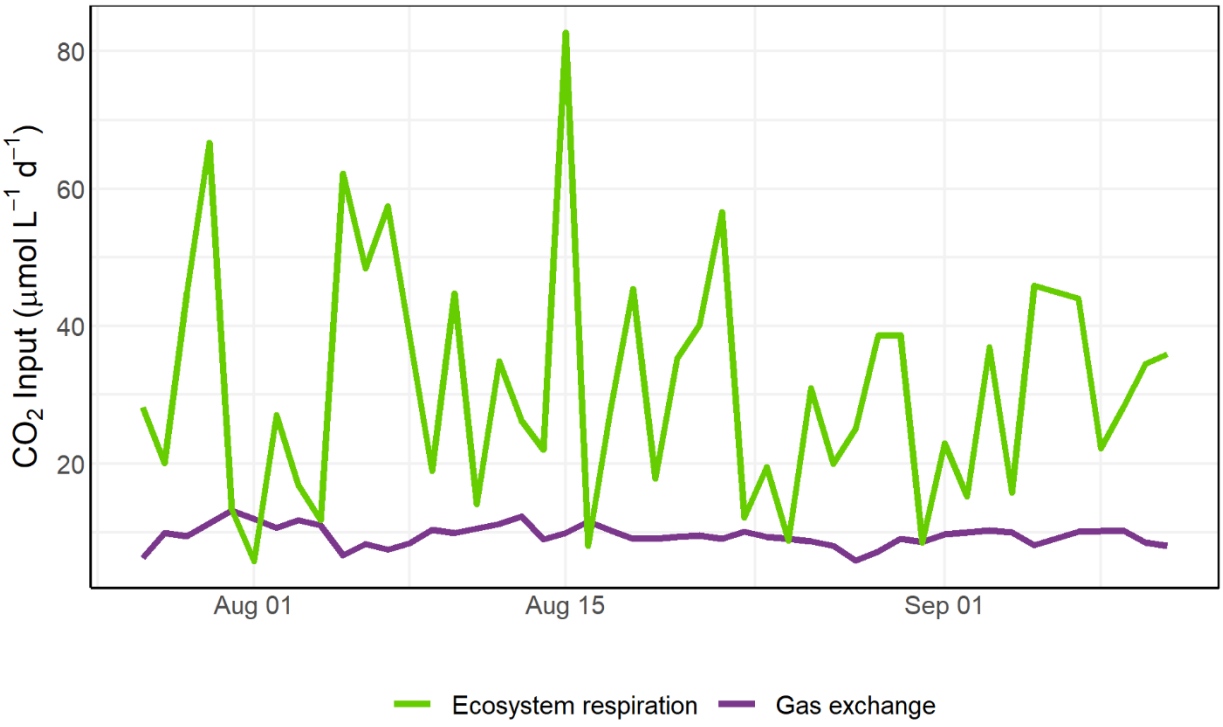

Figure A10: Rates of gross primary productivity (GPP), net ecosystem productivity (NEP) and ecosystem respiration (ER) at 1 m in L227 at centre buoy during late summer 2018, and from May-September 2019. I converted the rate of R from µmol O_2 L^{-1} d^{-1} produced to µmol CO_2 L^{-1} d^{-1} consumed with a respiratory quotient of 0.81 (Berggren et al., 2012).

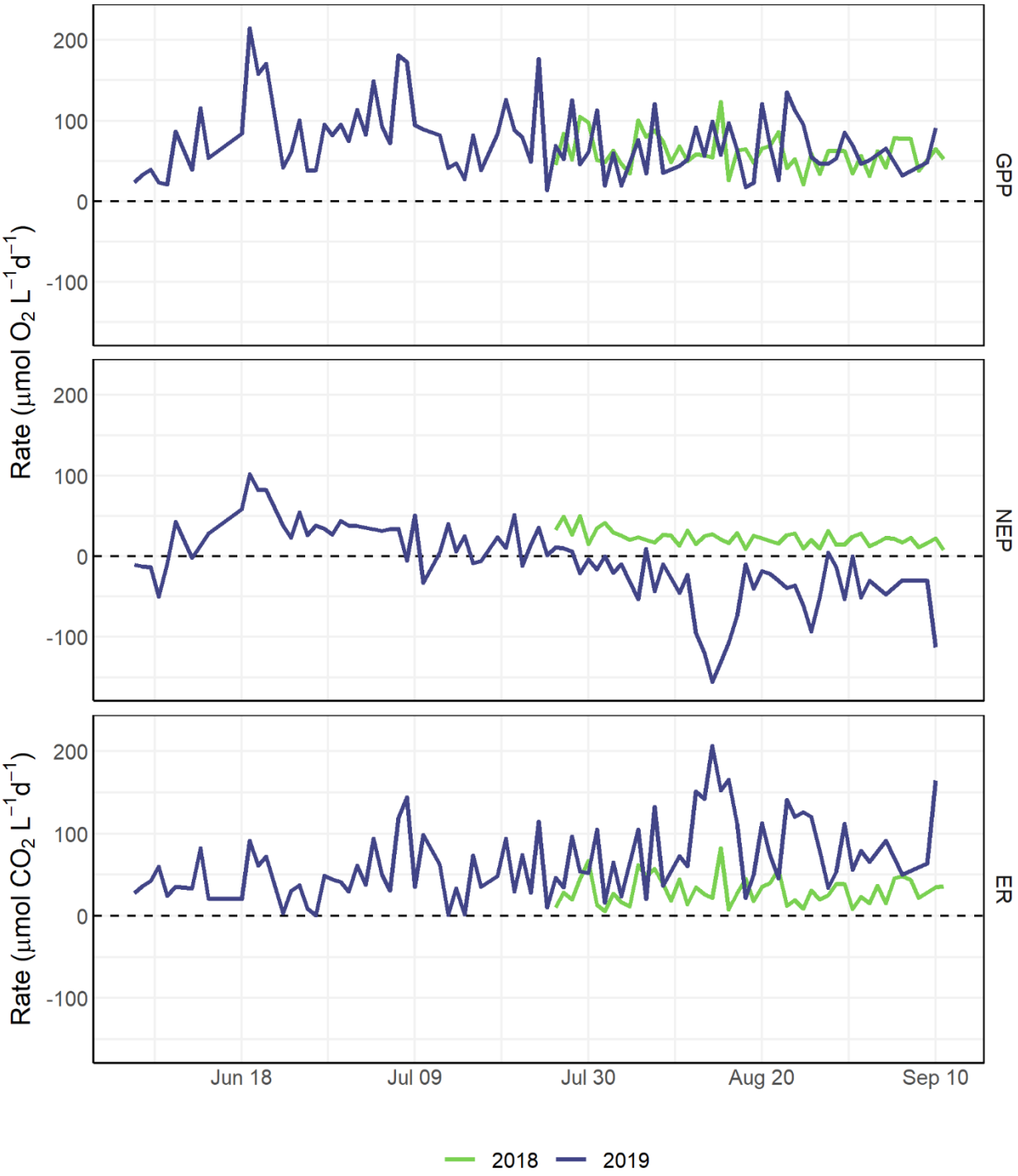

Figure A11: The relationship between δ^{13}C-POC, Chl a, and [DIC] at 3 m in L227 from 2011-2018. Researchers collected all δ^{13}C-POC samples from a depth of 3 m at CB. Chl a and [DIC] samples in 2011-2016 are from the integrated metalimnion, while samples in 2017-2018 are from 3 m.

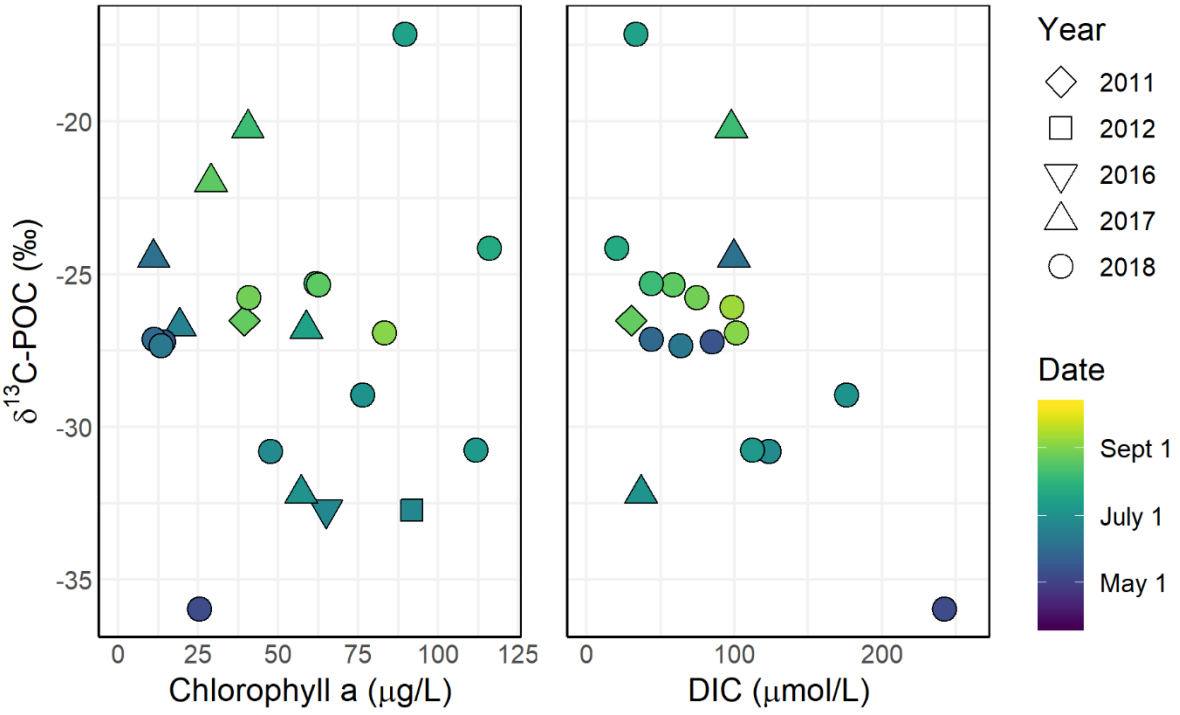

References

Åberg, J., Jansson, M., & Jonsson, A. (2010). Importance of water temperature and thermal stratification dynamics for temporal variation of surface water CO_2 in a boreal lake. *Journal of Geophysical Research, 115(G2)*. https://doi.org/10.1029/2009JG001085

Anderson, N.J., Heathcote, A.J., & Engstrom, D.R. (2020). Anthropogenic alteration of nutrient supply increases the global freshwater carbon sink. *Science Advances, 6*(16). https://doi.org/10.1126/sciadv.aaw2145

Bade, D.L., Carpenter, S.R., Cole, J.J., Hanson, P.C., & Hesslein, R.H. (2004). Controls of δ^{13}C-DIC in lakes: Geochemistry, lake metabolism, and morphometry. *Limnology and Oceanography, 49*(4), 1160-1172. https://doi.org/10.4319/lo.2004.49.4.1160

Bade, D.L., & Cole, J.J. (2006). Impact of chemically enhanced diffusion on dissolved inorganic carbon stable isotopes in a fertilized lake. *Journal of Geophysical Research, 11*, C01014. https://doi.org/10.1029/2004JC002684

Bade, D.L., Pace, M.L., Cole, J.J., & Carpenter, S.R. (2006). Can algal photosynthetic inorganic carbon isotope fractionation be predicted in lakes using existing models? *Aquatic Sciences, 68*, 142-153. https://doi.org/10.1007/s00027-006-0818-5

Badger, M.R. (2003). The roles of carbonic anhydrases in photosynthetic CO_2 concentrating mechanisms. *Photosynthesis Research, 77*, 83-94. https://doi.org/10.1023/A:1025821717773

Badger, M.R., & Price, G.D. (2003). CO2 concentrating mechanisms in cyanobacteria: molecular components, their diversity and evolution. Journal of Experimental Botany, 54(383), 609-622. https://doi.org/10.1093/jxb/erg076

Balmer, M.B., & Downing, J.A. (2011). Carbon dioxide concentrations in eutrophic lakes: undersaturation implies atmospheric uptake. *Inland Waters, 1*(2), 125-132. https://doi.org/10.5268/IW-1.2.366

Bastviken, D., Cole, J.J., Pace, M.L., Van de Bogert, M.C. (2008). Fates of methane from different lake habitats: Connecting whole-lake budgets and CH_4 emissions. *Biogeosciences, 113*(G2). https://doi.org/10.1029/2007JG000608

Battin, T.J., Luyssaert, S., Kaplan, L.A., Aufdenkampe, A.K., Richter, A., & Tranvik, L.J. (2009). The boundless carbon cycle. *Nature Geoscience, 2*, 598-600. https://doi.org/10.1038/ngeo618

Berggren, M., Lapierre, J.L., & del Giorgio, P.A. (2012). Magnitude and regulation of bacterioplankton respiratory quotients across freshwater environmental gradients. *The ISME Journal, 6*, 984-993. https://doi.org/10.1038/ismej.2011.157

Bogard, M.J., & del Giorgio, P.A. (2016). The role of metabolism in modulating CO_2 fluxes in boreal lakes. *Global Biogeochemical Cycles, 30*(10), 1509-1525. https://doi.org/10.1002/2016GB005463

Bontes, B.M., Pel, R., Ibelings, B.W., Boschker, H.T.S., Middelburg, J.J., & Van Donk, E. (2006). The effects of biomanipulation on the biogeochemistry, carbon isotopic composition and pelagic food web relations of a shallow lake. *Biogeosciences, 3*, 69-83. https://doi.org/10.5194/bg-3-69-2006

Brugnoli, E., & Farquhar, G.D. (2000). Photosynthetic fractionation of carbon isotopes. In: Leegood, R.C., Sharkey, T.D., & von Caemmerer, S. (Eds.) *Photosynthesis: Advances in Photosynthesis and Respiration* (Vol 9, pp. 399-434). Springer. https://doi.org/10.1007/0-306-48137-5

Carpenter, S.R., Caraco, N.F., Correll, D.L., Howarth, R.W., Sharpley, A.N., & Smith, V.H. (1998). Nonpoint pollution of surface waters with phosphorus and nitrogen. *Ecological Applications, 8*(3), 559-568. https://doi.org/10.1890/1051-0761(1998)008[0559:NPOSWW]2.0.CO;2

Carpenter, S.R. (2008). Phosphorus control is critical to mitigating eutrophication. *Proceedings of the National Academy of Sciences, 105*(32), 11039-11040. https://doi.org/10.1073/pnas.0806112105

Charlton, M.N., Milne, J.E., Booth, W.G., & Chiocchio, F. (1993). Lake Erie offshore in 1990: Resoration and resilience in the central basin. *Journal of Great Lakes Research, 19*(2), 291-309. https://doi.org/10.1016/S0380-1330(93)71218-6

Chapin, F.S., III, Woodwell, G.M., Randerson, J.T., Tastetter, E.B., Lovett, G.M., Baldocchi, D.D., Clark, D.A., Harmon, M.E., Schimel, D.S., Valentini, R., Wirth, C., Aber, J.S., Cole, J.J., Goulden, M.K., Harden, W.J., Heimann, M., Howarth, R.W., Matson, P.A., McGuire, A.D., … Schulze, E.D. (2006). Reconciling carbon-cycle concepts, terminology, and methods. *Ecosystems, 9*, 1041-1050. https://doi.org/10.1007/s10021-005-0105-7

Cole, J.J., Caraco, N.F., Kling, G.W., & Kratz, T.K. (1994). Carbon dioxide supersaturation in the surface waters of lakes. *Science, 265*(5178), 1568-1570. https://doi.org/10.1126/science.265.5178.1568

Cole, J.J., Prairie, Y.T., Caraco, N.F., McDowell, W.H., Tranvik, L.J., Striegl, R.G., Duarte, C.M., Kortelainen, P., Downing, J.A., Middelburg, J.J., & Melack, J. (2007). Plumbing the global carbon cycle: Integrating inland waters into the terrestrial carbon budget. *Ecosystems, 10*, 172-185. https://doi.org/10.1007/s10021-006-9013-8

Coloso, J.J., Cole, J.J., & Pace, M.L. (2011). Short-term variation in thermal stratification complicates estimation of lake metabolism. *Aquatic Sciences, 73*, (305-315). https://link.springer.com/article/10.1007/s00027-010-0177-0

del Giorgio, P.A., & Peters, P.H. (1993). Balance between phytoplankton production and plankton respiration in lakes. *Canadian Journal of Fisheries and Aquatic Sciences, 50*(2), 282-289. https://doi.org/10.1139/f93-032

DelSontro, T, Beaulieu, J.J., & Downing, J.A. (2018). Greenhouse gas emissions from lakes and impoundments: Upscaling in the face of global change. *Limnology and Oceanography Letters, 3*(3), 64-75. https://doi.org/10.1002/lol2.10073

Dove, A., & Chapra, S.C. (2015). Long-term trends of nutrients and trophic response variables for the Great Lakes. *Limnology and Oceanography, 60*(2), 696-721. https://doi.org/10.1002/lno.10055

Dubois, K., Carignan, R., & Veizer, J. (2009). Can pelagic net heterotrophy account for carbon fluxes from eastern Canadian lakes? *Applied Geochemistry, 24*(5), 988-998. https://doi.org/10.1016/j.apgeochem.2009.03.001

Elser, J.J., Sterner, R.W., Galford, A.E., Chrzanowski, T.H., Findlay, D.K., Mills, K.H., Paterson, M.J., Stainton, M.P., & Schindler, D.W. (2000). Pelagic C:N:P stoichiometry in a eutrophied lake: Responses to a whole-lake food-web manipulation. *Ecosystems, 3*, 292-307. https://doi.org/10.1007/s100210000027

Emerson, S. (1975). Chemically enhanced CO_2 gas exchange in a eutrophic lake: A general model. *Limnology and Oceanography, 20*(5), 743-753. https://doi.org/10.4319/lo.1975.20.5.0743

Environment and Climate Change Canada. (2019). *National Inventory Report 1990–2017: Greenhouse Gas Sources and Sinks in Canada: Executive Summary*. http://publications.gc.ca/pub?id=9.816345&sl=0

Falkowski, P.G. (1991). Species variability in the fractionation of ^{13}C and ^{12}C by marine phytoplankton. *Journal of Plankton Research, 13,* 21-28. https://doi.org/10.1093/oxfordjournals.plankt.a042367

Falkowski, P.G., & Raven, J.A. (2007). *Aquatic Photosynthesis* (2nd Ed.). Princeton University Press.

Farquhar, G.D. & Richards, R.A. (1984). Isotopic composition of plant carbon correlates with water-use efficiency of wheat genotypes. *Australian Journal of Plant Physiology, 11*(6), 539-552. https://doi.org/10.1071/PP9840539

Farquhar, G.D., Ehleringer, J.R., & Hubick, K.T. (1989). Carbon isotope discrimination and photosynthesis. *Annual Review of Plant Physiology and Plant Molecular Biology, 40*, 503-537. https://doi.org/10.1146/annurev.pp.40.060189.002443

Flett, R.J., Schindler, D.W., Hamilton, R.D., & Campbell, N.E.R. (1980). Nitrogen fixation in Canadian Precambrian shield lakes. *Canadian Journal of Fisheries and Aquatic Sciences, 37*(3), 494-505. https://doi.org/10.1139/f80-064

Flinn, N.A.P. (2012). The use of stable nitrogen and carbon isotopes to examine the sources, sinks and cycling of nitrogen in a small, artificially eutrophic Boreal lake [Master's thesis, University of Waterloo]. UWSpace.

Fielding, A.S., Turpin, D.H., Guy, R.D., Calvert, S.E., Crawford, D.W., & Harrison, P.J. (1998). Influence of the carbon concentrating mechanism on carbon stable isotope discrimination by the marine diatom *Thalassiosira pseudonana*. *Canadian Journal of Botany, 76*(6), 1098-1103. https://doi.org/10.1139/b98-069

Finlay, J.C. (2003). Controls of streamwater dissolved inorganic carbon dynamics in a forested watershed. *Biogeochemistry, 62*, 231-252. https://doi.org/10.1023/A:1021183023963

Fogel, M.L., & Cifuentes, L.A. 1993. Isotope fractionation during primary production. In Engel, M.H. & Macko, S.A. (Eds.), *Organic Geochemistry* (pp. 73–98). Plenum Press. https://doi.org/10.1007/978-1-4615-2890-6

Gammons, C.H., Babcock, J.N., Parker, S.R., & Poulson, S.R. (2011). Diel cycling and stable isotopes of dissolved oxygen, dissolved inorganic carbon, and nitrogenous species in a stream receiving treated municipal sewage. *Chemical Geology, 283*(1-2), 44-55. https://doi.org/10.1016/j.chemgeo.2010.07.006

Giordano, M., Beardall, J., & Raven, J.A. (2005). CO_2 concentrating mechanisms in algae: Mechanisms, environmental modulation, and evolution. Annual Review of Plant Biology, *56*, 99-131. https://doi.org/10.1146/annurev.arplant.56.032604.144052

Goldman, J.C., McCarthy, J.J., & Peavey, D.G. (1979). Growth rate influence on the chemical composition of phytoplankton in oceanic waters. *Nature, 279*, 210-215. https://doi.org/10.1038/279210a0

Gu, B., Chapman, A.D., & Schelske, C.L. (2006). Factors controlling seasonal variations in stable isotope composition of particulate organic matter in a soft water eutrophic lake. *Limnology and Oceanography, 51*(6), 283-2848. https://doi.org/10.4319/lo.2006.51.6.2837

Hanson, P.C., Carpenter, S.R., Armstrong, D.E., Stanley, E.H., & Kratz, T.K. (2006). Lake dissolved inorganic carbon and dissolved oxygen: changing drivers from days to decades. *Ecological Monographs, 76*(3), 343-363. https://doi.org/10.1890/0012-9615(2006)076[0343:LDICAD]2.0.CO;2

Hanson, P.C., Carpenter, S.R., Kimura, N., Wu, C., Cornelius, S.P., & Kratz, T.K. (2008). Evaluation of metabolism models for free-water dissolved oxygen methods in lakes. *Limnology and Oceanography: Methods, 6*(9), 454-465. https://doi.org/10.4319/lom.2008.6.454

Harned, H.S., & Scholes, S.R., Jr. (1941). The ionization constant of HCO_3^- from 0 to 50°. *Journal of the American Chemical Society, 63*(6), 1706-1709. https://doi.org/10.1021/ja01851a058

Harned, H.S., & Davies, R., Jr. (1943). The ionization constant of carbonic acid in water and the solubility of carbon dioxide in water and aqueous salt solutions from 0 to 50°. *Journal of the American Chemical Society, 65*(10), 2030-2037. https://doi.org/10.1021/ja01250a059

Hayes, J.M. (1993). Factors controlling ^{13}C contents of sedimentary organic compounds: Principles and evidence. *Marine Geology, 113*, 111-125. https://doi.org/10.1016/0025-3227(93)90153-M

Healey, F.P., & Hendzel, L.L. (1980). Physiological indicators of nutrient deficiency in lake phytoplankton. *Canadian Journal of Fisheries and Aquatic Sciences, 37*(3), 442-453. https://doi.org/10.1139/f80-058

Hecky, R.E., Campbell, P., Hendzel, L.L. (1993). The stoichiometry of carbon, nitrogen, and phosphorus in particulate matter of lakes and oceans. *Limnology and Oceanography, 38*(4), 709-724. https://doi.org/10.4319/lo.1993.38.4.0709

Heisler, J., Glibert, P.M., Burkholder, J.M., Anderson, D.M., Cochlan, W., Dennison, W.C., Dortch, Q., Gobler, C.J., Heil, C.A., Humphries, E., Lewitus, A., Magnien, R., Marshall, H.G., Sellner, K., Stockwell, D.A., Stoecker, D.J., & Suddleson, M. (2008). Eutrophication and harmful algal blooms: A scientific consensus. *Harmful Algae, 8*(1), 3-13. https://doi.org/10.1016/j.hal.2008.08.006

Herczeg, A.L., & Fairbanks, R.G. (1987). Anomalous carbon isotope fractionation between atmospheric CO_2 and dissolved inorganic carbon induced by intense photosynthesis. *Goechimica et Cosmochimica Acta, 51*(4), 895-899. https://doi.org/10.1016/0016-7037(87)90102-5

Higgins, S.N., Paterson, M.J., Hecky, R.E., Schindler, D.W., Venkiteswaran, J.J., & Findlay, D.L. (2018). Biological nitrogen fixation prevents the response of a eutrophic lake to reduced loading of nitrogen: Evidence from a 46-year whole-lake experiment. *Ecosystems, 21*, 1088-1100. https://doi.org/10.1007/s10021-017-0204-2

Hoagland, P., & Scatasta, S. (2006). The economic effects of harmful algal blooms. In Granéli, E. & Turner, J. (Eds.), *Ecology of Harmful Algae* (pp. 391-402). Springer. https://doi.org/10.1007/978-3-540-32210-8_30

Hoover, T.E., & Berkshire, D.C. (1969). Effects of hydration on carbon dioxide exchange across an air-water interface. *Journal of Geophysical Research, 74*(2), 456-464. https://doi.org/10.1029/JB074i002p00456

Jähne, B., Heinz, G., & Dietrich, W. (1987). Measurement of the diffusion coefficients of sparingly soluble gases in water. *Journal of Geophysical Research Oceans, 92*(C10), 10767-10776.

Jansson, M., Karlsson, J., & Jonsson, A. (2012). Carbon dioxide supersaturation promotes primary production in lakes. *Ecology Letters, 15*, 527-532. https://doi.org/10.1111/j.1461-0248.2012.01762.x

Kaplan, A., & Reinhold, L. (1999). CO_2 concentrating mechanisms in photosynthetic microorganisms. *Annual Review of Plant Physiology and Plant Molecular Biology, 50*, 539-570. https://doi.org/10.1146/annurev.arplant.50.1.539

Karlsson, J., Jansson, M., & Jonsson, A. (2007). Respiration of allochthonous organic carbon in unproductive forest lakes determined by the Keeling plot method. *Limnology and Oceanography, 52*(2), 603-608. https://doi.org/10.4319/lo.2007.52.2.0603

Kasinak, J.E., Holt, B.M., Chislock, M.F., & Wilson, A.E. (2014). Benchtop fluorometry of phycocyanin as a rapid approach for estimating cyanobacterial biovolume. *Journal of Plankton Research, 37*(1), 248-257. https://doi.org/10.1093/plankt/fbu096

Kragh, T., & Sand-Jensen, J. (2018). Carbon limitation of lake productivity. *Biological Sciences, 285*. https://doi.org/10.1098/rspb.2018.1415

Lammers, J.M., Reichart, G.J., & Middelburg, J.J. (2017). Seasonal variability in phytoplankton stable carbon isotope ratios and bacterial carbon sources in a shallow Dutch lake. *Limnology and Oceanography, 62*, 2773-2787. https://doi.org/10.1002/lno.10605

Lehmann, M. F., Bernasconi, S. M., Mckenzie, J. A., Barbieri, A., Simona, M., & Veronesi, M. (2004). Seasonal variation of the $\delta^{13}C$ and $\delta^{15}N$ of particulate and dissolved carbon and nitrogen in Lake Lugano: Constraints on biogeochemical cycling in a eutrophic lake. *Limnology and Oceanography, 49*(2), 415-429. https://doi.org/10.4319/lo.2004.49.2.0415

Lewis, W.K., & Whitman, W.G. (1924). Principles of gas absorption. *Industrial and Engineering Chemistry, 16*(12), 1215-1220. https://doi.org/10.1021/ie50180a002

Molot, L.A., & Dillon, P.J. (1997). Photolytic regulation of dissolved organic carbon in northern lakes. *Global Biogeochemical Cycles, 11*(3), 357-365. https://doi.org/10.1029/97GB01198

Molot, L.A., Watson, S.B., Creed, E.F., Trick, C.G., McCabe, S.K., Verschoor, M.J., Sorichetti, R.J., Powe, C., Venkiteswaran, J.J., & Schiff, S.L. (2014). A noval model for cyanobacteria bloom formation: the critical role of anoxia and ferrous iron. *Freshwater Biology, 59*, 1323-1340. https://doi.org/10.1111/fwb.12334

Mook, W.G., Bommerson, J.C., & Staverman, W.H. (1974). Carbon isotope fractionation between dissolved bicarbonate and gaseous carbon dioxide. *Earth and Planetary Science Letters, 22*(2), 169-176. https://doi.org/10.1016/0012-821X(74)90078-8

Morales-Williams, A.M., Wanamaker, A.D., Jr., & Downing, J.A. (2017). Cyanobacterial carbon concentrating mechanisms facilitate sustained CO_2 depletion in eutrophic lakes. *Biogeosciences, 14*, 2865-2875. https://doi.org/10.5194/bg-14-2865-2017

Morales-Williams, A.M., Wanamaker, A.D., Jr., Williams, C.J., & Downing, J.A. (2020). Eutrophication drives extreme seasonal CO_2 flux in lake ecosystems. *Ecosystems*. https://doi.org/10.1007/s10021-020-00527-2

Odum, H.T. (1956). Primary production in flowing waters. *Limnology and Oceanography, 1*(2), 102-117. https://doi.org/10.4319/lo.1956.1.2.0102

Pacheco, F.S., Roland, F., & Downing, J.A. (2014). Eutrophication reverses whole-lake carbon budgets. *Inland Waters, 4*(1), 41-48. https://doi.org/10.5268/IW-4.1.614

Paerl, H.W. (1990). Physiological Ecology and Regulation of N_2 Fixation in Natural Waters. In Marshall, K.C. (Ed.), *Advances in microbial ecology, vol 11* (pp. 305-344). Springer US. https://doi.org/10.1007/978-1-4684-7612-5_8

Paerl, H.W., & Huisman, J. (2009). Climate change: a catalyst for global expansion of harmful cyanobacterial blooms. *Environmental Microbiology Reports, 1*(1), 27-37. https://doi.org/10.1111/j.1758-2229.2008.00004.x

Parker, S.R., Poulson, S.R., Gammons, C.H., & DeGrandpre, M.D. (2005). Biogeochemical controls on diel cycling of stable isotopes of dissolved inorganic carbon in the Big Hole River, Montana. *Environmental Science and Technology, 39*(18), 7134-7140. https://doi.org/10.1021/es0505595

Peeters, F., Atamanchuk, D., Tengber, A., Encinas-Fernàndez, J., & Hofmann, H. (2016). Lake metabolism: Comparison of lake metabolic rates estimated from a diel CO_{2-} and the common diel O_{2-} technique. *PLoS One, 11*(12). https://doi.org/10.1371/journal.pone.0168393

Pel, R., Hoogveld, H., & Floris, V. (2003). Using the hidden isotopic heterogeneity in phyto- and zooplankton to unmask disparity in trophic carbon transfer. *Limnology and Oceanography, 48*(6), 2200-2207. https://doi.org/10.4319/lo.2003.48.6.2200

R Core Team (2019). R: A language and environment for statistical computing. R Foundation for Statistical Computing. https://www.R-project.org/

Raymond, P.A., Caraco, N.F., & Cole, J.J. (1997). Carbon dioxide concentration and atmospheric flux in the Hudson River. *Estuaries, 20*, 381-390. https://doi.org/10.2307/1352351

Raymond, P.A., Hartmann, J., Lauerwald, R., Sobek, S., McDonald, C., Hoover, M., Butman, D., Striegl, R., Mayorga, E., Humborg, C., Kortelainen, P., Dürr, H., Meybeck, M., Ciais, P., & Guth, P. (2013). Global carbon dioxide emissions from inland waters. *Nature, 503*, 355-359. https://doi.org/10.1038/nature12760

Redfield, A.C. (1958). The biological control of chemical factors in the environment. *American Scientist, 46*(3), 205-221. https://www.jstor.org/stable/27827150

Rocher-Ros, G., Sponseller, R.A., Bergström, A., Myrstener, M., & Giesler, R. (2019). Stream metabolism controls diel patterns and evasion of CO_2 in Arctic streams. *Global Change Biology*, *26*(3), 1400-1413. https://doi.org/10.1111/gcb.14895

Rudd, J.W.M., & Hamilton, R.D. (1978). Methane cycling in a eutrophic shield lake and its effects on whole lake metabolism. *Limnology and Oceanography, 23*(2), 337-348. https://doi.org/10.4319/lo.1978.23.2.0337

Sanches, L.F., Guenet, B., Marinho, C.C., Barros, N., & de Assis Esteves, F. (2019). Global regulation of methane emission from natural lakes. *Scientific Reports, 9*. https://doi.org/10.1038/s41598-018-36519-5

Sander, R. (2015). Compilation of Henry's law constants (version 4.0) for water as solvent. *Atmospheric Chemistry and Physics, 15,* 4399-4981. https://doi.org/10.5194/acp-15-4399-2015

Sandilands, K. (2018). *Light attenuation information sheet.* Unpublished internal document, IISD Experimental Lakes Area.

Schindler, D.W., Brunskill, G.J., Emerson, S., Broecker, W.S., & Peng, T.H. (1972). Atmospheric carbon dioxide: Its role in maintaining phytoplankton standing crops. *Science, 177*(4055), 1192-1194. https://doi.org/10.1126/science.178.4057.204

Schindler, D.W. & Fee, E.J. (1973). Diurnal variation of dissolved inorganic carbon and its use in estimating primary production and CO_2 invasion in Lake 227. *Journal of Fisheries Research Board of Canada, 30*, 1501-1510. https://doi.org/10.1139/f73-240

Schindler, D.W., Hecky, R.E., Findlay, D.L., Stainton, M.P., Parker, B.R., Paterson, M.J., Beaty, K.G., Lyng, M., & Kasian, S.E.M. (2008). Eutrophication of lakes cannot be controlled by reducing nitrogen input: Results of a 37-year whole-ecosystem experiment. *Proceedings of the National Academy of Sciences, 105*(32), 11254-11258. https://doi.org/10.1073/pnas.0805108105

Schindler, D.W. & Vallentyne, J.R. (2008). *The algal bowl: overfertilization of the world's freshwaters and estuaries.* University of Alberta Press.

Schindler, D.W. (2009). A personal history of the Experimental Lakes Project. *Canadian Journal of Fisheries and Aquatic Sciences, 66*(11), 1837-1847. https://doi.org/10.1139/F09-134

Schindler, D.W. (2012). The dilemma of controlling cultural eutrophication of lakes. *Proceedings of the Royal Society B, 279*, 4322-4333. https://doi.org/10.1098/rspb.2012.1032

Scripps CO_2 Program (2020, July). *Global stations isotopic ^{13}C trends*. https://scrippsco2.ucsd.edu/

Sharkey, T.D., & Berry, J.A. (1985). Carbon isotope fractionation of algae as influenced by an inducible CO_2 concentrating mechanism. In Lucas, W.J. & Berry, J.A. (Eds.), *Inorganic Carbon Uptake by Aquatic Photosynthetic Organisms* (389-401). The American Society for Plant Physiologists. https://doi.org/10.1111/j.1399-3054.1985.tb08687.x

Smith, R.B., Bass, B., Sawyer, D., Depew, D., & Watson, S.B. (2019). Estimating the economic costs of algal blooms in the Canadian Lake Erie Basin. *Harmful Algae, 87*, 101624. https://doi.org/10.1016/j.hal.2019.101624

Solomon, C.T., Carpenter, S.R., Clayton, M.K, Cole, J.J., Coloso, J.J., Pace, M.L., Vander Zanden, M.J., & Weidel, B.C. (2011). Terrestrial, benthic, and pelagic resource use in lakes: results from a three-isotope Bayesian mixing model. *Ecology, 92*(5), 1115-1125. https://doi.org/10.1890/10-1185.1

Spence, C., Beaty, K., Blanchfield, P.J., Hrenchuk, L., & MacKay, M.D. (2018). The impact of a loss of hydrologic connectivity on boreal lake thermal and evaporative regimes. *Limnology and Oceanography, 63*(5), 2028-2044. https://doi.org/10.1002/lno.10822

Stainton, M.P., Capel, M.J., Armstrong, F.A.J. (1977). *The chemical analysis of fresh water* (Miscellaneous special publication 25, 2nd Ed.). Fisheries and Environment Canada, Fisheries and Marine Service. https://cat.fsl-bsf.scitech.gc.ca/record=b3659354~S6

Stumm, W., & Morgan, J.J. (1996). *Aquatic chemistry: Chemical equilibria and rates in natural waters* (3rd Ed.). John Wiley & Sons, Inc.

Sulzman, E.W. (2007). Stable isotope chemistry and measurement: a primer. In Michener, R. & Lajtha, K. (Eds.), *Stable Isotopes in Ecology and Environmental Science* (2nd Ed., pp. 1-21). Blackwell Publishing Ltd. https://doi.org/10.1002/9780470691854

Sunda, W.G. (2006). Trace metals and harmful algal blooms. In Granéli, E. & Turner, J. (Eds.), *Ecology of Harmful Algae* (pp. 391-402). Springer. https://doi.org/10.1007/978-3-540-32210-8_16

Tans, P., & Keeling, R. (2020). *Trends in atmospheric carbon dioxide*. www.esrl.noaa.gov/gmd/ccgg/trends/

Tranvik, L.J., Downing, J.A., Cotner, J.B., Loiselle, S.A., Striegl, R.G., Ballatore, T.J., Dillon, P., Finlay, K., Fortino, K., Knoll, L.B., Kortelainen, P.L., Kutser, T., Larsen, S., Laurion, I., Leech, D.M., McCallister, S.L., McKnight, D.M., Melack, J.M., Overholt, E., … Weyhenmeyer, G.A. (2009). Lakes and reservoirs as regulators of carbon cycling and climate. *Limnology and Oceanography*, *54*, 2298-2314. https://doi.org/10.4319/lo.2009.54.6_part_2.2298

Van Dam, B.R., Tobias, C., Holbach, A., Paerl, H.W., & Zhu, G. (2018). CO_2 limited conditions favor cyanobacteria in a hypereutrophic lake: An empirical and theoretical stable isotope study. *Limnology and Oceanography, 63*(4), 1643-1659. https://doi.org/10.1002/lno.10798

Venkiteswaran, J.J., Schiff, S.L., St. Louis, V.L., Matthews, C.J.D., Boudreau, N.M., Joyce, E.M., Beaty, K.G., & Bodaly, R.A. (2013). Processes affecting greenhouse gas production in experimental boreal reservoirs. *Global Biogeochemical Cycles, 27*(2). 567-577. https://doi.org/10.1002/gbc.20046

Verspagen, J.M.H., Vad de Waal, D.B., Finke, J.F., Visser, P.M., Van Donk, E., & Huisman, J. (2014). Rising CO_2 levels will intensify phytoplankton blooms in eutrophic and hypereutrophic lakes. *PLoS ONE, 9*(8). https://doi.org/10.1371/journal.pone.0104325

Vuorio, K., Meili, M., & Sarvala, J. (2006). Taxon-specific variation in the stable isotopic signatures ($\delta^{13}C$ and $\delta^{15}N$) of lake phytoplankton. *Freshwater Biology, 51*, 807-822. https://doi.org/10.1111/j.1365-2427.2006.01529.x

Wang, X., Conway, W., Burns, R., McCann, N., & Maeder, M. (2010). Comprehensive study of the hydration and dehydration reactions of carbon dioxide in aqueous solution. *The Journal of Physical Chemistry A, 114*(4), 1734-1740. https://doi.org/10.1021/jp909019u

Wang, S., Yeager, K.M., & Lu, W. (2016). Carbon isotope fractionation in phytoplankton as a potential proxy for pH rather than for [CO_2(aq)]: Observations from a carbonate lake. *Limnology and Oceanography, 61,* 1259-1270. https://doi.org/10.1002/lno.10289

Watson, S.B., Whitton, B.A., Higgins, S.N., Paerl, H.W., Brooks, B.W., & Wehr, J.D. (2015). Harmful algal blooms. In Wehr, J.D., Sheath R.G., & Kocioleg, J.P. (Eds.), *Freshwater algae of North America: Ecology and classification* (2nd Ed., pp. 873-920). Academic Press. https://doi.org/10.1016/B978-0-12-385876-4.00020-7

Watson, S.B., Miller, C.J., Arhonditsis, G.B., Boyer, G.L., Carmichael, W.W., Charlton, M.N., Confesor, R., Depew, D.C., Höök, T.O., Ludsin, S.A., Matisoff, G., McElmurry, S.P., Murray, M.W., Richards, R.P., Rao, Y.R., Steffen, M.M., & Wilhelm, S.W. (2016). The re-eutrophication of Lake Erie: Harmful algal blooms and hypoxia. *Harmful Algae*, 56, 44-66. https://doi.org/10.1016/j.hal.2016.04.010

Wetzel, R.G. (2001). *Limnology* (3rd Ed.). Academic Press.

Whiticar, M.J. (1999). Carbon and hydrogen isotope systematics of bacterial formation and oxidation of methane. *Chemical Geology, 1-3*(30), 291-314. https://doi.org/10.1016/S0009-2541(99)00092-3

Williams, P., & del Giorgio, P.A. (2005). Respiration in aquatic ecosystems: History and background. In: del Giorgio, P.A., & Williams, P. (Eds.) *Respiration in Aquatic Ecosystems* (pp. 1-17). Oxford University Press. https://doi.org/10.1093/acprof:oso/9780198527084.001.0001

Wilkinson, G.M., Pace, M.L., & Cole, J.J. (2013). Terrestrial dominance of organic matter in north temperate lakes. *Global Biogeochemical Cycles, 27*(1), 43-51. https://doi.org/10.1029/2012GB004453

Winslow, L.A., Zward, J.A., Batt, R.D., Dugan, H.A., Woolway, R.I., R., Corman, J.R., Hanson, P.C., & Read, J.S. (2016). LakeMetabolizer: an R package for estimating lake metabolism from free-water oxygen using diverse statistical models. *Inland Waters, 6*, 622-636. https://doi.org/10.1080/IW-6.4.883

Wolfe, B., Kling, H.J., Brunskill, G.J., & Wilkinson, P. (1994). Multiple dating of a freeze core from Lake 227, an experimental fertilized lake with varved sediments. *Canadian Journal of Fisheries and Aquatic Sciences, 51*(10), 2274-2285. https://doi.org/10.1139/f94-231

Woodwell, G.M., & Whittaker, R.H. (1986). Primary production in terrestrial ecosystems. *American Zoologist, 8*(1), 19-30. https://doi.org/10.1093/icb/8.1.19

Zhang, J., Quay, P.D., & Wilbur, D.O. (1995). Carbon isotope fractionation during gas-water exchange and dissolution of CO_2. *Geochimica et Cosmochimica Acta, 59*(1), 107-114. https://doi.org/10.1016/0016-7037(95)91550-D